

1993

Hydrodynamic And Electrohydrodynamic Instability Of Shear Flows And The Numerical Simulation Of Viscous Droplets

Kenzu Abdella

Follow this and additional works at: <https://ir.lib.uwo.ca/digitizedtheses>

Recommended Citation

Abdella, Kenzu, "Hydrodynamic And Electrohydrodynamic Instability Of Shear Flows And The Numerical Simulation Of Viscous Droplets" (1993). *Digitized Theses*. 2203.
<https://ir.lib.uwo.ca/digitizedtheses/2203>

This Dissertation is brought to you for free and open access by the Digitized Special Collections at Scholarship@Western. It has been accepted for inclusion in Digitized Theses by an authorized administrator of Scholarship@Western. For more information, please contact tadam@uwo.ca, wlsadmin@uwo.ca.

**Hydrodynamic And Electrohydrodynamic
Instability Of Shear Flows
And The Numerical Simulation Of Viscous Droplets**

by

Kenzu Abdella

Department of Applied Mathematics

Submitted in partial fulfilment
of the requirements for the degree of
Doctor of Philosophy

Faculty of Graduate Studies
The University of Western Ontario
London, Ontario
March 1993

© Kenzu Abdella 1993



National Library
of Canada

Acquisitions and
Bibliographic Services Branch

395 Wellington Street
Ottawa, Ontario
K1A 0N4

Bibliothèque nationale
du Canada

Direction des acquisitions et
des services bibliographiques

395, rue Wellington
Ottawa (Ontario)
K1A 0N4

Your file *Votre référence*

Our file *Notre référence*

The author has granted an irrevocable non-exclusive licence allowing the National Library of Canada to reproduce, loan, distribute or sell copies of his/her thesis by any means and in any form or format, making this thesis available to interested persons.

L'auteur a accordé une licence irrévocable et non exclusive permettant à la Bibliothèque nationale du Canada de reproduire, prêter, distribuer ou vendre des copies de sa thèse de quelque manière et sous quelque forme que ce soit pour mettre des exemplaires de cette thèse à la disposition des personnes intéressées.

The author retains ownership of the copyright in his/her thesis. Neither the thesis nor substantial extracts from it may be printed or otherwise reproduced without his/her permission.

L'auteur conserve la propriété du droit d'auteur qui protège sa thèse. Ni la thèse ni des extraits substantiels de celle-ci ne doivent être imprimés ou autrement reproduits sans son autorisation.

ISBN 0-315-81279-6

Canada

Abstract

In this thesis, we investigate three fluid dynamic problems involving various physical mechanisms which exhibit interfacial instability. These problems have wide ranging industrial, scientific and engineering applications.

In the first problem, we investigate the linear stability of the unbounded Couette flow of two fluids separated by a plane interface. The exact dispersion relation is solved asymptotically and numerically to analyze the effects of the four stability parameters of the flow; the ratio of the viscosities, the ratio of the density, the surface tension and gravity. While our results confirm most of the earlier reported theories involving shear flows of fluids of equal densities, they also resolve the reported discrepancies between the numerical and the asymptotic solutions. For the general case of fluids with different densities, new asymptotic expressions for the growth rates of the flow are obtained and numerical calculations of marginal states are carried out in order to examine the effects of the stability parameters on the flow. The numerical results confirm the remarkable accuracy of our asymptotic expressions.

In the second problem, the electrohydrodynamic extension of the first problem is presented. Here, the plane interface is stressed by applying external electric fields normal to the interface. A linear stability analysis similar to that employed in the first problem is used to investigate the effects of six additional stability parameters on the stability of the flow; the ratio of the permittivities, the two conductivities, the two initial electric fields and the velocity of the upper fluid in the unperturbed motion. Various limiting cases having practical applications are investigated. We examine the effects of electrical shear stresses and initial streaming of the fluids on the onset of static instability. We also examine finite electric charge relaxation effects.

Finally, we investigate the dynamic behaviour of viscous droplets in the presence of applied electric fields in zero gravity conditions. Here, the full nonlinear equations of motion are solved numerically by adapting the NASA-VOF2D algorithm. The numerical computations carried out for axisymmetric droplets in zero gravity successfully simulate microgravity experiments conducted on KC-135 NASA aircraft flights. Further experimental and modelling modifications are discussed.

Acknowledgements

I wish to thank my supervisor Dr. Henning Rasmussen for his unfailing guidance, support and encouragement throughout my doctoral work. I am also grateful to Dr. Ion Inculet and the Applied Electrostatic Research Center for providing the experimental data for the water droplet problem, Dr. David Jeffrey for his constructive suggestions for the shear flow stability problem and for introducing me to the computer algebra system Maple, Dr. Robert Corless for lending his expertise in Maple, and the Canadian Space Agency for their generous financial support.

I wish to thank all the faculty and fellow graduate students of the applied mathematics department with whom I had useful discussions about the topics of the thesis, and especially Serge D'Alessio for his support and friendship. Many thanks to the applied mathematics department secretaries, Audrey Kagar, Pat Malone and Gayle McKenzie for their commitment to us, the graduate students.

Most importantly I would like to thank my wife Michele for her unfailing love and support throughout the course of this thesis. She has also been of great help in editing the text of the thesis. I wish to thank my father Abdella Sultan, my mother Zeineba Ali and my brothers and sisters including Fuad for their patience and confidence in me. This thesis is dedicated to them and to my wife Michele.

Finally, praise goes to Allah, the most benevolent, ever-merciful, all-knowing and all-powerful.

Contents

1	Introduction	1
2	Shear-flow Instability at the Interface Between Two Fluids	4
2.1	Introduction	4
2.2	Introduction to Hydrodynamic Stability	7
2.3	Linear Theory of Hydrodynamic Stability	8
2.3.1	The Normal Mode Method	9
2.4	Formulation of the Problem	11
2.4.1	The Governing Equations	11
2.4.2	Boundary Conditions	16
2.4.3	The Eigenvalue Problem	21
2.5	The Dispersion Relation	22
2.5.1	The Stability of the $m > 1$ Case	25
2.6	Asymptotic Analysis	26
2.6.1	Short Wavelength Approximations	26
2.6.2	Long Wavelength Approximations	34
2.6.3	Asymptotic Behaviour of c as $m \rightarrow 0$	35
2.6.4	Asymptotic Behaviour of c as $m \rightarrow 1$	38
2.6.5	Marginal Stability Curves	39
2.7	Numerical Procedure	41
2.8	Results and Discussion	44

2.8.1	Equal Densities	44
2.8.2	Unequal Densities	53
2.9	Conclusion	67
3	Electrohydrodynamic Instability of Two Superposed Fluids in Normal Electric Fields	69
3.1	Introduction	69
3.2	Formulation of the Problem	72
3.2.1	The Governing Equations	74
3.2.2	Boundary Conditions	78
3.3	The Dispersion Relation	81
3.4	Free Charge (EH-If) and Polarization Charge (EH-Ip) Configurations	86
3.4.1	The Principle of Exchange of Stabilities	89
3.5	Infinite Electric Charge Relaxation Limit	96
3.6	Instantaneous Charge Relaxation Limit	100
3.7	Finite Relaxation Time Effects	104
3.8	Concluding Remarks	106
4	Interfacial Deformation of Liquid Droplets by Applied Electric Fields at Zero Gravity	107
4.1	Introduction	107
4.2	Formulation of the Problem	111
4.2.1	Governing Equations	112
4.2.2	Boundary Conditions	114
4.3	Description of the Numerical Procedure	115
4.3.1	The Fluid Flow Model	115
4.3.2	The Electrostatic Model	126
4.4	The Initial Equilibrium Shape	133

4.5	Flow Chart of the Numerical Model	135
4.6	Numerical Results	137
4.7	Comparison of the Model With Experimental Results	138
4.8	Future Improvements and Considerations	140
4.9	Concluding Remarks	141
5	Conclusion	152
	Appendix	154
A	Airy Functions	154
B	The Coefficients c_{4s} and c_{5s}	156
C	Photographs From The Experiment	158
	Bibliography	164
	Vita	172

List of Figures

2.1	Schematic representation of the problem.	12
2.2	Marginal stability curve for $S = 0$ and $r = 1$	46
2.3	Marginal stability curves for $r = 1$ and small values of S	47
2.4	Marginal stability curves for $r = 1$ and large values of S	48
2.5	Maximum growth rates for various values of S when $r = 1$	51
2.6	Values of α corresponding to maximum growth rates when $r = 1$. . .	52
2.7	Marginal stability curve for various values of r , $g = 0$ and $S = 0$. . .	55
2.8	Marginal stability curves for $r = 1.25$, $S = 0.1$ and various values of g	57
2.9	Marginal stability curves for $r = 0.8$, $S = 0.1$ and for various values of g	58
2.10	Marginal stability curves for $r = 1.25$, $S = 0.0$ and various values of g	60
2.11	Neutral stability curve for $g = 1.0$, $S = 0.1$ and various values of r . .	63
2.12	Marginal stability curves for small values of α	64
2.13	Maximum growth rates for $r > 1$ and $r < 1$	65
2.14	Values of α corresponding to maximum growth rates for $r = 0.8$. . .	66
3.1	Schematic representation of the problem.	73
3.2	Marginal stability curves for the EH-I _f configuration with $\alpha^* = 4.47$, $a_1 - a_2 = 0.5$ and $V = 0.83$	92
3.3	Marginal stability curves for the EH-I _p configuration with $\alpha^* = 4.47$, $a_1 - a_2 = 0.5$ and $V = 0.83$	93
3.4	Electric field required to destabilize $\alpha^* = 4.47$ as a function of $a_1 - a_2$	94
3.5	Real part of c for marginal stability at $\alpha^* = 4.47$ as a function of $a_1 - a_2$	95

3.6	Marginal stability curves for the infinite charge relaxation limit with $a_1 - a_2 = 0.05$	98
3.7	Marginal stability curves for the infinite charge relaxation limit with $q=0.31$	99
3.8	Marginal stability curve for the case of instantaneous relaxation limit, $Q = 0.5$ and $a_1 - a_2 = 0.05$	103
4.1	Schematic representation of the the physical problem	112
4.2	A typical computational mesh	117
4.3	Location of variables in a typical mesh cell	117
4.4	Definition of d_s and d_c for the surface pressure interpolation.	122
4.5	The rectangular mesh used to solve the electrostatic problem	127
4.6	Definition of the h 's for the surface cells	128
4.7	Selection of metal nodes	132
4.8	Equilibrium profile of a sessile droplet.	133
4.9	Equilibrium droplet profile at $t = 0$ milliseconds. The contact angle is 82 degrees.	143
4.10	Droplet profile at $t = 25.6$ milliseconds.	144
4.11	Droplet profile at $t = 28.3$ milliseconds.	145
4.12	Droplet profile at $t = 28.5$ milliseconds. First breakup occurs.	146
4.13	Droplet profile at $t = 36$ milliseconds.	147
4.14	Droplet profile at $t = 28.5$ milliseconds. Second breakup occurs.	148
4.15	Droplet profile at $t = 51$ milliseconds.	149
4.16	Droplet profile at $t = 52$ milliseconds.	150
4.17	Droplet profile at $t = 54$ milliseconds. Third breakup has occurred.	151
C.1	The over all view of the microgravity experimental apparatus.	158

C.2	The experimental droplet profile for water on a brass electrode before breakup	159
C.3	The experimental droplet profile for water on a brass electrode just before breakup	159
C.4	The experimental droplet profile for water on a brass electrode after breakup	160
C.5	The nonaxisymmetric droplet profile for water on a brass electrode after breakup	160
C.6	The experimental droplet profile for water on an aluminium electrode before breakup	161
C.7	The experimental droplet profile for water on an aluminium electrode just before breakup	161
C.8	The experimental droplet profile for water on an aluminium electrode after breakup	162
C.9	The nonaxisymmetric droplet profile for water on an aluminium electrode after breakup	162
C.10	The nonaxisymmetric droplet profile for water on an aluminium electrode before a second breakup	163
C.11	The droplet profile for a highly viscous material on a brass electrode	163

List of Tables

2.1	Imaginary parts of c computed from the asymptotic expression 2.118 and from the numerical method	43
2.2	The imaginary parts of c computed from the asymptotic expression 2.103 and from the numerical method	43
2.3	Comparison between 2.119 and the numerical method for $r = 1$	45
2.4	Comparison between 2.120 and the numerical method for $r = 1$	49
2.5	Imaginary parts of c to illustrate the zero-gravity zero-surface tension case with $\alpha = 2.0$	53
2.6	Comparison of the imaginary parts of c between equation 2.101 and the numerical method where $r = 1.5$, $S = 0$, $m = 0.05$ and $g = 1.0$. .	54
2.7	Comparison of α intercepts between 2.115 and the numerical method for $S = 0.1$ and $g = 1.0$	61
2.8	Comparison of α intercepts between 2.115 and the numerical method for $S = 0.1$ and $g = 1.0$	61

The author of this thesis has granted The University of Western Ontario a non-exclusive license to reproduce and distribute copies of this thesis to users of Western Libraries. Copyright remains with the author.

Electronic theses and dissertations available in The University of Western Ontario's institutional repository (Scholarship@Western) are solely for the purpose of private study and research. They may not be copied or reproduced, except as permitted by copyright laws, without written authority of the copyright owner. Any commercial use or publication is strictly prohibited.

The original copyright license attesting to these terms and signed by the author of this thesis may be found in the original print version of the thesis, held by Western Libraries.

The thesis approval page signed by the examining committee may also be found in the original print version of the thesis held in Western Libraries.

Please contact Western Libraries for further information:

E-mail: libadmin@uwo.ca

Telephone: (519) 661-2111 Ext. 84796

Web site: <http://www.lib.uwo.ca/>

Chapter 1

Introduction

In this thesis, we consider three fluid dynamic problems involving physical mechanisms which exhibit unstable behaviour. The first two problems deal with the hydrodynamic and electrohydrodynamic instability of the shear flow at the interface between two fluids. The third problem involves the development of computational methods to describe the dynamic deformation of large viscous droplets subjected to external electric fields in a zero gravity environment. These problems have many practical applications in industry and engineering including underwater explosions, atmospheric electrifications, electrostatic spraying and the orientation of fluids in zero gravity.

In chapter 2 we analyze the unbounded Couette flow of two fluids which are separated by a plane interface by employing a linear stability analysis. We assume that the fluids have different viscosities, densities and equilibrium velocities. Surface tension acts at the interface and there is a gravitational body force. The exact dispersion relation relating the stability parameters is derived in terms of the Airy functions and their integrals. The stability of the system depends on four parameters including the ratio of viscosities, the ratio of the densities, gravity and surface tension. The dispersion relation is solved both numerically and asymptotically.

The asymptotic analysis carried out for large wavenumbers α removes the restriction imposed by Hooper and Boyd on the allowable values of surface tension [33].

Their analysis for large wavenumbers, which was based on the Orr-Sommerfeld equation for the problem, required that the surface tension S be scaled in such a way that $S\alpha^3$ remained order unity. We base our analysis on the exact dispersion relation and we obtain a new functional form of the asymptotic expression containing higher powers of α without placing any restriction on the surface tension. The asymptotic analysis is also extended for small wavenumbers to include the case of unequal fluid densities. Both the large and the small wavenumber limits contain new terms due to the presence of gravity.

When the two densities are equal, our results qualitatively agree with the findings of Hooper and Boyd. However, they encountered several discrepancies between their numerical and asymptotic solutions which are resolved using our analysis. This confirms the validity of the extended asymptotic analysis and corrects their numerical results. Our numerical results are used to show that the large wavenumber expansion is remarkably accurate even for moderate wavenumbers. Even so, our results do not replace numerical solutions, because it is shown that predictions of stability based solely on asymptotic results can be erroneous. In general terms, the flow is unstable for viscosity ratios far from 1 and stable for ratios near 1 provided that surface tension is present or gravity is stabilizing. The instability is *not* generally at short wavelengths as previously reported by Hooper and Boyd.

In chapter 3 we examine the electrohydrodynamic extension of the first problem. The interface is stressed by applying external electric fields normal to the plane interface. In addition to the assumptions made in the first problem, the fluids are assumed to have different conductivities and permittivities. A linear stability analysis similar to that employed in the first problem is used to investigate the stability of the system. The stability of the system depends on the following ten parameters; the ratio of the viscosities, the ratio of the densities, the surface tension, gravity, the ratio of the permittivities, the two conductivities, the two initial electric fields and the velocity

field of the upper fluid in the unperturbed motion.

We consider various limiting cases with the relaxation time as the limiting parameter and we investigate the onset of instability and the destabilizing effects of the equilibrium motion. The effects of electrical shear stresses are investigated in the infinite and instantaneous relaxation charge limit. We also examine the finite charge relaxation effects and develop conditions for the incipience of static instability.

Finally, in chapter 4, we investigate the dynamic evolution of viscous droplets in the presence of applied electric fields in zero gravity conditions. Due to the applied electric fields, an electric charge is induced on the droplet surface resulting in an outwardly directed pressure which forces the droplet into a cone. Under suitable conditions, small droplets are ejected from the cone.

Here, unlike in the first two problems, we solve the full nonlinear equations of motion. The core of the model is adapted from the NASA VOF2D algorithm for transient two-dimensional flows with free surfaces. Numerical computations are carried out with axisymmetric and zero gravity assumptions and are then compared with experimental data collected from microgravity experiments conducted on KC-135 NASA aircraft flights. While a number of modifications are suggested, the numerical model successfully simulates the actual deformation process.

Chapter 2

Shear-flow Instability at the Interface Between Two Fluids

2.1 Introduction

In this chapter we consider the parallel flow of two fluids of different viscosities and different densities separated by a planar interface. At each side of the interface the flow is the unbounded Couette flow. The linear stability of the flow is analysed by deriving the exact dispersion relation and solving it numerically and asymptotically.

The linear stability of parallel shear flows, both in bounded and unbounded domains, has been studied by many authors using asymptotic and approximate analyses [69], [43], [52] and [20]. Yih considered the flow of two fluids of different viscosities between two parallel rigid plane boundaries and separated by an interface parallel to the boundaries [83]. Using non-singular perturbation methods, he showed that when the fluids are set in motion by either an applied pressure gradient (Poiseuille flow) or by the relative motion of the boundaries (Couette flow) the interface was unstable for arbitrarily small Reynold numbers. However, it was not known if the rigid boundaries played an important role in this instability.

In 1983, Hooper and Boyd, referred to in this thesis as HB, addressed this question [33]. They examined the stability of the unbounded flow configuration shown in figure 2.1. By solving the exact dispersion relation containing the stability parameters

$m = \mu_2/\mu_1$ where μ_1 and μ_2 are the constant viscosities of the upper and the lower fluid respectively, a non-dimensionalised surface tension S , the wavenumber α , and the wave velocity of the disturbance c , they showed that, in the absence of surface tension, the flow with equal densities is always unstable with respect to short wavelength disturbances.

However, their numerical procedure suffered from several shortcomings. First, it was restricted to the case of equal densities; the case of unequal densities was tackled using asymptotic techniques only. Second, the calculations could not be completed for small ratios of the viscosities precisely the domain in which a comparison with asymptotic analysis would be most revealing. Finally, if the numerical results they obtained for moderate viscosity ratios are extrapolated to small ratios, then significant discrepancies with the asymptotic analysis are evident, casting doubt on at least one of the methods employed. The difficulties of the numerical computations made it quite possible that they, rather than the asymptotic methods, were in error and, perhaps on this supposition, these asymptotic methods have been used since, in spite of uncertainties.

One of the difficulties HB faced in their numerical calculations was that the dispersion relation describing the stability of the flow contained Airy functions having complex arguments, and the methods available to them for computing these functions were not efficient.

In this chapter, we re-examine the unbounded shear flow problem of two fluids of different densities and viscosities. The presence of the density jump introduces the stability parameters $r = \rho_2/\rho_1$ and a non-dimensionalized acceleration g . We compute the Airy functions using recently developed methods for evaluating Airy functions with complex arguments [4], [12]. We obtain improved agreement between the numerical solutions and the asymptotic analysis and we extend the numerical treatment to cases not covered by HB. We also rework the asymptotic analysis, start-

ing from a different point, because their analysis placed restrictions on the allowable values of surface tension. To be specific, their analysis for large wavenumbers α required that the surface tension S was scaled in such a way that $S\alpha^3$ remained order unity. Their analysis was based on the Orr-Sommerfeld equation for the problem, whereas we start from the dispersion relation:

The findings of HB suggest that a more comprehensive analysis is needed. They showed that, for zero surface tension, the flow is unstable for all viscosity ratios. Surface tension is a stabilising influence, but will only make the flow stable provided that the ratio of viscosities is not too different from 1. Since it is unlikely that fluids having different viscosities will have the same densities, we investigate the effect of density differences on the stability. The asymptotic analysis of HB shows that a density difference can be as important an agent for stability as surface tension; indeed, this is confirmed by an asymptotic analysis for large wavenumbers.

One of the difficulties arising from these generalisations of the flow problem is the increase in the number of parameters. There are now four independent stability parameters governing the problem; m , r , S , and g . Our primary results are presented in stability diagrams where the ratio of viscosities is the primary parameter. The ratio of viscosities was chosen because it was the parameter employed by HB and because it is supported by the asymptotic analysis to some extent. However, we leave open the question of whether another parameter may be more appropriate. A comparison with the asymptotic results shows that analytic expressions for the marginal stability curves can be found that are accurate over a wide range of parameters. Numerous stability plots are not therefore required, although the analytic approximations can be misleading when compared with full numerical solutions.

In sections 2.2 and 2.3 we set out the mathematical techniques used in hydrodynamic stability analysis. In section 2.4 we formulate the mathematical model of the problem. In section 2.5 we derive the dispersion relation which, for fluids of equal

densities, reduces to that derived in HB. In section 2.6 we present some asymptotic estimates while in section 2.7 we outline the numerical procedure used to solve the dispersion relation relating the four stability parameters, the wavenumber α and the wave speed c . Results for both equal and unequal densities are presented in section 2.8. As the parameters approach asymptotic limits, the numerical results and the asymptotic approximations obtained are in excellent agreement. Finally, conclusions are presented in section 2.9.

2.2 Introduction to Hydrodynamic Stability

Hydrodynamic stability has been studied quite extensively for over a century. It is of particular importance in the study of the initial stages of fluid flow transitions from laminar to turbulent flow. These transitions usually involve different types of instabilities. Therefore, in order to gain an understanding of the physical mechanism of this transition process, the study of hydrodynamic stability is essential. The various types of instabilities include thermal convective instability [64], capillary instability [63] and shear flow instability [59]. In this chapter we deal with shear flow instability at the interface between two fluids. This is commonly known as interfacial instability. Among the well known examples of interfacial instability are the Kelvin-Helmholz instability [39] and the Rayleigh-Taylor instability [74]. These are both special cases of the problem that is considered in this chapter.

Interfacial instabilities are responsible for a wide range of natural phenomena [62]. In his investigation of liquid jets, Lord Rayleigh demonstrated that resonance as well as acoustic stimulation could give rise to interfacial instability [62]. Later, Harrison further investigated the same problem by considering the effect of viscosity [24]. Lamb explained the abnormal resistance experienced by ships where there is a layer of fresh water over salt water in terms of interfacial oscillations [41]. More recently, Taylor studied interfacial instability theoretically [74] and Lewis studied it experimentally

[42] to explain the loss of energy in successive pulsations of underwater explosion bubbles.

In real systems, these natural phenomena described by an interfacial instability process may be influenced by many physical factors such as molecular diffusion across the interface, evaporation and condensation. In this thesis, the effects of these factors are assumed to be negligible. We consider the effects of other factors including interfacial surface tension, gravity, density and viscosity.

A mathematical theory covering the development of instability due to arbitrary finite disturbances is generally too complex to solve and, moreover, since the nature of the disturbances is often too difficult for experimental control, experimental comparisons are not always possible to perform. Therefore, most stability analyses are based on a perturbation theory[16]. The linear theory of stability gives an adequate representation of flows with small disturbances and it can also predict the onset of instability. Even in the case of finite amplitude disturbances, valuable insights can be gained through the linear theory. In this thesis we use linear stability theory to predict the conditions and the nature of stability at the interface between two superposed fluids. In the next section we discuss the principles of this theory.

2.3 Linear Theory of Hydrodynamic Stability

The linear theory for a particular flow starts with the basic state solutions of the system representing the unperturbed flow. These solutions describe the characteristics of the steady state equilibrium. Then, small perturbations are introduced to these solutions and their evolution in time is investigated. The common method of analysis is called the normal mode method [16]. This method consists of solving the linearized equations of motion subject to the linearized boundary conditions for the small perturbations about the basic state. The perturbations that result in a time increasing departure from the basic state solutions are classified as unstable.

2.3.1 The Normal Mode Method

We begin by perturbing the basic flow as follows:

$$Q(\mathbf{r}, t) = Q_b(\mathbf{r}) + q'(\mathbf{r}, t) \quad (2.1)$$

where Q represents any quantity associated with the flow, Q_b represents the basic state value of quantity Q and q' represents the small perturbation about the basic state quantity Q_b . The perturbed flow quantities are introduced into the equations of motion which are then linearized with respect to the primed quantities and their derivatives. In other words, all terms involving quadratic and higher order terms in the primed quantities are neglected. A complete investigation of stability is accomplished by Fourier analysis of arbitrary spatial disturbance. The immediate advantage of linearity is that there are no interactions between the different Fourier components so that the equations can be broken down into separate sets of equations for each Fourier component [10]. Then, the stability or instability with respect to that component is examined.

Therefore, we assume that the perturbations are spacially sinusoidal and time dependent of the form

$$q' \propto \exp i(\mathbf{k} \cdot \mathbf{r} - \sigma t) \quad (2.2)$$

where

$$\sigma = \sigma_r + i\sigma_i \quad (2.3)$$

is the complex wave speed and \mathbf{k} is the wavenumber. This assumption reduces the linear partial differential equations of motion to ordinary differential equations. By imposing appropriate boundary conditions upon the solutions of the resulting ordinary differential equations, we formulate an eigenvalue problem. The relation between σ , the perturbing wavenumber \mathbf{k} and the other stability parameters of the particular flow such as viscosity and surface tension is called the *dispersion relation*. The roots of the dispersion relation are the eigenvalues σ . The stability or the instability of the

flow is then determined by the sign of these roots. If σ_i is negative for all values of k , then all infinitesimal perturbations of the original flow decay exponentially. This is a necessary condition for *stability*. If σ_i is positive for any values of k , then the corresponding perturbation will be exponentially amplified. This is a sufficient condition for *instability*.

If $\sigma_i = 0$ for some values of k , then the flow is said to be *neutrally stable* with respect to the corresponding perturbations. If, in this case, $\sigma_i > 0$ for some neighbouring values of the stability parameters on which the eigenvalues depend, then the flow is said to be *marginally stable*. Thus, marginal stability separates the stable and the unstable classes of all infinitesimal disturbances for the given basic state. The locus of the marginal stability states in the space of the stability parameters forms the *marginal stability curve (or surface)*. The conditions of stability for a given flow are usually determined by investigating the nature and the structure of these curves [10].

The state of marginal stability is divided into two according to the ways in which the perturbations evolve. If $\sigma_r = 0$, then the disturbance will grow or decay exponentially. Here, the transition from stability to instability takes place via a marginal state exhibiting a steady secondary flow, such as the case of convection cells that arise when a fluid is heated from below [10]. When this type of behaviour prevails there is said to be an *exchange of stability* [38]¹. On the other hand, if $\sigma_r \neq 0$, then the disturbances will decay or grow in oscillatory motion and the transition from stability to instability occurs via a marginal state exhibiting oscillatory motion with characteristic frequency. This type of behaviour is called *over stability* [17]. It tends to occur when a destabilizing influence and a feature giving rise to wave motions, such as stratification, are present simultaneously.

¹This definition can be traced back to Poincare [61] but Jeffreys [38] first used this definition in the present sense.

2.4 Formulation of the Problem

We consider the two dimensional flow of two incompressible and viscous fluids of constant viscosities μ_1 and μ_2 with constant densities ρ_1 and ρ_2 . In the unperturbed state, the two fluids are separated by the interface $y^* = 0$, where x^* and y^* are the usual Cartesian coordinates. We use subscripts 1 and 2 to refer to fluid properties and fluid flow quantities above and below the interface respectively. Gravity g^* acts in the negative y^* direction. The basic unperturbed flow in this two-layer model is described by the following velocity field,

$$\tilde{u}_1(x^*, y^*) = (\tilde{\omega}_1 y^*, 0) \quad (2.4)$$

$$\tilde{u}_2(x^*, y^*) = (\tilde{\omega}_2 y^*, 0)$$

where $\tilde{\omega}_1$ and $\tilde{\omega}_2$ are constant vorticities above and below the interface respectively.

The schematic representation of the problem is shown in figure 2.1.

The continuity of shear stress at the interface $y^* = 0$ implies that

$$\tilde{\omega}_1 = m\tilde{\omega}_2 \quad (2.5)$$

where $m = \frac{\mu_2}{\mu_1}$. As we will see later, the viscosity ratio m turns out to be one of the stability parameters in the dispersion relation.

2.4.1 The Governing Equations

The general equations of motion of a two dimensional incompressible flow are,

$$\begin{aligned} \frac{\partial u^*}{\partial t^*} + u^* \frac{\partial u^*}{\partial x^*} + v^* \frac{\partial u^*}{\partial y^*} &= -\frac{1}{\rho} \frac{\partial p^*}{\partial x^*} + \nu \nabla^2 u^* \\ \frac{\partial v^*}{\partial t^*} + u^* \frac{\partial v^*}{\partial x^*} + v^* \frac{\partial v^*}{\partial y^*} &= -\frac{1}{\rho} \frac{\partial p^*}{\partial y^*} - g^* + \nu \nabla^2 v^* \\ \frac{\partial u^*}{\partial x^*} + \frac{\partial v^*}{\partial y^*} &= 0 \end{aligned} \quad (2.6)$$

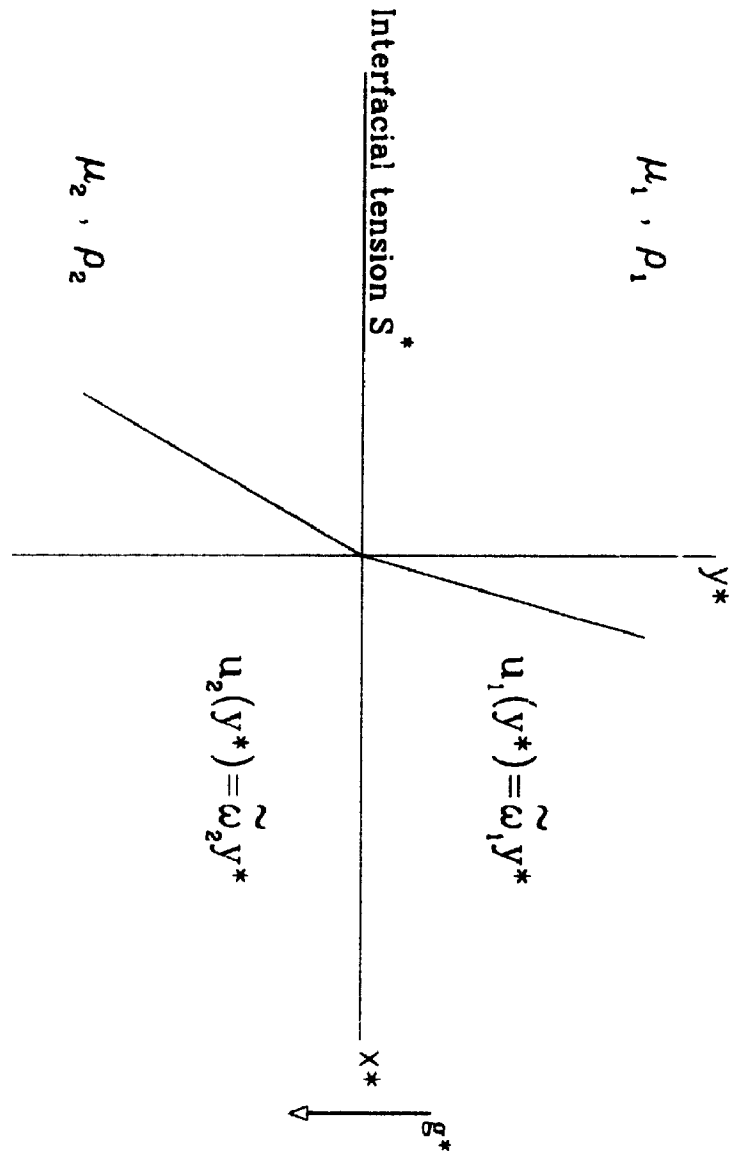


Figure 2.1: Schematic representation of the problem.

where $u^*(x^*, y^*, t^*)$ is the fluid velocity parallel to the x^* axis, $v^*(x^*, y^*, t^*)$ is the velocity parallel to the y^* axis, $p^*(x^*, y^*, t^*)$ is the pressure, and ν is the kinematic viscosity.

Following HB's methods, we begin by non-dimensionalizing the equations of motion with respect to the lower fluid using the following changes of variables:

$$\begin{aligned}(\hat{x}, \hat{y}) &= \left(\frac{\rho_2 \tilde{\omega}_2}{\mu_2} \right)^{1/2} (x^*, y^*) \\(u, v) &= \left(\frac{\rho_2}{\tilde{\omega}_2 \mu_2} \right)^{1/2} (u^*, v^*) \\p &= \frac{1}{\tilde{\omega}_2 \mu_2} p^* \\g &= \left(\frac{\rho_2}{\mu_2 \tilde{\omega}_2^3} \right)^{1/2} g^* \\t &= \tilde{\omega}_2 t^*.\end{aligned}$$

Then, the equations of motion given by 2.6 become

$$\begin{aligned}\frac{\partial u_i}{\partial t} + u_i \frac{\partial u_i}{\partial \hat{x}} + v_i \frac{\partial u_i}{\partial \hat{y}} &= -\frac{\rho_2}{\rho_i} \frac{\partial p_i}{\partial \hat{x}} + \nu \nabla^2 \hat{u}_i \\ \frac{\partial v_i}{\partial t} + u_i \frac{\partial v_i}{\partial \hat{x}} + v_i \frac{\partial v_i}{\partial \hat{y}} &= -\frac{\rho_2}{\rho_i} \frac{\partial p_i}{\partial \hat{y}} - g + \nu \nabla^2 \hat{v}_i \\ \frac{\partial u_i}{\partial \hat{x}} + \frac{\partial v_i}{\partial \hat{y}} &= 0\end{aligned}\tag{2.7}$$

where $i = 1$ for the upper fluid and $i = 2$ for the lower fluid.

We now impose small perturbations on the basic flow as follows and investigate their evolution in time :

$$\begin{aligned}u_i &= \hat{u}_i + u'(\hat{x}, \hat{y}, t) \\v_i &= \hat{v}_i + v'(\hat{x}, \hat{y}, t) \\p_i &= \hat{p}_i + p'(\hat{x}, \hat{y}, t)\end{aligned}\tag{2.8}$$

where the tilde superscript is used to indicate quantities of the basic flow, and the primed quantities denote small disturbances. In terms of the new variables, the basic state quantities are given by

$$\begin{aligned}\tilde{u}_i &= \frac{\tilde{\omega}_i}{\tilde{\omega}_2} \hat{y} \\ \tilde{v}_i &= 0 \\ \frac{\rho_2}{\rho_i} \frac{\partial \tilde{p}_i}{\partial \hat{y}} &= -g.\end{aligned}\quad (2.9)$$

Therefore, by introducing the equations 2.8 and 2.9 into equation 2.7, we obtain the following nonlinear partial differential equations for the disturbances :

$$\begin{aligned}\frac{\partial u'_i}{\partial t} + \frac{\tilde{\omega}_i}{\tilde{\omega}_2} \hat{y} \frac{\partial u'_i}{\partial \hat{x}} + \frac{\tilde{\omega}_i}{\tilde{\omega}_2} v'_i + \left\{ u'_i \frac{\partial u'_i}{\partial \hat{x}} + v'_i \frac{\partial u'_i}{\partial \hat{y}} \right\} &= -\frac{\rho_2}{\rho_i} \frac{\partial p'_i}{\partial \hat{x}} + \frac{\mu_i}{\mu_2} \frac{\rho_2}{\rho_i} \nabla^2 u'_i \\ \frac{\partial v'_i}{\partial t} + \frac{\tilde{\omega}_i}{\tilde{\omega}_2} \hat{y} \frac{\partial v'_i}{\partial \hat{x}} + \left\{ u'_i \frac{\partial v'_i}{\partial \hat{x}} + v'_i \frac{\partial v'_i}{\partial \hat{y}} \right\} &= -\frac{\rho_2}{\rho_i} \frac{\partial p'_i}{\partial \hat{y}} + \frac{\mu_i}{\mu_2} \frac{\rho_2}{\rho_i} \nabla^2 v'_i \\ \frac{\partial u'_i}{\partial \hat{x}} + \frac{\partial v'_i}{\partial \hat{y}} &= 0.\end{aligned}\quad (2.10)$$

We now linearize these equations by neglecting the products of the perturbations and their derivatives as they appear in parentheses on the left-hand sides of the first two equations. Then we obtain the following linear equations for the primed quantities:

$$\begin{aligned}\frac{\partial u'_i}{\partial t} + \frac{\tilde{\omega}_i}{\tilde{\omega}_2} \hat{y} \frac{\partial u'_i}{\partial \hat{x}} + \frac{\tilde{\omega}_i}{\tilde{\omega}_2} v'_i &= -\frac{\rho_2}{\rho_i} \frac{\partial p'_i}{\partial \hat{x}} + \frac{\mu_i}{\mu_2} \frac{\rho_2}{\rho_i} \nabla^2 u'_i \\ \frac{\partial v'_i}{\partial t} + \frac{\tilde{\omega}_i}{\tilde{\omega}_2} \hat{y} \frac{\partial v'_i}{\partial \hat{x}} &= -\frac{\rho_2}{\rho_i} \frac{\partial p'_i}{\partial \hat{y}} + \frac{\mu_i}{\mu_2} \frac{\rho_2}{\rho_i} \nabla^2 v'_i \\ \frac{\partial u'_i}{\partial \hat{x}} + \frac{\partial v'_i}{\partial \hat{y}} &= 0.\end{aligned}\quad (2.11)$$

The stream function $\psi_i(\hat{x}, \hat{y}, t)$ can now be defined such that the relations

$$\begin{aligned}u'_i &= \frac{\partial \psi_i}{\partial \hat{y}} \\ v'_i &= -\frac{\partial \psi_i}{\partial \hat{x}}\end{aligned}\quad (2.12)$$

satisfy the continuity equation given by the third equation of 2.11. Since the coefficients of equations 2.11 are only functions of \hat{y} , the equations admit sinusoidal solutions which depend on \hat{x} and t . We then consider solutions of the form

$$\begin{aligned}(\psi_i(\hat{x}, \hat{y}, t)) &= (\phi_i(\hat{y})) e^{i\alpha(\hat{x}-\hat{c}t)} \\(p'_i(\hat{x}, \hat{y}, t)) &= (p_i(\hat{y})) e^{i\alpha(\hat{x}-\hat{c}t)}\end{aligned}\quad (2.13)$$

in which we take the real parts of these expressions in order to obtain the physical quantities. Since we require the solutions to be bounded as \hat{x} go to ∞ , the wavenumber α must be real. The wave speed $\hat{c} = \hat{c}_r + i\hat{c}_i$ represents waves which travel in the direction $(\alpha, 0)$ with phase speed $\alpha\hat{c}_r$ and which grow or decay in time like $e^{(\alpha\hat{c}_i t)}$.

For convenience, we rescale the coordinates and phase speed by changing the following variables as done by HB:

$$\begin{aligned}(x, y) &= \alpha(\hat{x}, \hat{y}) \\c &= \alpha\hat{c}.\end{aligned}\quad (2.14)$$

Then, substituting equations 2.12, 2.13 and 2.14 into equation 2.11, operating with the derivatives in x and t and eliminating the exponential factors, we obtain the following equations:

$$cD\phi_i - \frac{\tilde{\omega}_i}{\tilde{\omega}_2}yD\phi_i + \frac{\tilde{\omega}_i}{\tilde{\omega}_2}\phi_i = \alpha^2\frac{\rho_2}{\rho_i}p_i + i\frac{\mu_i}{\mu_2}\frac{\rho_2}{\rho_i}\alpha^2(D^2 - 1)D\phi_i \quad (2.15)$$

$$-c\phi_i + \frac{\tilde{\omega}_i}{\tilde{\omega}_2}y\phi_i = -\alpha^2\frac{\rho_2}{\rho_i}Dp_i + \frac{\mu_i}{\mu_2}\frac{\rho_2}{\rho_i}\alpha^2(D^2 - 1)\phi_i \quad (2.16)$$

where $D = \frac{d}{dy}$, indicating the derivative with respect to y . To eliminate p_i , we differentiate equation 2.15 and add it to equation 2.16 and obtain

$$(D^2 - 1)^2\phi_i = i\frac{\mu_2}{\mu_i}\frac{\rho_i}{\rho_2}\alpha^{-2}\left(y\frac{\tilde{\omega}_i}{\tilde{\omega}_2} - c\right)(D^2 - 1)\phi_i. \quad (2.17)$$

Therefore, the coefficients of the stream functions ϕ_1 and ϕ_2 satisfy

$$(D^2 - 1)^2\phi_1 = \frac{im}{r}\alpha^{-2}(my - c)(D^2 - 1)\phi_1 \quad (2.18)$$

$$(D^2 - 1)^2 \phi_2 = i\alpha^{-2}(y - c)(D^2 - 1)\phi_2 \quad (2.19)$$

where

$$m = \frac{\mu_2}{\mu_1} = \frac{\tilde{\omega}_1}{\tilde{\omega}_2} \quad r = \frac{\rho_2}{\rho_1}.$$

These equations are the Orr-Sommerfeld equations and they correspond to equations (4a) and (4b) in HB.

If we denote the vorticities of the disturbances by

$$\omega'_i(x, y, t) = \omega_i(y)e^{i(x-ct)} \quad (2.20)$$

then

$$\omega_i(y) = -(D^2 - 1)\phi_i. \quad (2.21)$$

Therefore, in terms of the vorticity coefficients, equations 2.17, 2.18 and 2.19 become

$$(D^2 - 1)\omega_1 = \frac{im}{r}\alpha^{-2}(my - c)\omega_1 \quad (2.22)$$

$$(D^2 - 1)\omega_2 = i\alpha^{-2}(y - c)\omega_2. \quad (2.23)$$

Equations 2.21, 2.22 and 2.23, together with the appropriate boundary conditions, define the stability problem.

2.4.2 Boundary Conditions

In addition to the requirement that both ϕ_i and w_i go to zero as y goes to ∞ for $i = 1$ and as y goes to $-\infty$ for $i = 2$, we must also impose the following boundary conditions at the interface [5].

(a) Kinematic Condition.

The kinematic condition requires that the fluids move with the common interface and that neither fluid crosses this interface. Therefore, the normal velocity of both fluids must equal the velocity of the interface, whose location is described by

$$F(x, y, t) = \eta(x, t) - y = 0 \quad (2.24)$$

where the general distortion of the interface can be represented as a superposition of normal modes given by

$$\eta(x, t) = \epsilon e^{i(x-ct)}. \quad (2.25)$$

If we denote the normal unit vector to the interface by $\hat{\mathbf{n}}$ and if we denote the velocity of the interface by \mathbf{v}_n , then the kinematic condition implies that

$$\mathbf{v}_1 \cdot \hat{\mathbf{n}} = \mathbf{v}_2 \cdot \hat{\mathbf{n}} = \mathbf{v}_n \cdot \hat{\mathbf{n}} \quad (2.26)$$

at $y = \eta(x, t)$. Here

$$\mathbf{v}_1(x, y, t) = (my + u'_1(x, y, t), v'_1(x, y, t)) \quad (2.27)$$

and

$$\mathbf{v}_2(x, y, t) = (y + u'_2(x, y, t), v'_2(x, y, t)). \quad (2.28)$$

Now recall that

$$\hat{\mathbf{n}} = \frac{\nabla F}{|\nabla F|} = \frac{\left(\frac{\partial \eta}{\partial x}, -1\right)}{\sqrt{1 + \left(\frac{\partial \eta}{\partial x}\right)^2}}. \quad (2.29)$$

Since the surface moves with the fluid, we obtain

$$\frac{DF}{Dt} = \frac{\partial F}{\partial t} + \mathbf{v}_n \cdot \nabla F = 0 \quad (2.30)$$

at $y = \eta(x, t)$.

With equation 2.26 this gives

$$\frac{\partial F}{\partial t} + \mathbf{v}_i \cdot \nabla F = 0 \quad (2.31)$$

for $i = 1, 2$. Therefore, we obtain

$$-\frac{\partial \eta}{\partial t} = my \frac{\partial \eta}{\partial x} + u'_1 \frac{\partial \eta}{\partial x} - v'_1 = y \frac{\partial \eta}{\partial x} + u'_2 \frac{\partial \eta}{\partial x} - v'_2 \quad (2.32)$$

at $y = \eta(x, t)$. Then, expanding about $y = 0$ and evaluating at $y = \eta(x, t)$ we obtain

$$-\frac{\partial \eta}{\partial t} = v'_1|_{y=0} + \text{higher order terms} \quad (2.33)$$

which, after neglecting the higher order terms, gives us

$$ic\epsilon = i\phi(0) \quad (2.34)$$

so that

$$\eta(x, t) = \frac{\phi_1(0)}{c} e^{i(x-ct)}. \quad (2.35)$$

When the following boundary conditions on the velocities and on the stresses are applied, this expression is used for η .

(b) Continuity of Velocity.

The continuity of the normal velocity which follows from the kinematic condition above, when linearized requires that

$$v_1 = v_2 \quad (2.36)$$

at $y = \eta(x, t)$ and, therefore,

$$v'_1(0) + \left. \frac{\partial v'_1}{\partial y} \right|_{y=0} \eta + \dots = v'_2(0) + \left. \frac{\partial v'_2}{\partial y} \right|_{y=0} \eta + \dots \quad (2.37)$$

By neglecting the nonlinear terms we obtain

$$\phi_1(0) = \phi_2(0) = \phi(0). \quad (2.38)$$

Since there is no slip between the fluids in the direction of the flow, the tangential velocities are also continuous. This requires that

$$u_1 = u_2 \quad (2.39)$$

at $y = \eta(x, t)$. Therefore,

$$m\eta + u'_1(0) + \left. \frac{\partial u'_1}{\partial y} \right|_{y=0} \eta + \dots = \eta + u'_2(0) + \left. \frac{\partial u'_2}{\partial y} \right|_{y=0} \eta + \dots \quad (2.40)$$

which, after linearization and after cancelling the exponential factor, gives

$$D\phi_1(0) + m\epsilon - D\phi_2(0) - \epsilon = 0. \quad (2.41)$$

Then, substituting for ϵ from equation 2.34, we obtain

$$D\phi_1(0) - D\phi_2(0) = \frac{(1-m)}{c}\phi(0). \quad (2.42)$$

(c) Interfacial Stress Conditions.

At the interface of the two fluids, the shear stress must be continuous. For small disturbances this implies that

$$\frac{1}{m} \left(\frac{\partial u_1}{\partial y} + \frac{\partial v_1}{\partial x} \right) - \left(\frac{\partial u_2}{\partial y} + \frac{\partial v_2}{\partial x} \right) = 0 \quad (2.43)$$

at $y = \eta(x, t)$. Again, expanding about $y = 0$ and multiplying by m we obtain

$$\frac{\partial u_1}{\partial y} + \frac{\partial^2 u_1}{\partial y^2} \eta + \frac{\partial v_1}{\partial x} + \frac{\partial^2 v_1}{\partial x \partial y} \eta + \dots - m \left(\frac{\partial u_2}{\partial y} + \frac{\partial^2 u_1}{\partial y^2} \eta + \frac{\partial v_2}{\partial x} + \frac{\partial^2 v_2}{\partial x \partial y} \eta + \dots \right) = 0 \quad (2.44)$$

where the partial derivatives are evaluated at $y = 0$. Then, after linearizing and substituting for the velocities, the shear stress condition becomes

$$D^2 \phi_1(0) + \phi_1(0) = m(D^2 \phi_2(0) + \phi_2(0)). \quad (2.45)$$

The normal stress condition at the interface requires that for small disturbances the jump in the nondimensionalized normal stress given by

$$\left(-p_1 + \frac{\rho_1}{\rho_2} g \hat{y} + \frac{2}{m} \frac{\partial v_1}{\partial \hat{y}} \right) - \left(-p_2 + g \hat{y} + 2 \frac{\partial v_2}{\partial \hat{y}} \right) \quad (2.46)$$

is balanced by the effective nondimensionalized pressure due to surface tension which is given by

$$\frac{S^*}{\tilde{\omega}_2 \mu_2 R^*} \quad (2.47)$$

where S^* is the actual surface tension coefficient and R^* is the actual radius of curvature of the interface. We then nondimensionalize the radius of curvature and the surface tension coefficient by

$$R = \left(\frac{\rho_2 \tilde{\omega}_2}{\mu_2} \right)^{\frac{1}{2}} R^* \quad (2.48)$$

$$S = \left(\frac{\rho_2}{\dot{\omega}_2 \mu_2^3} \right)^{\frac{1}{2}} S^*. \quad (2.49)$$

The stress condition can then be rewritten as

$$-p_1 + \frac{\rho_1}{\rho_2} g \hat{y} + \frac{2}{m} \frac{\partial v_1}{\partial \hat{y}} + p_2 - g \hat{y} - 2 \frac{\partial v_2}{\partial \hat{y}} = \frac{S}{R} \quad (2.50)$$

where the nondimensionalized radius of curvature is given by

$$\frac{1}{R} = - \frac{\frac{\partial^2 \eta}{\partial \hat{x}^2}}{\left(1 + \left(\frac{\partial \eta}{\partial \hat{x}} \right)^2 \right)^{\frac{1}{2}}}. \quad (2.51)$$

Here, the negative sign is chosen so that the jump is positive when $\frac{\partial^2 \eta}{\partial \hat{x}^2}$ is negative.

After expanding equation 2.50 about $\hat{y} = 0$ and linearizing, we obtain the following equation in terms of the rescaled variables x and y :

$$(p_2(0) - p_1(0))\alpha + \left(\frac{1}{r} - 1 \right) g \eta + \frac{2}{m} \alpha \left. \frac{\partial v_1}{\partial y} \right|_{y=0} - 2\alpha \left. \frac{\partial v_2}{\partial y} \right|_{y=0} = -S\alpha^2 \frac{\partial^2 \eta}{\partial x^2}. \quad (2.52)$$

In terms of the stream function coefficients this becomes

$$(p_2(0) - p_1(0))\alpha + \left(\frac{1}{r} - 1 \right) g \frac{\phi_1(0)}{c} + 2\alpha i \left(D\phi_2(0) - \frac{D\phi_1(0)}{m} \right) = S\alpha^2 \frac{\phi(0)}{c}. \quad (2.53)$$

However, from equation 2.15 we have

$$p_2(0) - p_1(0) = \frac{1}{\alpha^2} c D \left(\phi_2 - \frac{\phi_1}{r} \right) + \frac{i}{\alpha^2} \left(\phi_2 - m \frac{\phi_1}{r} \right) - i (D^3 - D) \left(\phi_2 - \frac{\phi_1}{m} \right) \quad (2.54)$$

where the ϕ_1 , ϕ_2 and their derivatives are evaluated at $y = 0$. Therefore, substituting

equation 2.54 into equation 2.53, utilizing equation 2.42, and multiplying by $\frac{mi}{\alpha}$ we obtain

$$\begin{aligned} & i \alpha^{-2} m \left(1 - \frac{1}{r} \right) (c D \phi_2(0) + \phi(0)) \\ & - im\alpha \left(S + \alpha^{-2} \left(1 - \frac{1}{r} \right) g \right) \left(\frac{D\phi_1(0) - D\phi_2(0)}{1 - m} \right) \\ & = (D^3 - 3D) \phi_1(0) - m (D^3 - 3D) \phi_2(0). \end{aligned} \quad (2.55)$$

2.4.3 The Eigenvalue Problem

In summary, the following two fourth order linear differential equations describe the stability problem:

$$(D^2 - 1)^2 \phi_1 = \frac{im}{r} \alpha^{-2} (my - c)(D^2 - 1)\phi_1 \quad (2.56)$$

$$(D^2 - 1)^2 \phi_2 = i\alpha^{-2} (y - c)(D^2 - 1)\phi_2 \quad (2.57)$$

where ϕ_i are related to ω_i by

$$\omega_1(y) = -(D^2 - 1)\phi_1 \quad (2.58)$$

and

$$\omega_2(y) = -(D^2 - 1)\phi_2 \quad (2.59)$$

subject to the following eight requirements on ϕ_1 and ϕ_2 .

At infinity ($y = y_1 = \infty$ and $y = y_2 = -\infty$) the disturbances must vanish :

$$\phi_1(y_1) = 0 \quad (2.60)$$

$$\omega_1(y_1) = 0 \quad (2.61)$$

$$\phi_2(y_2) = 0 \quad (2.62)$$

$$\omega_2(y_2) = 0. \quad (2.63)$$

At the interface ($y = 0$) the following conditions must hold :

$$\phi_1(0) = \phi_2(0) = \phi(0) \quad (2.64)$$

$$D\phi_1(0) - D\phi_2(0) = \frac{(1 - m)}{c} \phi(0) \quad (2.65)$$

$$D^2\phi_1(0) + \phi_1(0) = m(D^2\phi_2(0) + \phi_2(0)) \quad (2.66)$$

$$\begin{aligned}
& i \alpha^{-2} m \left(1 - \frac{1}{r}\right) (cD\phi_2(0) + \phi(0)) \\
& - im\alpha \left(S + \alpha^{-2} \left(1 - \frac{1}{r}\right) g\right) \left(\frac{D\phi_1(0) - D\phi_2(0)}{1 - m}\right) \\
& = (D^3 - 3D) \phi_1(0) - m (D^3 - 3D) \phi_2(0).
\end{aligned} \tag{2.67}$$

2.5 The Dispersion Relation

It is well known that, for problems of the type considered in this chapter, the Orr-Sommerfeld equations can be solved exactly in terms of the Airy functions [16]. In order to solve the eigenvalue problem given in the last section we make the following changes of variables:

$$\begin{aligned}
z_1 &= m^{2/3} r^{-1/3} \alpha^{-2/3} e^{-i\pi/2} \left(y - \frac{c}{m} - i\alpha^2 r m^{-2}\right) \\
z_2 &= \alpha^{-2/3} e^{-i\pi/2} (y - c - i\alpha^2) \\
\omega_i(y) &= \xi_i(z_i).
\end{aligned} \tag{2.68}$$

Then the vorticity equations become

$$\frac{d^2 \xi_1}{dz_1^2} - z_1 \xi_1 = 0 \tag{2.69}$$

$$\frac{d^2 \xi_2}{dz_2^2} - z_2 \xi_2 = 0. \tag{2.70}$$

These equations are in the form of the Airy equation and therefore their solutions are given by

$$\xi_1 = a_1 Ai(z_1) + b_1 Ai(z_1 e^{\theta_1}) \tag{2.71}$$

$$\xi_2 = a_2 Ai(z_2) + b_2 Ai(z_2 e^{\theta_2}) \tag{2.72}$$

where Ai denotes the Airy function and $\theta_i = 2\pi/3$ or $-2\pi/3$ [1]. Then, the boundary conditions 2.61 and 2.63 imply that the vorticities ω_i must tend to zero as $y \rightarrow \infty$ or $y \rightarrow -\infty$, so that $a_1 = a_2 = 0$, $\theta_1 = 2\pi/3$ and $\theta_2 = -2\pi/3$. Therefore,

$$\omega_1(y) = b_1 A_1(y) \tag{2.73}$$

$$\omega_2(y) = b_2 A_2(y) \quad (2.74)$$

where

$$A_1(y) = Ai\left(z_1 e^{\frac{2y}{3}}\right) = Ai\left(m^{2/3} r^{-1/3} \alpha^{-2/3} \left(y - \frac{c}{m} - i\alpha^2 r m^{-2}\right) e^{i\pi/6}\right) \quad (2.75)$$

$$A_2(y) = Ai\left(z_2 e^{-\frac{2y}{3}}\right) = Ai\left(\alpha^{-2/3} (y - c - i\alpha^2) e^{5i\pi/6}\right).$$

Consequently, we obtain the following equations for ϕ_1 and ϕ_2 :

$$(D^2 - 1)\phi_1 = b_1 A_1(y) \quad (2.76)$$

$$(D^2 - 1)\phi_2 = b_2 A_2(y). \quad (2.77)$$

After solving these second order linear differential equations with the boundary conditions at infinity given by equations 2.60 and 2.62, we obtain the following expressions for the stream functions:

$$\phi_1 = c_1 e^{-y} + b_1 \left(e^{-y} \int_0^y e^s A_1(s) ds + e^y \int_y^\infty e^{-s} A_1(s) ds \right) \quad (2.78)$$

$$\phi_2 = c_2 e^y + b_2 \left(e^y \int_0^y e^{-s} A_2(s) ds + e^{-y} \int_y^{-\infty} e^s A_2(s) ds \right) \quad (2.79)$$

where c_1 and c_2 are constants.

Finally, applying the remaining four boundary conditions given by the equations 2.64 through 2.67, we obtain four linear equations for the four unknown constants c_1 , b_1 , c_2 and b_2 . The linear homogenous system of equations can then be written as

$$\mathbf{A} \mathbf{h} = 0 \quad (2.80)$$

where $\mathbf{h}^T = (c_1, c_2, b_1, b_2)$ and where the matrix \mathbf{A} is given by

$$\mathbf{A} = \begin{pmatrix} 1 & -1 & J_1 & J_2 \\ -1 + m/c & -1 - 1/c & (1 + m/c)J_1 & (-1 + 1/c)J_2 \\ 2 & -2m & 2J_1 - 2A_1 & -m(-2J_2 + 2A_2) \\ \phi_{4,1} & \phi_{4,2} & \phi_{4,3} & \phi_{4,4} \end{pmatrix}. \quad (2.81)$$

Here

$$\begin{aligned} \phi_{4,1} &= 2 - \frac{i\alpha m}{1-m} \left(S + \alpha^{-2} \left(1 - \frac{1}{r}\right) g \right) \\ \phi_{4,2} &= 2m - \frac{i\alpha m}{1-m} \left(S + \alpha^{-2} \left(1 - \frac{1}{r}\right) g \right) - i m \alpha^{-2} \left(1 - \frac{1}{r}\right) (1-c) J_2 \\ \phi_{4,3} &= -2(J_1 + A'_1) + \frac{i\alpha m J_1}{1-m} \left(S + \alpha^{-2} \left(1 - \frac{1}{r}\right) g \right) \\ \phi_{4,4} &= 2m(J_2 - A'_2) - \frac{i\alpha m J_2}{1-m} \left(S + \alpha^{-2} \left(1 - \frac{1}{r}\right) g \right) - i m \alpha^{-2} \left(1 - \frac{1}{r}\right) (1+c) \end{aligned} \quad (2.82)$$

and

$$\begin{aligned} J_1 &= \int_0^\infty e^{-s} A_1(s) ds \\ J_2 &= \int_0^\infty e^{-s} A_2(-s) ds \\ A_1 &= A_1(0) \\ A_2 &= A_2(0) \\ A'_1 &= \left. \frac{dA_1(y)}{dy} \right|_{y=0} \\ A'_2 &= \left. \frac{dA_2(y)}{dy} \right|_{y=0}. \end{aligned} \quad (2.83)$$

For a non-trivial solution of 2.80, we require the determinant of \mathbf{A} to vanish. This gives the following dispersion relation for the nondimensional quantities α, c, m, r, g and S

$$F(\alpha, c, m, r, g, S) = 0 \quad (2.84)$$

where

$$F = F_1 + \frac{F_2}{c} \quad (2.85)$$

and

$$\begin{aligned}
 F_1 &= 2m(1-m)J_1(A_2 + A'_2) + 2m(A'_1A_2 - A'_2A_1) + 2(1-m)(A'_1 - A_1)J_2 \\
 &+ 4(1-m)^2J_1J_2 + \frac{im(1-\frac{1}{r})}{\alpha^2}((2(1-m)J_1J_2 + m(c+1)A_2J_1 + (c-m)A_1J_2)) \\
 F_2 &= 2(1-m)m(J_1A_2 + A_1J_2) - iam(S + \alpha^{-2}(1-\frac{1}{r})g)(J_2A_1 + mJ_1A_2) \\
 &+ m(1-m)A'_1A_2 - m(1-m)A'_2A_1.
 \end{aligned}$$

This reduces to HB's dispersion relation given by equation (25) when $r = 1$.

To analyze the stability of this problem we investigate the dependence of the eigenvalues c on the other stability parameters such as m , r and S . In the following sections, we examine the solutions of this dispersion relation and investigate the stability of the flow.

2.5.1 The Stability of the $m > 1$ Case

The dispersion relation does not have to be studied for all values of m . It is sufficient to consider only the $m \leq 1$ case, because the solution for $m > 1$ can be found from the solution for $m < 1$. If $\phi_1(y, \alpha, m, r, S, g, c)$, $\phi_2(y, \alpha, m, r, S, g, c)$ and $c(\alpha, m, r, S, g)$ are the solutions of the above eigenvalue problem given in section 2.4.3, then we can show that the functions

$$\phi_2^*\left(-y, \frac{\alpha r^{\frac{1}{2}}}{m}, \frac{1}{m}, \frac{1}{r}, \frac{Sm}{r^{\frac{1}{2}}}, -\frac{g}{r^{\frac{1}{2}}m}, -\frac{c^*}{m}\right)$$

$$\phi_1^*\left(-y, \frac{\alpha r^{\frac{1}{2}}}{m}, \frac{1}{m}, \frac{1}{r}, \frac{Sm}{r^{\frac{1}{2}}}, -\frac{g}{r^{\frac{1}{2}}m}, -\frac{c^*}{m}\right)$$

and the eigenvalue

$$\frac{c^*\left(\frac{\alpha r^{\frac{1}{2}}}{m}, \frac{1}{m}, \frac{1}{r}, \frac{Sm}{r^{\frac{1}{2}}}, -\frac{g}{r^{\frac{1}{2}}m}\right)}{m}$$

are also solutions of the above eigenvalue problem.

This can also be directly observed from the dispersion relation as there exists the

relation

$$\Gamma(y, \alpha, m, r, S, g, c) \Big|_{y=0} = \Gamma^* \left(-y, \frac{\alpha r^{\frac{1}{2}}}{m}, \frac{1}{m}, \frac{1}{r}, \frac{Sm}{r^{\frac{1}{2}}}, -\frac{g}{r^{\frac{1}{2}}m}, -\frac{c^*}{m} \right) \Big|_{y=0}$$

where $*$ denotes the complex conjugate and Γ is related to the dispersion relation function F by

$$\Gamma(y, \alpha, m, r, S, g, c) \Big|_{y=0} = F(\alpha, m, r, S, g, c).$$

Note that, in order to take advantage of this relation, one must consider negative values of g . In other words, one must consider problems in which gravity acts in the positive y direction. However, we observe that, in the absence of gravity, the stability of the flow is independent of the actual positioning of the more viscous fluid. Only the direction of the propagation velocity is reversed when the positions of fluid 1 and fluid 2 are interchanged.

2.6 Asymptotic Analysis

The dispersion relation found in the previous section is a highly complicated expression. The eigenvalues c appear explicitly in the dispersion relation and implicitly in the argument of the Airy functions and their integrals which are part of the dispersion relation. Therefore, in general, it is not possible to solve this relation analytically. In this section we find various approximations to the dispersion relation and therefore to the eigenvalues c by considering limiting cases of the stability parameters and of the wavenumber α .

2.6.1 Short Wavelength Approximations

In this approximation we examine the behaviour of the eigenvalues c as the wavenumber α approaches ∞ . Since α appears in the arguments of $A_1, A_2, A'_1, A'_2, J_1$ and J_2 , we must find asymptotic approximations for these functions as α goes to ∞ . Let us

first approximate J_1 , which is given by

$$J_1 = \int_0^{\infty} e^{-s} A_1(s) ds. \quad (2.86)$$

This can be rewritten as

$$J_1 = e^{\left(\frac{c}{m} + \frac{i\alpha^2}{m^2} - \frac{i\pi}{6}\right)} \int_{l_1}^{u_1} e^{-\alpha^2 w e^{-\frac{i\pi}{6}}} \text{Ai}\left(m^{\frac{2}{3}} r^{-\frac{1}{3}} \alpha^{\frac{1}{3}} w\right) dw \quad (2.87)$$

where

$$l_1 = \alpha^{-2} e^{-\frac{3i\pi}{6}} \left(\frac{c}{m} + \frac{i\alpha^2 r}{m^2}\right) = e^{-\frac{i\pi}{3}} \frac{r}{m^2} \left(1 - \frac{icm}{r\alpha^2}\right)$$

$$w = \alpha^{-2} e^{\frac{i\pi}{6}} \left(y - \frac{c}{m} - \frac{i\alpha^2}{m^2}\right) = \alpha^{-2} e^{\frac{i\pi}{6}} y + l_1$$

and $u_1 = \infty e^{\frac{i\pi}{6}}$. Therefore, if $\alpha^{\frac{1}{3}} w$ is large and $|\arg(w)| < \pi$ for all values of w in the range of the integral, then we can approximate the Airy function in the integrand using the following asymptotic expressions for the Airy functions with large arguments (see Appendix A):

$$\text{Ai}\left(m^{\frac{2}{3}} r^{-\frac{1}{3}} \alpha^{\frac{1}{3}} w\right) = \frac{1}{2} \pi^{-\frac{1}{2}} k_1 w^{-\frac{1}{4}} \left(1 - k_2 w^{-\frac{3}{2}} + k_3 w^{-3}\right) e^{-\frac{2}{3} \alpha^2 r^{-\frac{1}{3}} m w^{\frac{3}{2}}} \quad (2.88)$$

where

$$k_1 = r^{\frac{1}{2}} m^{-\frac{1}{6}} \alpha^{-\frac{1}{3}}$$

$$k_2 = \frac{5}{48} r^{\frac{1}{2}} m^{-1} \alpha^{-2}$$

$$k_3 = \frac{385}{4608} r m^{-2} \alpha^{-4}.$$

Then, J_1 can be written as

$$J_1 = \frac{1}{2} \pi^{-\frac{1}{2}} \alpha^2 e^{-\left(\frac{c}{m} + \frac{i\alpha^2 r}{m^2}\right)} \int_{l_1}^{u_1} e^{-\alpha^2 \left(w e^{-\frac{i\pi}{6}} + \frac{2}{3} r^{-\frac{1}{3}} m w^{\frac{3}{2}}\right)} k_1 w^{-\frac{1}{4}} \left(1 - k_2 w^{-\frac{3}{2}} + k_3 w^{-3}\right) dw. \quad (2.89)$$

This integral is of the form

$$J_1 = \frac{1}{2} \pi^{-\frac{1}{2}} \alpha^2 e^{\left(\frac{c}{m} + \frac{i\alpha^2 r}{m^2} - \frac{i\pi}{6}\right)} \int_{l_1}^{u_1} q(w) e^{-\lambda p(w)} dw \quad (2.90)$$

where

$$q(w) = k_1 w^{-\frac{1}{2}} \left(1 - k_2 w^{-\frac{1}{2}} + k_3 w^{-3} \right) \quad (2.91)$$

$$p(w) = w e^{-\frac{w}{r}} + \frac{2}{3} r^{-\frac{1}{2}} m w^{\frac{3}{2}} \quad (2.92)$$

and $\lambda = \alpha^2$.

The function $p(w)$ attains its minimum value when

$$\frac{dp}{dw} = e^{-\frac{w}{r}} + r^{-\frac{1}{2}} m w^{\frac{1}{2}} = 0. \quad (2.93)$$

Therefore, the stationary points of $p(w)$ occur at $w_0 = r m^{-2} e^{\frac{4w}{3}}$. However, the asymptotic expression of the Airy function is valid only when $|\arg(w)| < \pi$ in the domain of the integration contour. Consequently, $p(w)$ has no stationary points.

Moreover

$$\operatorname{Re} \left(\frac{dp}{dw} \right) = \frac{\sqrt{3}}{2} + r^{-\frac{1}{2}} m |w^{\frac{1}{2}}| \cos \theta \quad (2.94)$$

where $\theta = \arg(w^{\frac{1}{2}})$. Since $-\frac{\pi}{2} < \theta < \frac{\pi}{2}$, $\operatorname{Re} \left(\frac{dp}{dw} \right) > 0$. Therefore, the contour of integration is a path of descent and, by Watson's lemma, the asymptotic expansion of the integral can be evaluated by considering the contributions from the lower end point of the integrand only.

To apply Watson's lemma, we expand the functions $p(w)$ and $q(w)$ about l_1 :

$$p(w) = p(l_1) + \sum_{s=0}^{\infty} p_s (w - l_1)^{s+1}$$

$$q(w) = q_0 + \sum_{s=1}^{\infty} q_s (w - l_1)^s.$$

Then, the asymptotic approximation of the integral is given by [57]

$$\int_{l_1}^{u_1} q(w) e^{-\lambda p(w)} dw = e^{-\lambda p(l_1)} \left(\frac{d_0}{\lambda} + \frac{d_1}{\lambda^2} + \frac{d_2}{\lambda^3} + o(\lambda^{-3}) \right) \quad (2.95)$$

where

$$\begin{aligned} d_0 &= \frac{q_0}{p_0} \\ d_1 &= \left(q_1 - \frac{2p_1 q_0}{p_0} \right) \frac{1}{p_0^2} \\ d_2 &= \left(q_2 - \frac{3p_1 q_1}{p_0} + (4p_1^2 - 2p_0 p_2) \frac{3q_0}{2p_0^2} \right) \frac{1}{p_0^3}. \end{aligned}$$

Therefore,

$$\begin{aligned} d_0 &= \frac{e^{\frac{ix}{6}} k_1 l_1^{-\frac{1}{4}} \left(1 - k_2 l_1^{-\frac{3}{2}} + k_3 l_1^{-3} \right)}{\left(1 + \left(1 - \frac{icm}{r\alpha^2} \right)^{\frac{1}{2}} \right)} \\ d_1 &= \frac{-im^2 d_0}{4 \left(1 + \left(1 - \frac{icm}{r\alpha^2} \right)^{\frac{1}{2}} \right)} \left(\frac{1}{\left(1 - \frac{icm}{r\alpha^2} \right)^{\frac{1}{2}}} + \frac{2}{\left(1 - \frac{icm}{r\alpha^2} \right)^{\frac{1}{2}} + \left(1 - \frac{icm}{r\alpha^2} \right)} \right) + d_{11} \end{aligned}$$

where

$$d_{11} = \frac{3k_1 k_2 l_1^{-\frac{11}{4}} e^{\frac{ix}{3}}}{\left(1 + \left(1 - \frac{icm}{r\alpha^2} \right)^{\frac{1}{2}} \right)^2}. \quad (2.96)$$

Now recall that

$$A_1 = A_1(0) = \frac{1}{2} \pi^{-\frac{1}{2}} k_1 l_1^{-\frac{1}{4}} \left(1 - k_2 l_1^{-\frac{3}{2}} + k_3 l_1^{-3} \right) e^{-\frac{2}{3} \alpha^2 r - \frac{1}{2} m l_1^{\frac{3}{2}}} \quad (2.97)$$

so that the leading terms of $\frac{J_1}{A_1}$ are given by

$$\begin{aligned} \frac{J_1}{A_1} &= \frac{1}{1 + \left(1 - \frac{icm}{r\alpha^2} \right)^{\frac{1}{2}}} - \frac{\frac{im^2}{4\alpha^2 r}}{\left(1 + \left(1 - \frac{icm}{r\alpha^2} \right)^{\frac{1}{2}} \right)^2 \left(1 - \frac{icm}{r\alpha^2} \right)^{\frac{1}{2}}} \\ &\quad - \frac{\frac{im^2}{2\alpha^2 r}}{\left(1 + \left(1 - \frac{icm}{r\alpha^2} \right)^{\frac{1}{2}} \right)^2 \left(\left(1 - \frac{icm}{r\alpha^2} \right)^{\frac{1}{2}} + \left(1 - \frac{icm}{r\alpha^2} \right) \right)} \\ &\quad + \frac{\frac{d_2}{\alpha^4}}{k_1 l_1^{-\frac{1}{4}} \left(1 - k_2 l_1^{-\frac{3}{2}} + k_3 l_1^{-3} \right)} + o(\alpha^{-4}). \end{aligned}$$

This approximation is valid when $|\arg(l_1)| < \pi$ or $-\frac{2\pi}{3} < \arg\left(1 - \frac{icm}{r\alpha^2}\right) < \frac{4\pi}{3}$.

Similar calculations result in the following approximation for the leading terms of $\frac{J_2}{A_2}$

$$\begin{aligned} \frac{J_2}{A_2} = & \frac{1}{1 + \left(1 - \frac{ic}{\alpha^2}\right)^{\frac{1}{2}}} + \frac{\frac{i}{4\alpha^2}}{\left(1 + \left(1 - \frac{ic}{\alpha^2}\right)^{\frac{1}{2}}\right)^2 \left(1 - \frac{ic}{\alpha^2}\right)^{\frac{1}{2}}} \\ & + \frac{\frac{i}{2\alpha^2}}{\left(1 + \left(1 - \frac{ic}{\alpha^2}\right)^{\frac{1}{2}}\right)^2 \left(\left(1 - \frac{ic}{\alpha^2}\right)^{\frac{1}{2}} + \left(1 - \frac{ic}{\alpha^2}\right)\right)} \\ & + \frac{\frac{d_2}{\alpha^4}}{k_1 l_2^{-\frac{1}{4}} \left(1 - k_2 l_2^{-\frac{3}{2}} + k_3 l_2^{-3}\right)} + o(\alpha^{-4}). \end{aligned}$$

This is valid when $-\frac{4\pi}{3} < \arg\left(1 - \frac{ic}{\alpha^2}\right) < \frac{2\pi}{3}$.

To find the leading terms of A'_1 and A'_2 for large α , we use equation A.3 and A.4 in appendix A which for large Z is given by

$$\frac{Ai'(Z)}{Ai(Z)} = -\left(Z^{\frac{1}{2}} + \frac{1}{4Z} - \frac{5}{32Z^{5/2}} + \frac{15}{64Z^4}\right). \quad (2.98)$$

Therefore, using $Z(y) = \alpha^{-\frac{2}{3}} r^{-\frac{1}{3}} m^{\frac{2}{3}} e^{\frac{iy}{\alpha}} \left(y - \frac{c}{m} - \frac{i\alpha^2 r}{m^2}\right)$, we obtain

$$\frac{A'_1}{A_1} = -\alpha^{-\frac{2}{3}} r^{-\frac{1}{3}} m^{\frac{2}{3}} e^{\frac{iy}{\alpha}} \left(Z(0)^{\frac{1}{2}} - \frac{1}{4Z(0)}\right).$$

Then, the leading term approximation of $\frac{A'_1}{A_1}$ becomes

$$\frac{A'_1}{A_1} = -\left(1 - \frac{icm}{r\alpha^2}\right)^{\frac{1}{2}} - \frac{\frac{im^2}{4\alpha^2 r}}{\left(1 - \frac{icm}{r\alpha^2}\right)} - \frac{\frac{5m^4}{32\alpha^4 r^2}}{\left(1 - \frac{icm}{r\alpha^2}\right)^{\frac{1}{2}}} + \frac{\frac{15im^6}{64\alpha^6 r^3}}{\left(1 - \frac{icm}{r\alpha^2}\right)^4}. \quad (2.99)$$

This expression is valid when $-\frac{2\pi}{3} < \arg\left(1 - \frac{icm}{r\alpha^2}\right) < \frac{4\pi}{3}$. This same condition was

required for the $\frac{J_1}{A_1}$ approximation. Similar computation gives

$$\frac{A'_2}{A_2} = - \left(1 - \frac{ic}{\alpha^2}\right)^{\frac{1}{2}} - \frac{\frac{i}{4\alpha^2}}{\left(1 - \frac{ic}{\alpha^2}\right)} - \frac{\frac{5}{32\alpha^4}}{\left(1 - \frac{ic}{\alpha^2}\right)^{\frac{3}{2}}} + \frac{\frac{15i}{64\alpha^6}}{\left(1 - \frac{ic}{\alpha^2}\right)^4} \quad (2.100)$$

which is valid when $\frac{-4\pi}{3} < \arg\left(1 - \frac{ic}{\alpha^2}\right) < \frac{2\pi}{3}$. This was the same condition that was required for the $\frac{J_2}{A_2}$ approximation.

To obtain an asymptotic expression for c as $\alpha \rightarrow \infty$, we assume that

$$c = c_0\alpha + c_1 + c_2\alpha^{-1} + c_3\alpha^{-2} + c_4\alpha^{-3} + c_5\alpha^{-4} + o(\alpha^{-4}). \quad (2.101)$$

This is a different assumption from that of HB, who assumed that $c = \hat{c}_0 + \hat{c}_1\alpha^{-2} + \hat{c}_2\alpha^{-4}$. The expression for \hat{c}_1 found by HB contained a term $S\alpha^3$, which, because of the scaling assumed for S , did not violate their assumptions. Their result, however, naturally led to the new ansatz given by equation 2.101, in order to free S of the restrictions placed on it. Substituting equation 2.101 into the above approximations for the Airy functions and their integrals we obtain

$$\begin{aligned} \frac{A'_1}{A_1} &= -1 + \frac{imc_0}{2r}\alpha^{-1} + \frac{m}{8r^2} (4rc_1i - mc_0^2 - 2mri) \alpha^{-2} \\ &\quad - \frac{m}{16r^3} (4mrc_0c_1 - 4m^2rc_0 + m^2c_0^3i - 8c_2r^2i) \alpha^{-3} \\ &\quad - \frac{m}{128r^4} \left(-5m^3c_0^4 - 32m^2r^2c_1 + 16mc_1^2r^2 + 32mc_0c_2r^2 + 20r^2m^3 \right. \\ &\quad \left. - 32m^3rc_0^2i - 64ir^3c_3 + 24m^2rc_1c_0^2 \right) \alpha^{-4}, \\ \frac{A'_2}{A_2} &= 1 - \frac{1}{2}ic_0\alpha^{-1} - \left(\frac{1}{2}c_1i - \frac{1}{8}c_0^2 + \frac{1}{4}i\right) \alpha^{-2} + \left(\frac{1}{4}c_0c_1 + \frac{1}{4}c_0 + \frac{1}{16}c_0^3i - \frac{1}{2}c_2i\right) \alpha^{-3} \\ &\quad + \frac{1}{128} \left(-5c_0^4 + 32c_1 + 16c_1^2 + 32c_0c_2 + 20 + 32c_0^2i - 64ic_3 + 24c_1c_0^2 \right) \alpha^{-4} \end{aligned}$$

and

$$\begin{aligned} \frac{J_1}{A_1} &= \frac{1}{2} + \frac{imc_0}{8r}\alpha^{-1} + \frac{m}{16r^2} (2rc_1i - mc_0^2 - 2mri) \alpha^{-2} \\ &\quad - \frac{m}{128r^3} (16mrc_0c_1 - 18m^2rc_0 - 16c_2r^2i + 5m^2c_0^3i) \alpha^{-3} \end{aligned}$$

$$\begin{aligned}
& - \frac{m}{256r^4} \left(30m^2irc_1c_0^2 - 32ir^3c_3 - 36m^3rc_0^2i + 32mc_0c_2r^2 + 16mc_1^2r^2 \right. \\
& \left. - 7m^3c_0^4 + 36m^3r^6 - 36m^2r^2c_1 \right) \alpha^{-4} \\
\frac{J_2}{A_2} &= \frac{1}{2} + \frac{1}{8}ic_0\alpha^{-1} + \left(\frac{1}{8}c_1i - \frac{1}{16}c_0^2 + \frac{1}{8}i \right) \alpha^{-2} + \frac{1}{128} (16c_0c_1 - 18c_0 - 16c_2i - 5c_0^3i) \alpha^{-3} \\
& - \frac{1}{256} \left[30ic_1c_0^2 - 32ic_3 + 36c_0^2i + 32c_0c_2 + 16c_1^2 \right. \\
& \left. - 7c_0^4 + 36 + 36c_1 \right] \alpha^{-4}.
\end{aligned}$$

After dividing the dispersion relation by A_1A_2 and substituting these expressions, we obtain the following approximation for the coefficients c_i :

$$\begin{aligned}
c_0 &= -\frac{imS}{2(1+m)} & (2.102) \\
c_1 &= -\left(3 + \frac{3}{r}\right) im^3S^2/16(1+m)^{-3} \\
c_2 &= -g\frac{im}{2(1+m)} + \frac{(-5m^2 - 3m + 3rm + 5r)m^2S}{8r(1+m)^3} \\
& - \frac{m^4i(r^2 + 20mr^2 + 20m + m^2 + 34rm)S^3}{128(1+m)^5r^2} \\
c_3 &= \frac{im(1-m)(r-m^2)}{2r(1+m)^2} + \frac{3igm^3(r^2-1)}{8r^2(1+m)^3} \\
& - \frac{m^5i(2m^4 + (13r+21)m^3 + 2(1+r)(85r^2 + 116r + 85)m^2)S^4}{1024(1+m)^7r^3} \\
& - \frac{m^5i(+r^2(13+21r)m + 2r^3)S^4}{1024(1+m)^7r^3} - \frac{(9m^4 + 112m^3 + 82m^3r)m^3S^2}{128r^2(1+m)^5} \\
& + \frac{(63m^2r^2 - 63m^2 + 112mr^2 + 82rm + 9r^2)m^3S^2}{128r^2(1+m)^5} \\
c_4 &= \frac{(r-1)(-5m^2 - 3m + 3rm + 5r)gm^2}{8r^2(1+m)^3} + Sc_{4s} \\
c_5 &= \frac{((1+9r^4)m^6 + (26+18r^4)m^5 + (9r^4 - 8r + 17)m^4)(m-1)}{32r^2(1+m)^4m} \\
& - \frac{(2r(13r-4)m^2 - 32m^3r + 44mr^2 + 10r^2)(m-1)}{32r^2(1+m)^4m} \\
& - \frac{(3r+3)(r-1)^2m^3ig^2}{16(1+m)^3r^3} + Sc_{5s}.
\end{aligned}$$

Expressions for c_{4s} and c_{5s} are obtained using the computer algebra system Maple [11]

and are presented in Appendix B. Equation 2.101 is the asymptotic representation for the growth rate for short wavelength instabilities. We note that c_3 was given by HB for the case where $r = 1$ and it agrees with our results when $S = 0$. If we let $S = 0$ and $r = 1$ in c_1 and c_4 , both coefficients become zero as was assumed by HB. When $S = 0$, our c_2 also reduces to the corresponding HB coefficient. Finally, c_3 reduces to the corresponding HB coefficient when $r = 1$ and $S = 0$. The main difference between our results and those of HB is the presence of the terms in S which they could not obtain because of their assumed scaling. Their approximation was obtained using a regular perturbation analysis of the fourth order differential equations in ϕ_1 and in ϕ_2 . In their analysis, it was necessary to make the assumption that $S = o(\alpha^{-3})$. This restriction on the values of S essentially led to a zero surface tension limit. In the method we employ of analyzing the asymptotic behaviour of the dispersion relation, HB's restriction is not required. The numerical computations we carry out both for the large and small values of the surface tension support our conclusion that equation 2.101 holds for any value of S .

As expected, in this short wavelength range, surface tension is a very important parameter. Equation 2.101 shows that surface tension always has a stabilizing effect. For the case $\rho_1 = \rho_2$, if there is no surface tension, the flow will always be unstable with respect to short wavelength instabilities caused by the jump in viscosity. In the absence of gravity, if $r < m^2$ then the viscosity jump stabilizes the short wavelength instability caused by the density jump. In other words, if the density of the bottom fluid is small enough, then the viscosity jump has a stabilizing effect. On the other hand, if the bottom fluid is dense enough or if $r > m^2$, then the viscosity jump causes instability. As expected, gravity is a stabilizing factor when $r > 1$ and it is a destabilizing factor when $r < 1$. When $r = 1$, gravity has no effect on stability.

2.6.2 Long Wavelength Approximations

The long wavelength approximations occur in the limit as α goes to zero. In this limit, the arguments of the functions A_1 and A_2 become very large. Therefore, we can use methods similar to the one used for the short wavelength approximations in order to obtain the following asymptotic expressions for the integrals and derivatives of these functions:

$$\begin{aligned} \frac{A'_1}{A_1} &= -\frac{\sqrt{m}ce^{-\frac{m}{4}\alpha}}{\sqrt{r}\alpha} + \frac{m}{4c} + \frac{\sqrt{r}(5m^2 - 16c^2)e^{-\frac{m}{4}\alpha}}{32\sqrt{m}c^{5/2}} \\ &\quad - \frac{r(16c^2 + 15m^2)i\alpha^2}{64c^4} + O(\alpha^3) \\ \frac{A'_2}{A_2} &= -\frac{\sqrt{c}e^{-\frac{m}{4}\alpha}}{\alpha} + \frac{1}{4c} + \frac{(16c^2 - 5)e^{-\frac{m}{4}\alpha}}{32c^{5/2}} - \frac{i(16c^2 - 15)\alpha^2}{64c^4} + O(\alpha^3) \\ \frac{J_1}{A_1} &= \frac{\sqrt{r}e^{-\frac{m}{4}\alpha}}{\sqrt{m}\sqrt{c}} + \frac{r(3m - 4c)i\alpha^2}{4mc^2} + O(\alpha^3) \\ \frac{J_2}{A_2} &= \frac{e^{-\frac{m}{4}\alpha}}{\sqrt{c}} - \frac{(4c + 3)i\alpha^2}{4c^2} + O(\alpha^3). \end{aligned} \tag{2.103}$$

Then we divide the dispersion relation by A_1A_2 and we use the above asymptotic expression to eliminate all the Airy functions present in the relation. Then, the following asymptotic expression is obtained:

$$c = \tilde{c}_0 + \tilde{c}_1\alpha + \tilde{c}_2\alpha^2 + o(\alpha^2) \tag{2.104}$$

where

$$c_0 = \frac{m - r}{1 + r}$$

$$c_1 = \frac{r(m+1)^2(r-1)^2(1-i)\sqrt{2}}{2(1+r)^{3/2}(r-m)^{3/2}(\sqrt{r}\sqrt{m}+1)} - \frac{g(r-1)}{r-m}$$

$$c_2 = \frac{c_{2n}}{c_{2d}}$$

and

$$\begin{aligned} c_{2n} = & (64rm(1+i)(r-1)c_0^7 - 16\sqrt{2}i\left((8r-5\sqrt{mr}^{3/2}+m-7rm \right. \\ & + 8r^{3/2}m^{3/2}-r^{5/2}\sqrt{m})c_0^6 - 16m(1+i)(r-1)(3rm-2rc_1 \\ & - 4r+2c_1)c_0^5 - 4\sqrt{2}\sqrt{m}\left(28mr^{3/2}i-4r^{5/2}i+3mr^{3/2}c_1^2 \right. \\ & - 4im^{3/2}+3rc_1^2\sqrt{m}+16\sqrt{m}i+3m\sqrt{r}c_1^2+32irm^{3/2}-24r^{3/2}i \\ & + 3c_1^2\sqrt{m}-44ir\sqrt{m})c_0^4 - 16m(1+i)(r-1)(3rm+2rg+2g)c_0^3 \\ & - \sqrt{2}m\left(5m^{3/2}r^{5/2}i+4c_1^2m-69ir+64irm-64mi+4m^{3/2}\sqrt{r}c_1^2 \right. \\ & + 59i-15m^{3/2}r^{3/2}i-4\sqrt{mr}^{3/2}c_1^2-4rc_1^2+16rgc_1+16\sqrt{mr}^{3/2}gc_1 \\ & - 16gc_1-16\sqrt{m}\sqrt{r}gc_1)c_0^2 + 8m(1+i)\left(rm^2c_1+3r^2mg+3r^2mc_1 \right. \\ & + 3mc_1-8mrc_1-3rmg-3rg+rc_1+3g)c_0 \\ & \left. - \sqrt{2}im\left(5r^{5/2}m^{3/2}-10r^{3/2}m^{3/2}-5r-59m+5m^{5/2}r^{3/2}+64rm\right)\sqrt{2} \right. \\ c_{2d} = & 32c_0^4m\left(3(r+1)\left(1+\sqrt{r}\sqrt{m}\right)c_0^2 - (m-r)\left(1+\sqrt{r}\sqrt{m}\right)\right). \end{aligned}$$

For $r = 1$, this reduces to

$$c = -\frac{1-m}{2} - \frac{2i(1+m)\alpha^2}{m} \quad (2.105)$$

which is the same equation as equation (26) in HB. Therefore, with respect to long wavelength disturbances, the flow is always stable when the densities of the two fluids are equal. As pointed out by HB, this result is not uniformly valid as $m \rightarrow 0$.

2.6.3 Asymptotic Behaviour of c as $m \rightarrow 0$

The limit of $m \rightarrow 0$ can occur either when, for fixed μ_2 , μ_1 tends to ∞ or when, for fixed μ_1 , μ_2 tends to zero. The former case represents the configuration of a viscous

fluid in the lower half plane bounded by a solid boundary at $y = 0$. The latter case represents a configuration of a viscous fluid with a zero-velocity profile on top and an inviscid fluid with a linear velocity profile on the bottom.

Analyses similar to section 2.6.1 show that as $m \rightarrow 0$

$$\frac{J_1}{A_1} = \frac{1}{2} + \frac{icm}{8\alpha^2 r} + o(m)$$

$$\frac{A'_1}{A_1} = -1 + \frac{icm}{2\alpha^2 r} + o(m)$$

and the dispersion relation reduces to

$$J_2 \left(-1 + \frac{m}{c} \left(1 - \frac{i\alpha S}{2} - \frac{i \left(1 - \frac{1}{r}\right) g}{2\alpha} - \frac{A'_2}{2J_2} \right) \right) - \quad (2.106)$$

$$J_2 \frac{m^2}{c} \left(\frac{1}{J_2} - \frac{1}{2J_2^2} - \frac{i\alpha S A'_2}{4J_2^2} - \frac{i \left(1 - \frac{1}{r}\right) g}{4\alpha J_2^2} - \frac{A'_2 (1 + A'_2)}{4J_2^3} \right) = 0.$$

Therefore, as $m \rightarrow 0$, the eigenvalues c either satisfy

$$J_2 = 0 \quad (2.107)$$

or they are given by

$$c = m \left(1 - \frac{i\alpha S}{2} - \frac{i \left(1 - \frac{1}{r}\right) g}{2\alpha} - \frac{A'_2}{2J_2} \right) \quad (2.108)$$

$$+ m^2 \left(\frac{1}{J_2} - \frac{1}{2J_2^2} - \frac{i\alpha S A'_2}{4J_2^2} - \frac{i \left(1 - \frac{1}{r}\right) g}{4\alpha J_2^2} - \frac{A'_2 (1 + A'_2)}{4J_2^3} \right) + o(m^2).$$

The Airy functions here are evaluated with $c = 0$ in their arguments.

Note that, in the case of fluids with different densities, the density ratio determines the stability of the flow. Only values of r larger than unity have a stabilizing effect. However, surface tension always acts as a stabilizing parameter. Note also that this approximation can be simplified further by considering the case of large values of α . When α is large, we can replace $\frac{A'_2}{J_2}$ with its asymptotic expression to obtain

$$c = \frac{mi}{2\alpha^2} \left(1 - \alpha^3 S - \left(1 - \frac{1}{r}\right) g\alpha \right). \quad (2.109)$$

This is consistent with the short wavelength approximation given by 2.101 as $m \rightarrow 0$.

Equation 2.107 represents the dispersion relation for the stability problem with the solid boundary conditions mentioned above. To see this, note that the eigenvalue problem in this case reduces to

$$(D^2 - 1)^2 \phi = i\alpha^2(y - c)(D^2 - 1)\phi$$

$$\phi(0) = \phi'(0) = 0$$

$$\phi(y_2) = \omega(y_2) = 0.$$

This leads to the linear system

$$\mathbf{A}\mathbf{h} = \mathbf{0}$$

where \mathbf{A} is given by

$$\mathbf{A} = \begin{pmatrix} 1 & -J_2 \\ 1 & J_2 \end{pmatrix}.$$

Therefore, for a nontrivial solution, J_2 must vanish.

Equation 2.108 represents the case of an inviscid fluid on the bottom. In this limit, our non-dimensionalization with respect to the lower fluid becomes singular. However, we can investigate this case by nondimensionalizing with respect to μ_1 and ρ_1 . This results in a dispersion relation given by

$$F\left(\alpha, \frac{c}{s_2}, m, r, g, \frac{S}{m}\right) = 0 \quad (2.110)$$

where F is defined as in equation 2.84, $m\left(1 - \frac{1}{r}\right)$ is replaced by $s_2(1 - \hat{r})$ and S and g are non-dimensionalized with respect to μ_1 , ρ_1 and τ where τ defines the basic state velocity field by

$$\mathbf{u}^*(x^*, y^*) = \begin{cases} (s_1\tau y^*, 0) & \text{if } y^* > 0 \\ (s_2\tau y^*, 0) & \text{otherwise} \end{cases} \quad (2.111)$$

The Airy functions in this case are defined by

$$A_1(y) = Ai\left(z_1 e^{\frac{2r}{3}}\right) = Ai\left(m^{1/3}\alpha^{-2/3}s_2^{1/3}\left(y - \frac{c}{m} - \frac{i\alpha^2 r}{s_2 m}\right)e^{i\pi/6}\right) \quad (2.112)$$

$$A_2(y) = Ai\left(z_2 e^{-\frac{2r}{3}}\right) = Ai\left(\alpha^{-2/3}r^{\frac{1}{3}}s_2^{\frac{1}{3}}m^{\frac{1}{3}}\left(y - c - \frac{im\alpha^2}{s_2 r}\right)e^{5i\pi/6}\right).$$

As $m \rightarrow 0$, we obtain the following approximations for the leading terms of the Airy functions and their integrals:

$$\begin{aligned}\frac{A'_1}{A_1} &= -\left(1 - \frac{ic}{\alpha^2}\right)^{\frac{1}{2}} \\ \frac{A'_2}{A_2} &= -i\left(\frac{irc}{m\alpha^2}\right)^{\frac{1}{2}} \\ \frac{J_1}{A_1} &= \frac{1}{1 + \left(1 - \frac{ic}{\alpha^2}\right)^{\frac{1}{2}}} \\ \frac{J_2}{A_2} &= \left(\frac{im\alpha^2}{cr}\right)^{\frac{1}{2}}.\end{aligned}$$

Therefore, the dispersion relation reduces to

$$(r+1)c^2 + (4\alpha^2 i + rs_2)c + 4\left(\left(1 - \frac{ic}{\alpha^2}\right)^{\frac{1}{2}} - 1\right)\alpha^4 - \alpha^3 S - (r-1)g\alpha. \quad (2.113)$$

As s_2 goes to zero, the problem reduces to the classic Rayleigh-Taylor problem which was first formulated and solved by Harrison [24] in 1908 and later confirmed by Chandrasekhar. Equation 2.113 is equivalent to Chandrasekhar's equation 113 [10].

2.6.4 Asymptotic Behaviour of c as $m \rightarrow 1$

In general, as $m \rightarrow 1$, the problem reduces to a configuration of two equally viscous fluids which are separated by an interface at $y = 0$. However, if r also approaches unity, then the problem reduces to the unbounded Couette flow of one fluid which is always stable [45].

As m approaches unity, the dispersion relation reduces to

$$\begin{aligned}2(A'_1 A_2 - A'_2 A_1) - \beta c(A_1 J_2 + J_1 A_2) + \beta(A_1 J_2 - J_1 A_2) \\ - \frac{ig}{c}\left(S + \alpha^{-2}\left(1 - \frac{1}{r}\right)g\right)(J_2 A_1 + J_1 A_2) = 0\end{aligned}$$

where

$$\beta = i\left(1 - \frac{1}{r}\right)\frac{1}{\alpha^2}.$$

For large values of α this yields

$$c = \frac{i}{4\alpha} \left(\left(\frac{1}{r} - 1 \right) g - \alpha^2 S \right). \quad (2.114)$$

However, this seems to suggest that, in the absence of surface tension, the Couette flow is neutrally stable. To resolve this apparent contradiction with $r = 1$, we reduce the dispersion relation in the limit $m \rightarrow 1$ to obtain

$$\pi^{-1} \alpha^{\frac{2}{3}} + \lim_{m \rightarrow 1} \left[\frac{1-m}{c} \left(2(J_1 A_2 + A_1 J_2) + \pi^{-1} \alpha^{\frac{2}{3}} \right) \right] = 0$$

where $\frac{1}{2} \pi^{-1} \alpha^{\frac{2}{3}}$ is the Wronskian of A_1 and A_2 . Therefore, to satisfy this equation for an arbitrary disturbance, the eigenvalue c must also approach zero as $1-m$ approaches zero. This leads to a trivial solution since it implies that the stream functions also go to zero. In this limit Chandrasekhar's result also leads to a trivial solution [10]. Later on we will consider this case again and show numerically that, for an initial disturbance, the eigenvalue c always goes to zero as $m \rightarrow 1$.

2.6.5 Marginal Stability Curves

As discussed in section 2.3, in order to investigate the growth or decay of a disturbance with specified values of r, m, g and S , we look at the marginal stability curves (ie. curves for which $\Im(c) = 0$ on the (m, α) plane. For fixed values of r, g and S , we can use the above asymptotic expressions to obtain the asymptotic behaviours of these curves.

The α -intercepts of the marginal stability curves can be obtained by setting the imaginary part of the $m \rightarrow 0$ limit given by 2.108 equal to zero:

$$\Im \left(1 - \frac{i\alpha S}{2} - \frac{i \left(1 - \frac{1}{r} \right) g}{2\alpha} - \frac{A_2'}{2J_2} \right) = 0 \quad (2.115)$$

where $\Im(f)$ represents the imaginary part of f . If $r < 1$ or S is small, then the α -intercepts are large. In either of these cases, the Airy functions and their integrals can be replaced by their asymptotic values. The intercepts are then given by

$$\alpha_{int} = \begin{cases} 2 \left(\frac{(\frac{1}{r} - 1)g}{3S} \right)^{\frac{1}{2}} \cos \left(\frac{1}{3}\theta \right) & \text{if } r \neq 1 \\ S^{\frac{1}{3}} & \text{if } r = 1 \end{cases} \quad (2.116)$$

where

$$\theta = \cos^{-1} \left(\frac{6.75Sr^3}{(1-r)^3g^3} \right)^{\frac{1}{2}}.$$

The portions of the marginal stability curves which correspond to large α values can be approximated by evaluating the imaginary part of equation 2.101. By using four terms this yields a cubic equation for α :

$$\alpha^3 - \frac{2(m+1)\Im(c_2)}{mS}\alpha - \frac{2(m+1)\Im(c_3)}{mS} = 0. \quad (2.117)$$

As m increases to unity, if the marginal stability curve intersects the $m = 1$ line at large α then the intercept will approximately be given by

$$\alpha_{m=1} = \left(\frac{(\frac{1}{r} - 1)g}{S} \right)^{\frac{1}{2}}. \quad (2.118)$$

Finally, by setting the imaginary part of 2.104 to zero, we obtain the following expression for the portion of the marginal stability curve with small values of α :

$$\alpha = \frac{\alpha_n}{\alpha_d} \quad (2.119)$$

where

$$\begin{aligned} \alpha_n &= 8m(\sqrt{rm} + 1)(r-m)^{5/2}(r+1)^{\frac{1}{2}}\sqrt{2}(r-1)^2(m+1) \\ \alpha_d &= -20m^2 - 4m^3 + 64r^4 + 16m^4 + 64r^5 - 248mr^3 - 196m^3r + 178m^3r^3 \\ &+ 7r^6m^3 + 32r^6m - 17r^5m^4 - 212r^5m^2 - 232r^3m^4 + 32m^{3/2}r^{3/2} - 432r^{5/2}m^{7/2} \\ &+ 128r^{3/2}m^{9/2} - 52r^5m + 276r^4m^3 - 6r^4m^4 - 41r^2m^3 - 362r^{3/2}m^{7/2} - 176mr^4 \\ &- 32m^{5/2}\sqrt{r} - 400m^{3/2}r^{9/2} + r^{9/2} - 480r^{7/2}m^{3/2} - 150r^{7/2} - m^{7/2} + 64r^{5/2}m^{9/2} \\ &+ 128\sqrt{mr}^{9/2} + 624r^{7/2}m^{5/2} - 85m^{7/2}\sqrt{r} + 184r^3m^2 + 64m^5r^2 + 149r^{3/2}m^{5/2} \\ &- 112r^{5/2}m^{3/2} - 41rm^4 - 36rm^2 + 650m^{5/2}r^{5/2} + 80\sqrt{mr}^{11/2} + 16r^2m \end{aligned}$$

$$\begin{aligned}
& - 64 m^{3/2} r^{11/2} + 48 \sqrt{mr} r^{7/2} - 46 r^5 m^3 - 138 r^2 m^4 + 28 r^6 m^2 + 64 m^5 r + 44 r m \\
& - 20 r^4 m^2 + 292 r^2 m^2 + 4 (r - m)^{1/2} (r + 1)^{1/2} \sqrt{2} (4 m r^3 - m^4 + 6 m^3 r + 6 m^3 r^3 \\
& - 12 r^{5/2} m^{7/2} + 4 r^{3/2} m^{9/2} - 12 r^2 m^3 + 6 r^{3/2} m^{7/2} - 4 m r^4 - 4 m^{3/2} r^{9/2} \\
& - 3 r^{9/2} m^{5/2} - m^{9/2} \sqrt{r} + 4 r^{7/2} m^{3/2} + 6 r^{7/2} m^{7/2} - 3 r^{5/2} m^{9/2} ; 12 r^{7/2} m^{5/2} \\
& + 12 r^3 m^2 + 4 r m^4 - 9 m^{5/2} r^{5/2} - 3 r^2 m^4 - 3 r^4 m^2 - 9 r^2 m^2 \\
& + g (3 m^2 - 2 m r^3 + 2 m r - 5 m + 8 m r^2 - 3 m r^4 - 2 m^2 r^3 - 8 m^2 r^2 \\
& + 5 m^2 r^4 + 2 m^2 r + 2 m^{3/2} r^{3/2} - 2 m^{3/2} r^{7/2} + 8 m^{3/2} r^{5/2} - 8 m^{5/2} r^{5/2} \\
& + 5 m^{5/2} r^{9/2} + 2 m^{5/2} r^{3/2} + 3 m^{5/2} \sqrt{r} 3 m^{3/2} r^{9/2} - 5 m^{3/2} \sqrt{r} - 2 m^{5/2} r^{7/2})).
\end{aligned}$$

This equation is valid for $m \leq r$. A similar expression is found for $m \geq r$. When $r = 1$, both expressions give $\alpha = 0$. This is consistent with equation 2.105.

2.7 Numerical Procedure

As discussed in section 2.5, in order to analyze the stability problem we must compute the roots of the dispersion relation 2.84 with respect to the eigenvalue c for any given m , α , g , S and r . As we have seen in the preceding section, only a few limiting cases yield asymptotic expressions for c . In general, we must implement a numerical procedure to solve the dispersion relation. The standard procedure is to use Newton's method or variations thereof, such as Muller's method. A different approach, used by HB for the case of equal densities where $r = 1$, is to search for a minima of $|F|^2$ with respect to c . In this thesis, we use both Newton's method and Muller's method [54]. Results obtained by these two methods differ by less than $O(10^{-7})$.

Since the dispersion relation 2.84 contains the Airy function and its integrals, an algorithm for the calculation of Airy functions with complex arguments must be used. Two such algorithms were used and produced very similar results. The first algorithm was developed by Amos [4] while the second one was reported in Corless, Jeffrey and Rasmussen [12]. The integration required in the evaluation of J_1 and

J_2 was also carried out using two different methods. Since the integrands are of the Gauss-Laguerre type, the first method we use is the Gauss-Laguerre quadrature formulae [72]. The second method is an IMSL numerical integration subroutine based on a globally adaptive scheme. It initially transforms the semi-infinite interval into the finite interval $[0,1]$ and then uses a 21-point Gauss-Kronrod rule to estimate the integral and the associated error [58]. The results found by the two integration methods are in excellent agreement.

In order to investigate the growth or decay of a disturbance with specified values of r, m, g and S , we look at the marginal stability curves as discussed in section 2.3.1. (i.e. curves for which $\Im(c) = 0$) on the (m, α) plane. The strategy for plotting the curve uses some qualitative features of the result. The curves all have the general shape that can be seen in figure 2.2. In particular, for small values of m there is a solution of the equation with a large value of α . Thus, once the values of r, g and S are chosen, we use the asymptotic expression for large values of α to calculate a starting value for c for $m = 0$. This value is then used as an initial approximation for determining the marginal curve points for large values of α . We then increase the value of m by a small amount and use the previous root as the initial approximation to evaluate the next point on the marginal curve. This procedure is continued until the critical value of m is reached. Once the critical value is reached, we decrease the value of m by a small amount and use the already computed value of c at the critical value as the initial approximation. We reduce α by a small amount until the point on the lower part of the marginal curve is obtained. This process is then continued until m is close to zero. In all the calculations, double precision is used and the residual of F is $(\times 10^{-13})$ or smaller.

Using the numerical method described above, we compute the imaginary parts of c for various values of α . For $r = 1$, the asymptotic expression for the imaginary

α	asymptotic	numerical
4	0.0026042	0.0025801
6	0.0011574	0.0011543
8	0.0006510	0.0006500
10	0.0004167	0.0004165

Table 2.1: Imaginary parts of c computed from the asymptotic expression 2.118 and from the numerical method

α	asymptotic $\Im(c)10^{-3}$	numerical $\Im(c)10^{-3}$
0.003	-0.054000	-0.053963
0.004	-0.096000	-0.095906
0.005	-0.150000	-0.149669
0.008	-0.380000	-0.382001

Table 2.2: The imaginary parts of c computed from the asymptotic expression 2.103 and from the numerical method

parts of c for large values of α given by 2.101 can be approximated by

$$c = \frac{im}{2(1+m)} \left(\frac{(1-m)^2}{\alpha^2} - \alpha S \right). \quad (2.120)$$

Table 2.1 compares the imaginary parts of c which are evaluated from the numerical procedure and those which are computed from the asymptotic expression for the case where $S = 0, r = 1$ and $m = 0.5$. As the table shows, for large values of α , the numerical solutions and the asymptotic solutions are in close agreement.

Similarly, for small values of α , we obtain a close agreement between the numerical calculation and the long wavelength approximation given by 2.105. This is demonstrated in table 2.2. We carried out further comparisons to test the numerical procedure which showed similar agreement with the asymptotic solutions.

2.8 Results and Discussion

The case of equal densities, $r = 1$, was the only one investigated numerically by HB. This case is discussed at the outset so that our results may be compared to theirs. For other values of r , HB used their asymptotic results to investigate the stability of the system. Since we have numerical results for these cases, we can test the predictions made on the basis of an asymptotic analysis alone. We shall demonstrate that numerical results are necessary in order to reach correct conclusions.

2.8.1 Equal Densities

HB investigated the case where the densities of the two fluids are equal, corresponding to $r = 1$ and $g = 0$. They found that, in the absence of surface tension, the flow is always unstable. Our results confirm this conclusion. Figure 2.2 depicts the marginal stability curve for zero surface tension. As discussed in section 2.6.4, as the viscosity ratio approaches unity, the flow becomes the unbounded Couette flow of one fluid. The stability curve conforms to the prediction resulting from the asymptotic analysis that, in this limit, the flow ceases to support any growing disturbance.

The stabilizing effect of surface tension can be seen in figure 2.3. As surface tension increases from zero, the flow becomes more stable with respect to short wavelength disturbances for m values closer to unity. However, the flow is still unstable since the surface tensions used for these curves are small.

The marginal curves for larger values of S are represented by the solid lines in figure 2.4. This figure shows that the instability caused by the viscosity jump is now stabilized for small values of m . As the viscosity ratio m approaches zero, the flow becomes more unstable and the surface tension is unable to stabilize it.

For m values higher than some critical amount m_c , the flow is always stable in the presence of surface tension. The values of m_c for the curves where $S = 0.5$, $S = 0.2$, $S = 0.1$ and $S = 0.02$ are 0.525, 0.650, 0.750, and 0.880 respectively. Flows with

S	Asymptotic	Numerical
0.1	2.1237	2.1240
0.2	1.6607	1.6610
0.3	1.4310	1.4317
0.5	1.1801	1.1814
0.9	0.9366	0.9371
1.0	0.8637	0.8643
1.5	0.7607	0.7610

Table 2.3: Comparison between 2.119 and the numerical method for $r = 1$.

viscosity ratios below these critical values are always unstable with respect to short wavelength disturbances.

The α -intercept of these curves decreases with increasing surface tension thereby reducing the number of unstable modes. For the purposes of comparison, 2.115 is used to evaluate the α -intercept of these curves. This is accomplished by simply solving

$$\Im \left(1 - \frac{A'_2}{2J_2} - \frac{i\alpha S}{2} \right) = 0. \quad (2.121)$$

Table 2.3 compares the results found from the numerical method and the asymptotic solutions. The close agreement is another indication that our numerical procedure is producing correct results.

Note that, for large values of α -intercepts, we can use the asymptotic expression given by 2.116 :

$$\alpha_{int} = \left(\frac{1}{S} \right)^{\frac{1}{3}}. \quad (2.122)$$

See table 2.4 for a comparison of this expression with the numerical solution.

HB calculated the α -intercepts from the asymptotic expressions and they obtained similar results. For example, for $S = 0.1$ they obtained $\alpha = 2.12$ and for $S = 0.5$ they

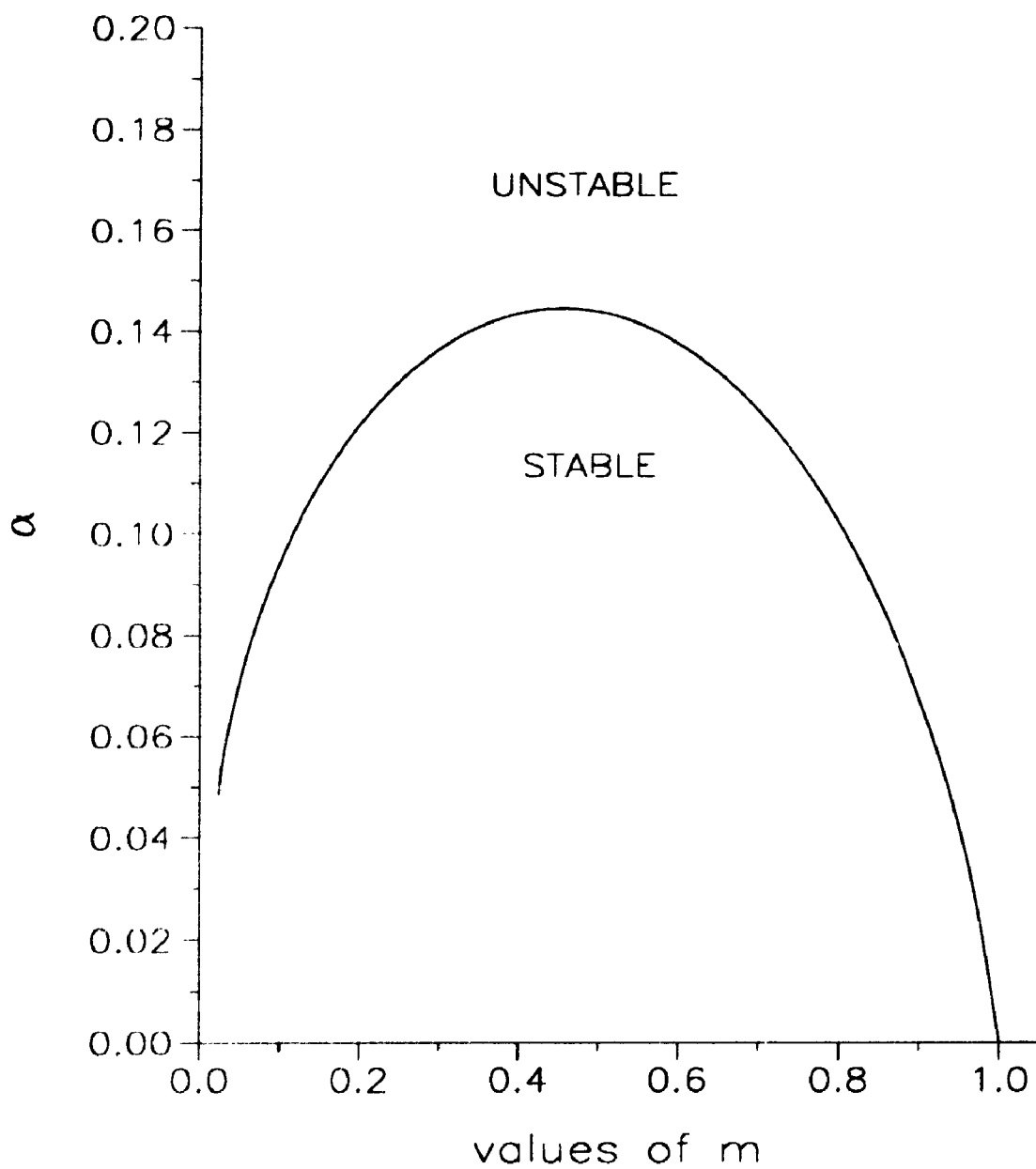


Figure 2.2: Marginal stability curve for $S = 0$ and $\tau = 1$

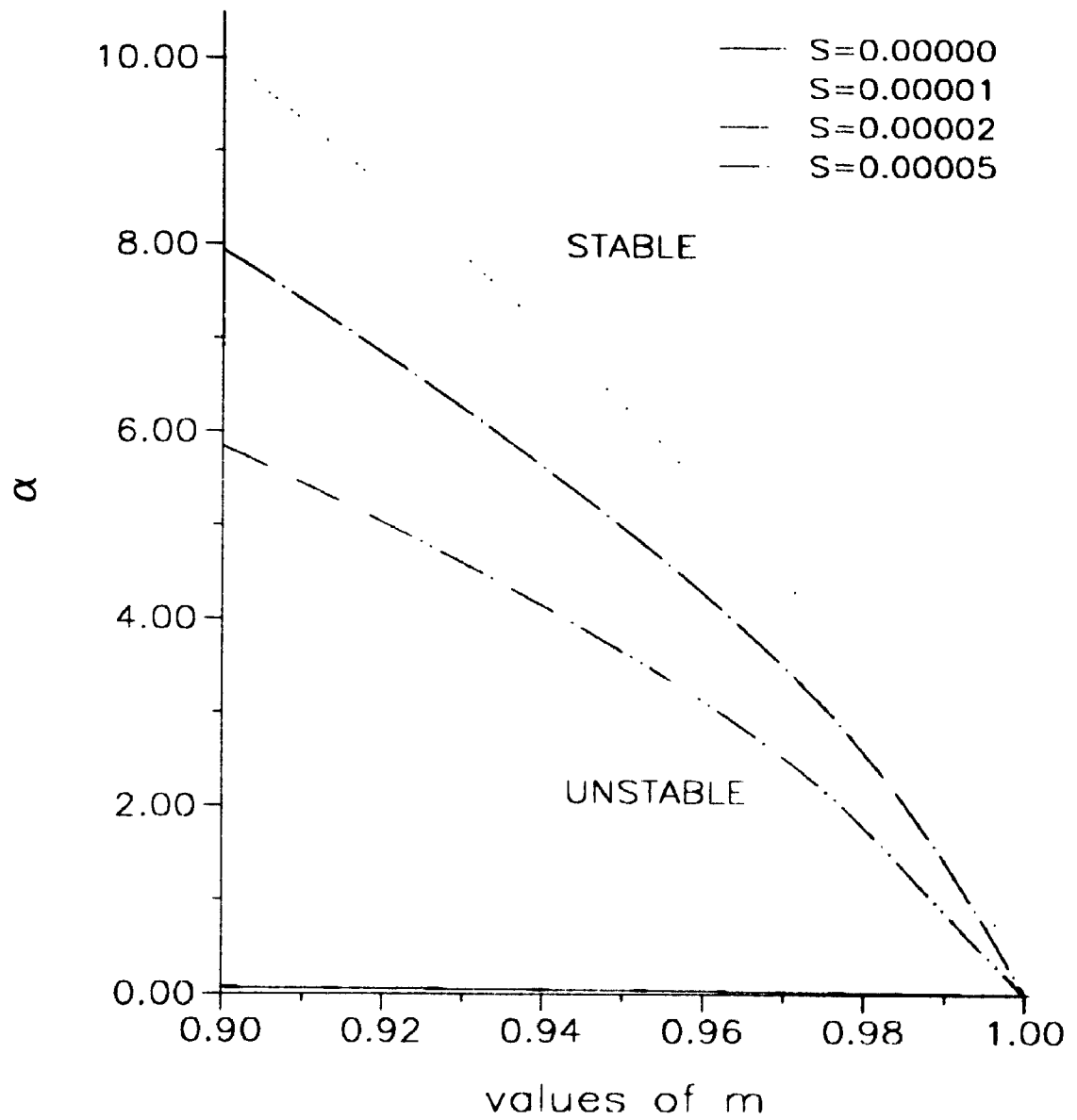


Figure 2.3: Marginal stability curves for $r = 1$ and small values of S

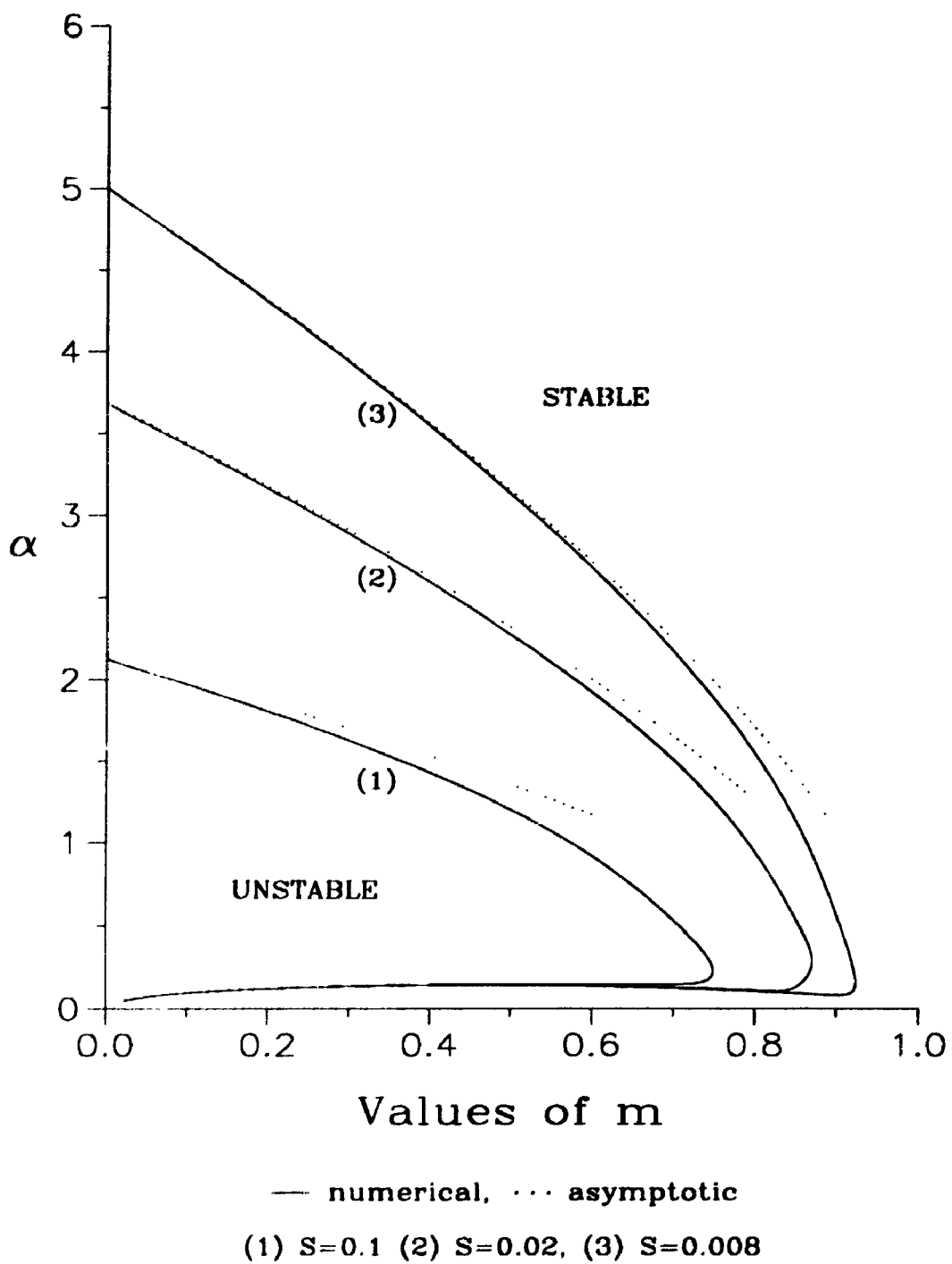


Figure 2.4: Marginal stability curves for $r = 1$ and large values of S

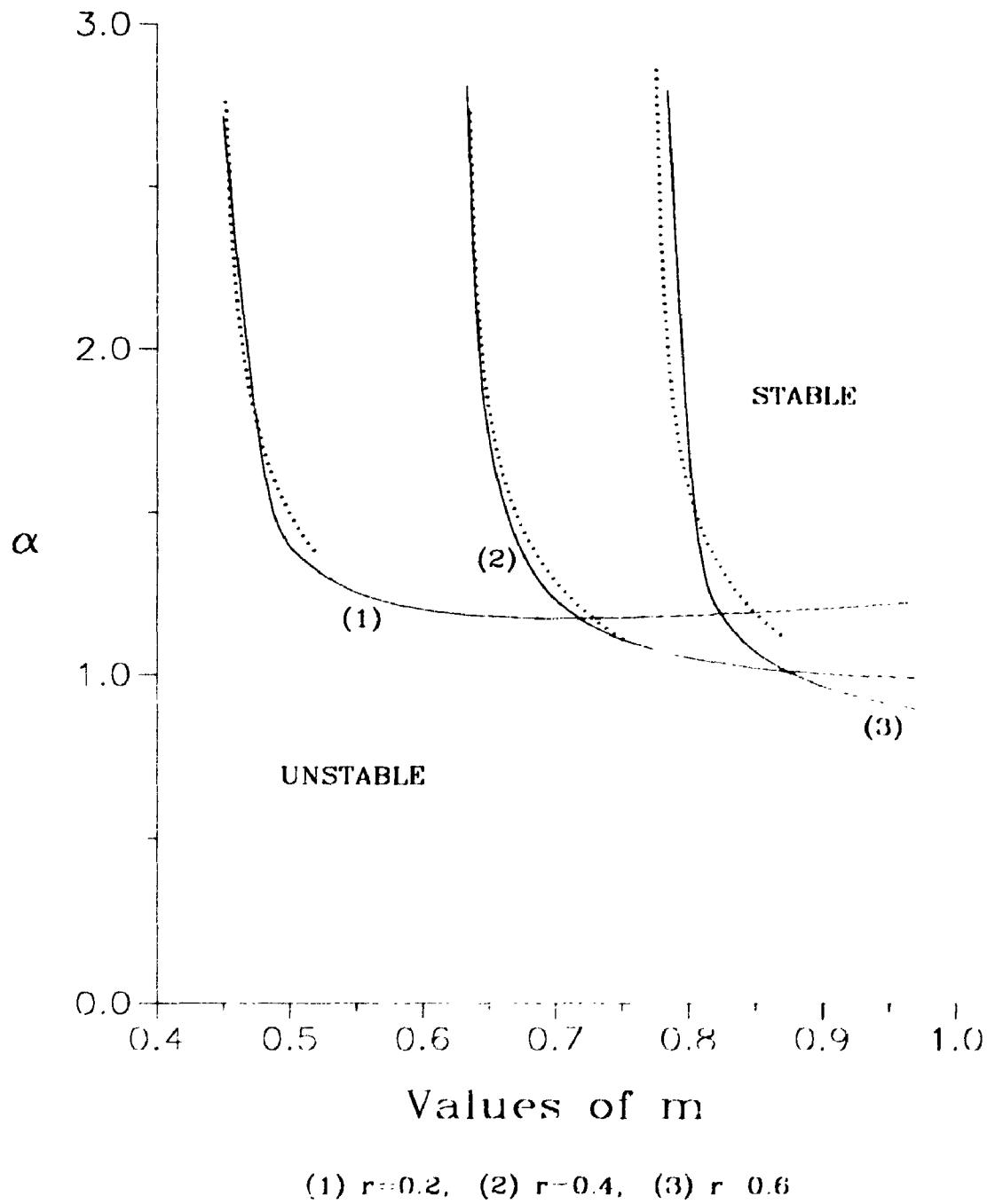


Figure 2.7: Marginal stability curve for various values of r , $g = 0$ and $S = 0$

The peaks of these curves decrease with increasing surface tension. Again, this is due to the stabilizing effect of surface tension. For $S = 0$, the peak occurs at $m = 0.11$ and at $\alpha = 0.29$ and has a value of 0.0674. For the case of the equal densities configuration, this value represents an upper bound for the growth rates of all possible disturbances. For small values of m , the growth rates can be evaluated from the asymptotic expression given by expression 2.108. For values of m less than 0.21, figure 2.5 depicts the maximum growth rate curves computed from the asymptotic expression for the case where $S = 0.0$. Note that, for very small values of m , this curve overlaps with all the other curves since, in this case, α is so small that the αS term is negligible. As m increases, however, these curves depart from each other because the surface tension effects become more important. Asymptotic curves computed for the other values of S also give similar results.

Figure 2.6 illustrates the values of α for which the maximum growth rates occur. These curves represent the most unstable modes for a given flow. Note that the most unstable modes corresponding to smaller values of S are shorter in wavelength. Due to the stabilizing influence of the surface tension, as S increases, the wavelengths of the most unstable modes lengthen.

In the next section we examine the effects of density jump and the effects of gravity by considering the unequal density case.

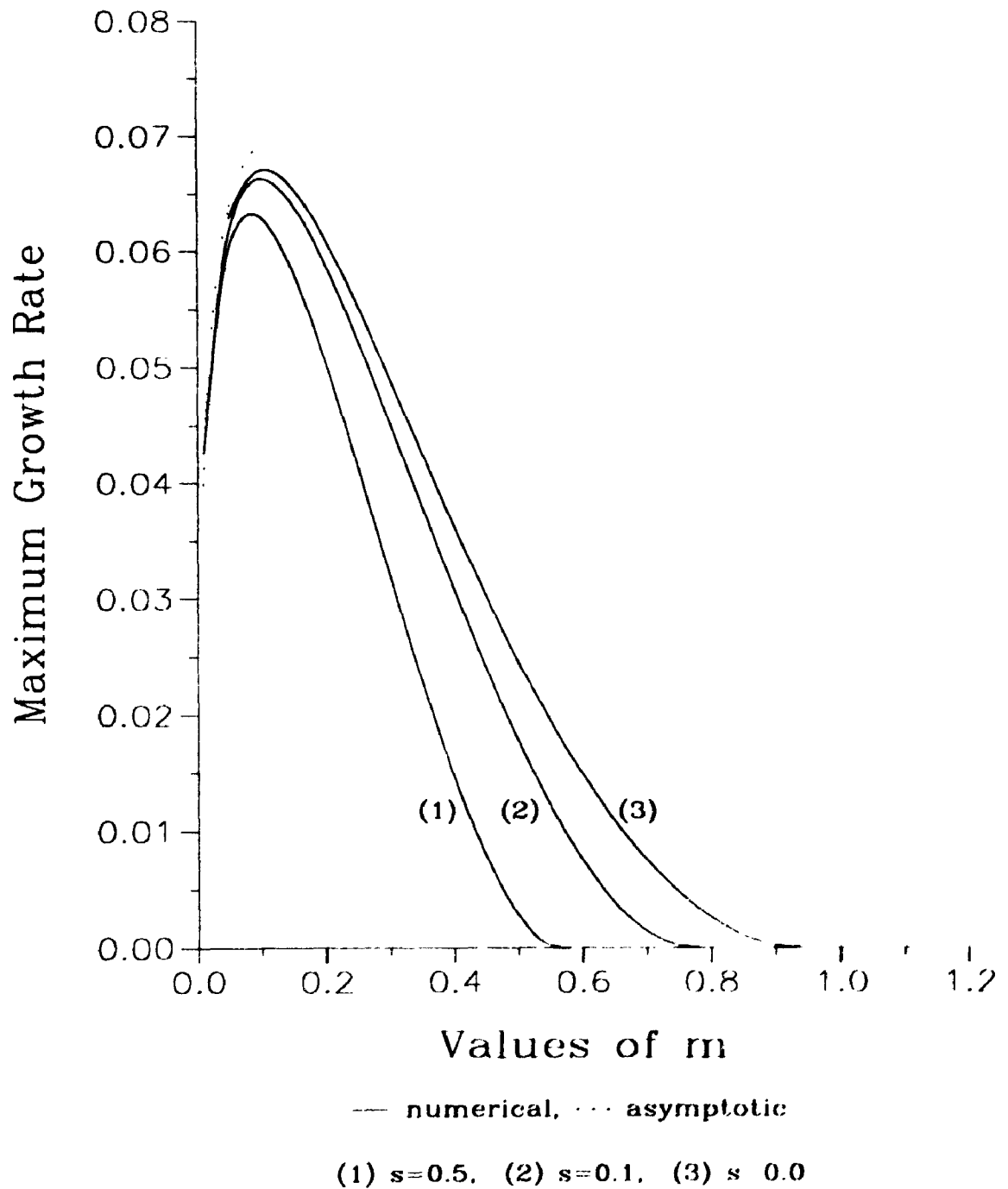
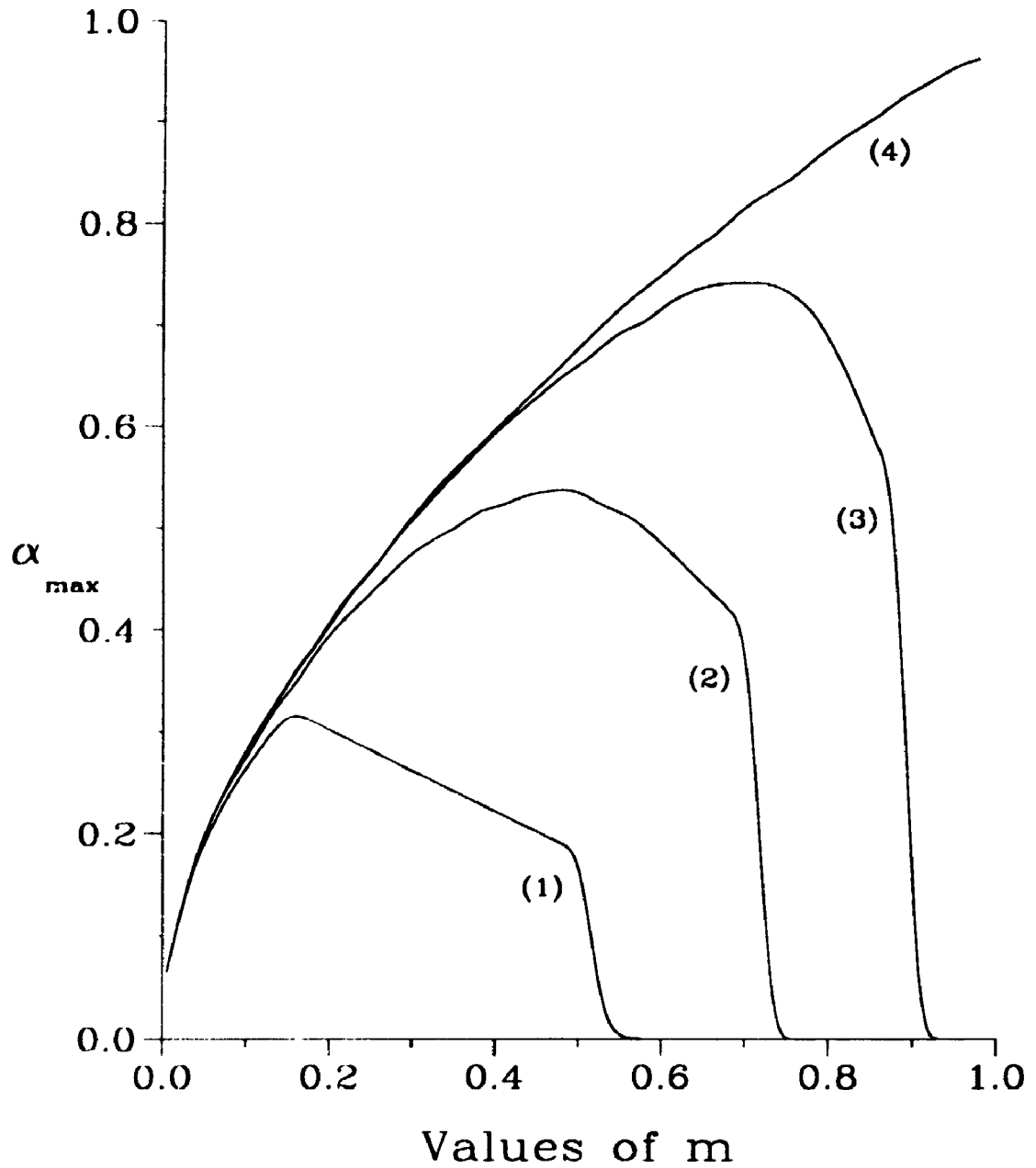


Figure 2.5: Maximum growth rates for various values of S when $r = 1$



(1) $s=0.5$, (2) $s=0.1$, (3) $s=0.008$, (4) $s=0.0$

Figure 2.6: Values of α corresponding to maximum growth rates when $r = 1$

2.8.2 Unequal Densities

Let us now consider the cases in which $r \neq 1$. The density difference can affect the stability of the interface in two ways. The first is through the change in the inertia of the fluid, and the second is through the response of the fluids to gravity. In order to investigate first the effect of inertia, we shall set $g = 0$. Since we consider only $m < 1$, then if $r < 1$, the less viscous fluid is also less dense. As in the case of equal densities, the surface tension has a very strong influence on the stability. Therefore, we consider the case where $S = 0$ at the outset.

In the absence of gravity and surface tension, 2.102 shows that the sign of $r - m^2$ determines the stability of the flow with respect to short wavelength disturbances. If the denser fluid is the less viscous, then the viscosity jump acts as a stabilizing influence as long as the ratio m is greater than $r^{\frac{1}{2}}$. On the other hand, if the less dense fluid is the less viscous, then the flow is always unstable (see table 2.5).

r	m	Numerical
0.30	0.60	-0.002343750
0.50	0.70	+0.000181661
0.90	0.95	-0.000004337
1.50	0.50	+0.011574074

Table 2.5: Imaginary parts of c to illustrate the zero-gravity zero-surface tension case with $\alpha = 2.0$

This behaviour was pointed out by HB. We cannot, however, extrapolate from this to conclude that the flow is stable if $r < m^2$ as HB did, because equation 2.101 says nothing about long wavelength stability, and a full numerical solution of the dispersion relation shows that the flow is always unstable where α is small. In figure 2.7 we plot the neutral curves for $S = g = 0$ and various values of r . It can be seen

that, for large α , the asymptotic statement is accurate; indeed, extending the analysis to a higher order in α shows that the neutral curves are given by

$$\frac{m(1-m)(r-m^2)}{2r(1+m)^2}\alpha^{-2} + O(\alpha^{-6}) = 0. \quad (2.123)$$

In figure 2.7, we plot the curves $K/(m^2 - r)$ using $K = 0.5$, a value chosen solely on the basis of convenience of presentation.

The effect of gravity on the stability of the flow is characterized by the reduced gravity

$$g_r = \left(\frac{1}{r} - 1\right)g. \quad (2.124)$$

If the lighter fluid is on top, then g_r is negative and, therefore, gravity is a stabilizing parameter. Otherwise gravity becomes a destabilizing influence. The stability of the flow, however, is determined by the magnitude of g_r . If the magnitude of g_r is small, then even the case where heavier fluid is on top can be stabilized by surface tension. Similarly, in the absence of surface tension, the case where lighter fluid is on top could be unstable if the magnitude of g_r is not large enough. This is illustrated in table 6 where the growth rates for the case where $r = 1.5$, $S = 0$, $m = 0.05$ and $g = 1.0$ are presented. Note that there is excellent agreement between the numerical and the asymptotic solution given by 2.101.

α	asymptotic	Numerical
4	0.00074112	0.00074844
5	0.00038135	0.00038376
6	0.00019928	0.00020036
7	0.00009800	0.00009861

Table 2.6: Comparison of the imaginary parts of c between equation 2.101 and the numerical method where $r = 1.5$, $S = 0$, $m = 0.05$ and $g = 1.0$.

The case where heavier fluid is on the bottom with various values of the nondimensional quantity g is depicted on the marginal stability curves of figure 2.8. As

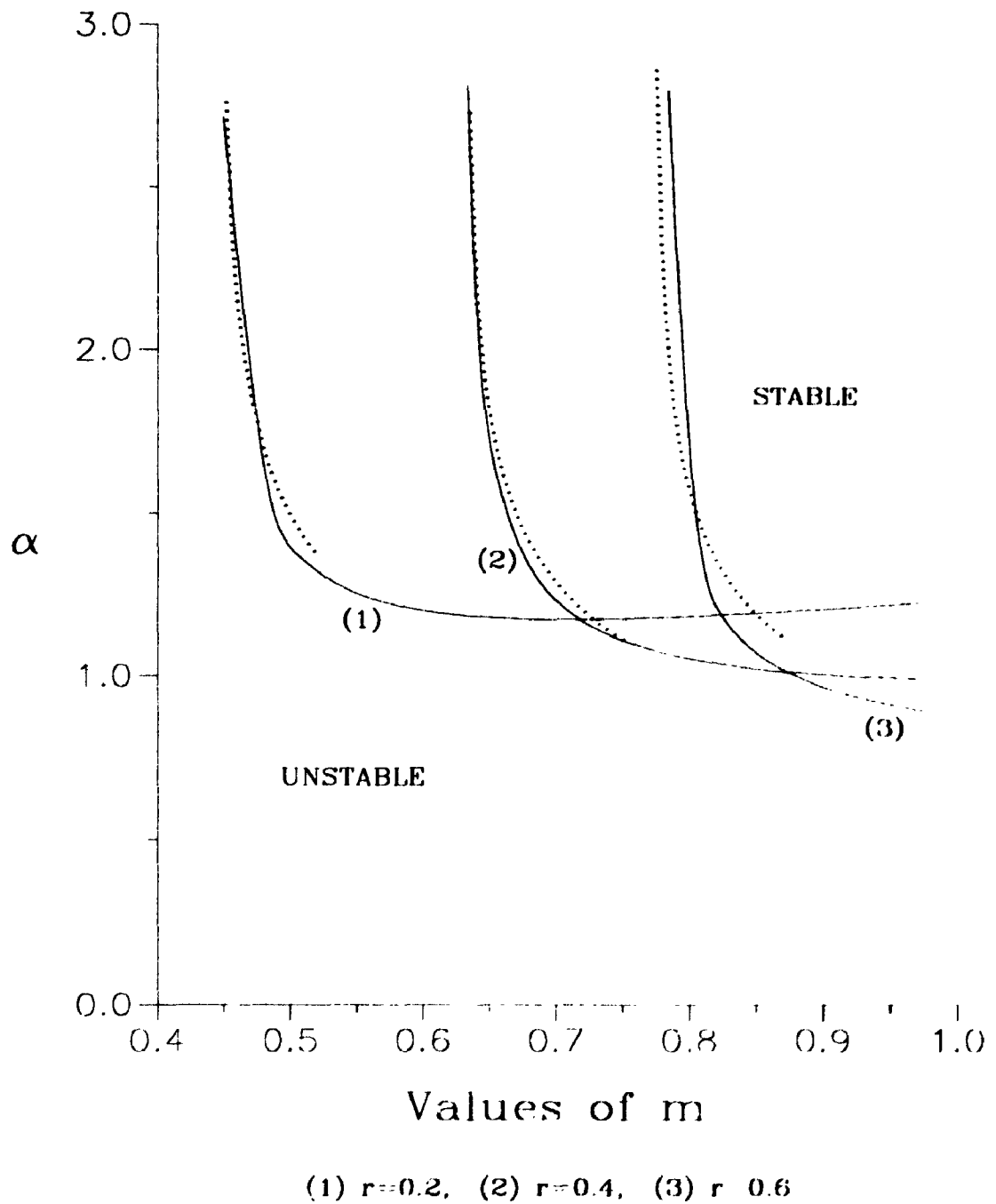


Figure 2.7: Marginal stability curve for various values of r , $g = 0$ and $S = 0$

in the case where $r = 1$, when g_r is non-positive, the flows become stable to all wavenumbers for $1 > m > m_c$, and the region of unstable wavenumbers is confined to smaller values of m . This region shrinks as g increases until it disappears when a critical value of the parameter g is used. For the particular example where $r = 1.25$ and $S = 0.1$, this critical value is 6.87. Similarly, the effect of g where the lighter fluid is on top is illustrated in figure 2.9 where the marginal stability curves for $r = 0.8$ and $S = 0.1$ are shown.

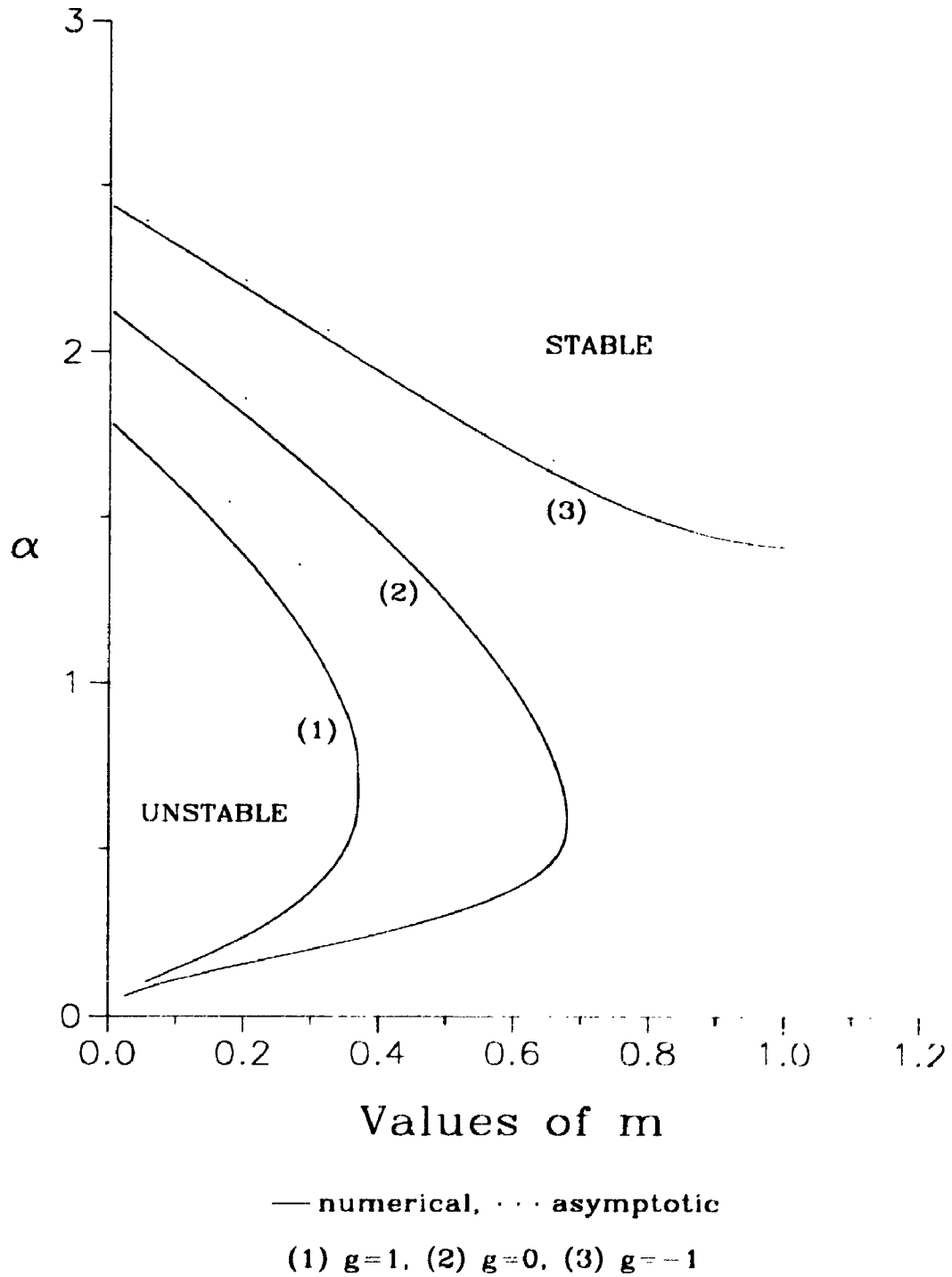


Figure 2.8: Marginal stability curves for $r = 1.25$, $S = 0.1$ and various values of g

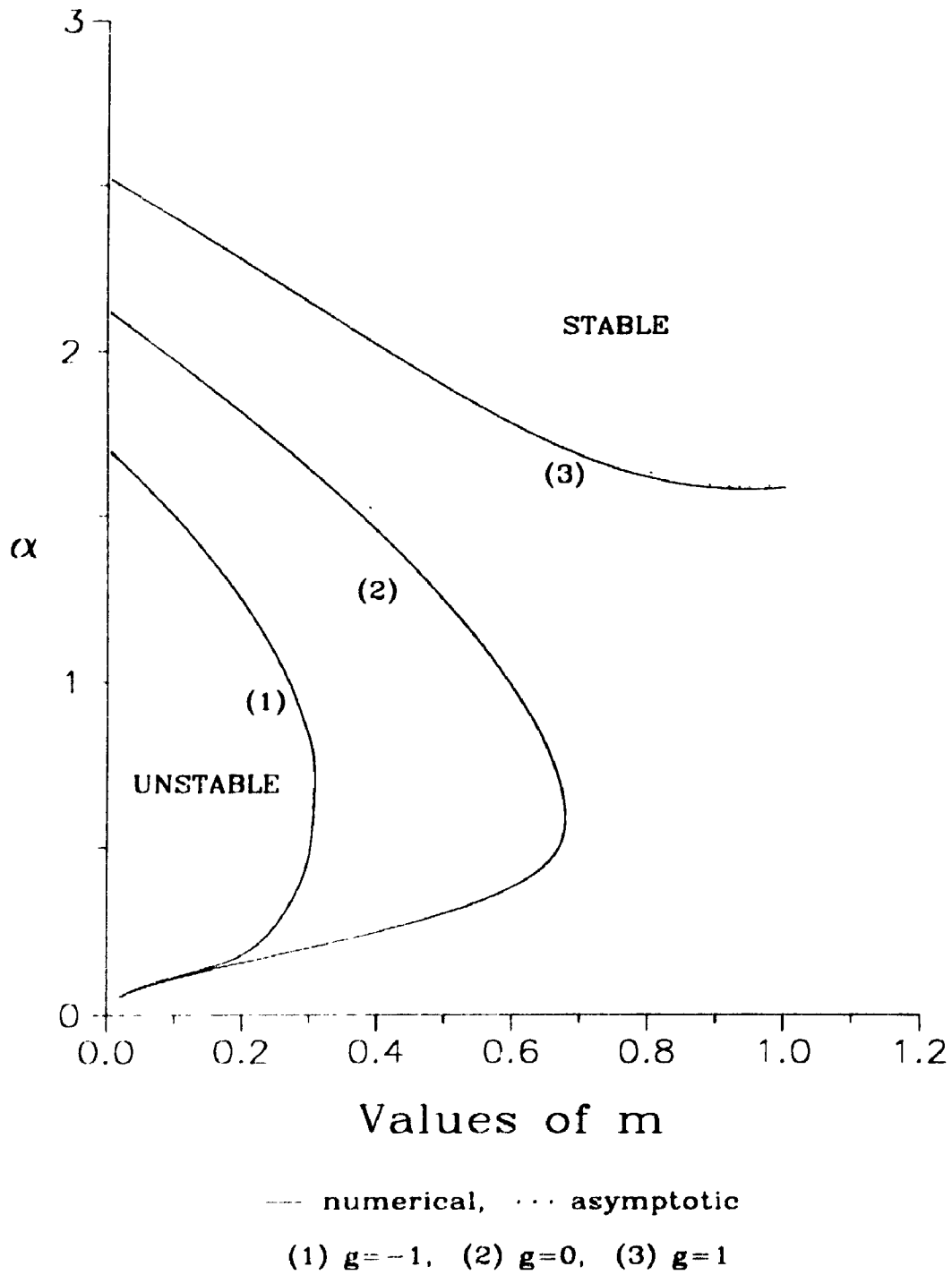


Figure 2.9: Marginal stability curves for $r = 0.8$, $S = 0.1$ and for various values of g

Again, note that both in figures 2.8 and 2.9 the asymptotic approximations computed using equation 2.117 are in excellent agreement with the numerically computed curves. The agreement between the asymptotically and the numerically computed curves for curve (3) of both of these figures is remarkable even for moderate values of α .

The effect of reduced gravity in the absence of surface tension is illustrated in figure 2.10. The upper branch of the marginal stability curves can be found approximately by setting the imaginary part of equation 2.101 to zero. The result is

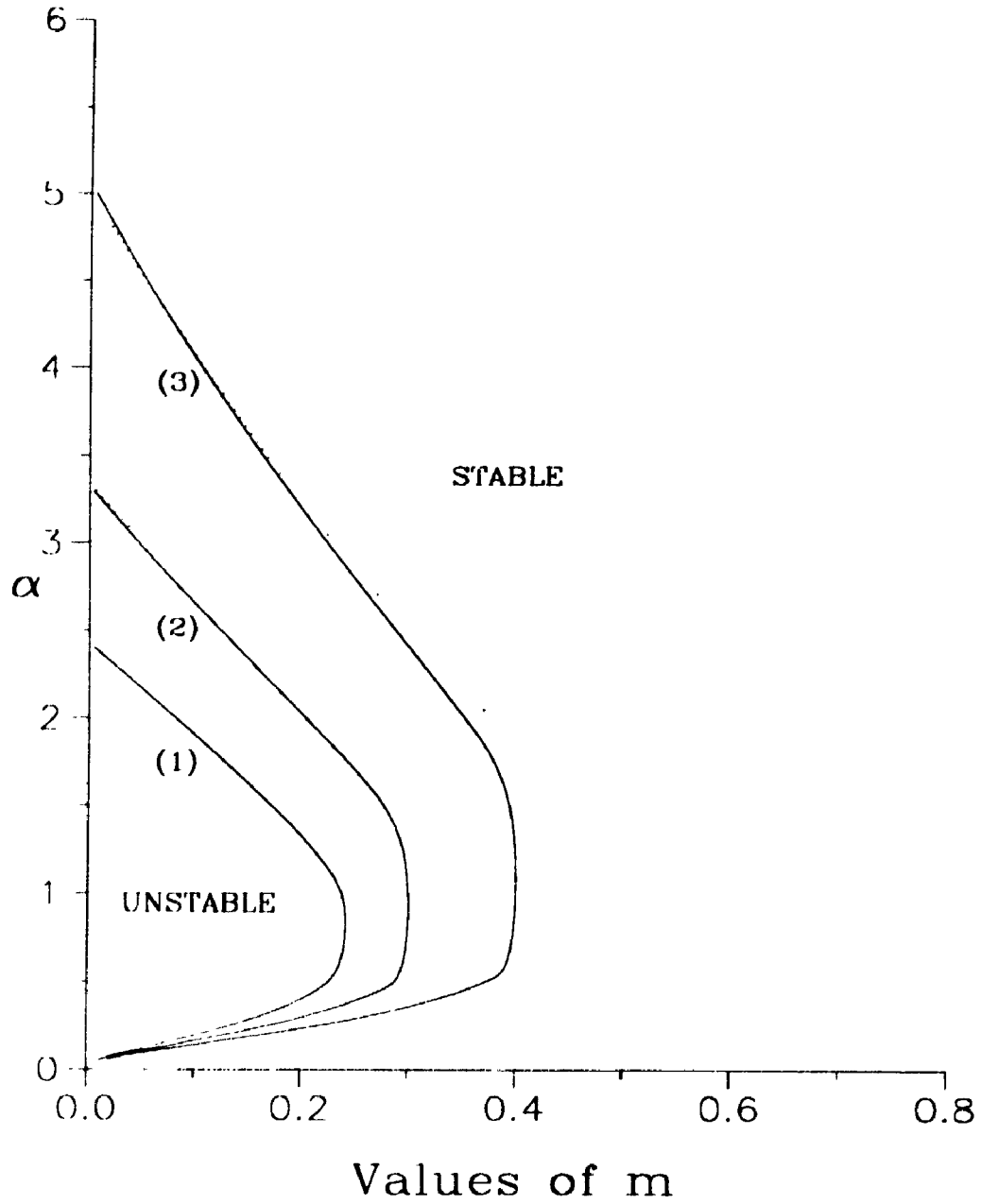
$$\alpha = \frac{(1-m)(r-m^2)}{r(1+m)g_r} + \frac{3m^2(r^2-1)}{r^2(1+m)^2}.$$

In particular, the intercept with the α -axis ($m = 0$) is, in this approximation, simply $1/g_r$ and the initial slope is $-2/g_r$. Both results are independent of r . The density ratio r is present in the definition of g_r but, aside from this, it clearly has only a secondary impact on the stability of the system. If g_r is not positive (and $S = 0$) then large wavenumbers will always be unstable. Put another way, the shear flow can destabilize the flow in spite of the fact that gravity is stabilizing it, provided that the viscosity ratio is small enough. It appears from the figure that there will always be a region of instability near $m = 0$, however high g_r may be. The rates of growth will, however, be very small.

The marginal stability curves of various configurations where heavier fluid is on top are depicted in figure 2.11. In all cases, the surface tension is 0.1 and g is 1.0. The α -intercepts of these curves are computed both numerically and asymptotically. The asymptotic values are obtained using equation 2.115.

As shown in table 2.7, our numerical solutions agree with the asymptotic solutions.

For values of $r < 1$ or for small values of S , the α -intercept is large. In either of these cases, the asymptotic expression 2.116 can be used to approximate the α -intercepts. Table 8 shows that the α_{int} computed from this expression agrees with the numerical computations.



--- numerical, ··· asymptotic

(1) $g=2$, (2) $g=1.5$, (3) $g=1$

Figure 2.10: Marginal stability curves for $r = 1.25$ $S = 0.0$ and various values of g

r	numerical	asymptotic
0.25	3.5700	3.5744
0.29	3.1899	3.1888
0.67	2.8912	2.8980
0.80	2.5175	2.5234
0.95	2.2047	2.2100

Table 2.7: Comparison of α intercepts between 2.115 and the numerical method for $S = 0.1$ and $g = 1.0$

r	numerical	asymptotic
0.25	3.5700	3.5771
0.29	3.1899	3.1891
0.67	2.8912	2.9051
0.80	2.5175	2.5378
0.95	2.2047	2.2358

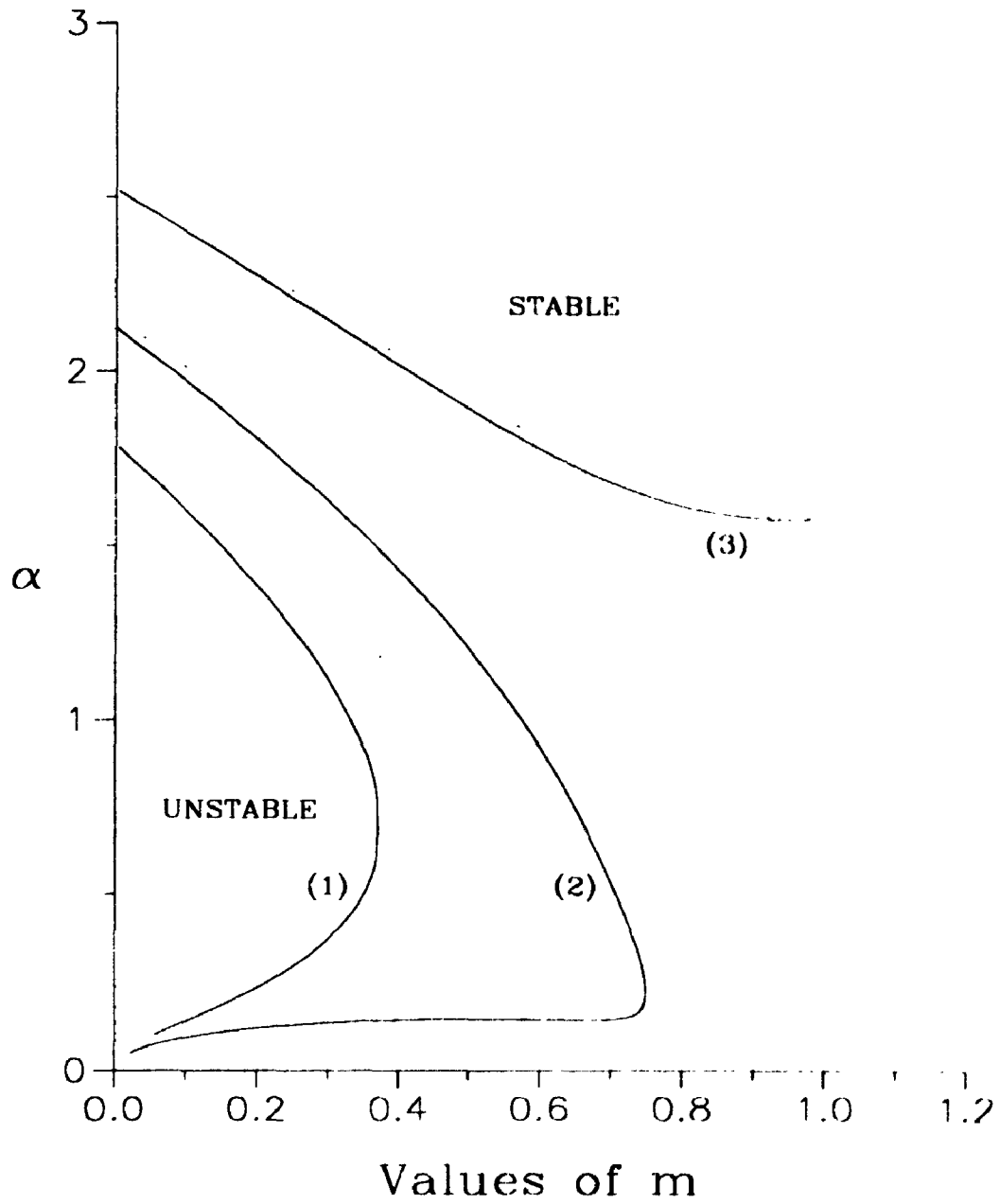
Table 2.8: Comparison of α intercepts between 2.115 and the numerical method for $S = 0.1$ and $g = 1.0$

As m approaches unity, the intercepts of the marginal stability curves with the line $m = 1$ are given by 2.118. It is easy to see that all the marginal stability curves are in accordance with this approximation. For $\frac{\rho_1}{\rho_2} = 2.0$, the value of the intercept at $m = 1$, calculated numerically, is 3.1624 while equation 2.118 approximates the intercept by a value of 3.1623.

The destabilizing effects of the density jump, illustrated in figure 2.11, show that, unlike the case of equal densities (see fig 2.2), the long wavelength disturbances are unstable. Furthermore, we observe that when the heavier fluid is on top (i.e. when $r < 1$) the flow is unstable even for values of m above the critical value m_c which was found for in the $r = 1$ case.

As $\alpha \rightarrow 0$, the long wavelength analyses discussed in section 2.6.2 show that for $r < 1$ and non-negative values of g there may exist a very small region of stability. This region is represented by a small area bounded by the marginal stability curve for small values of α given by equation 2.119. Since this region is very small, it is not apparent on the marginal stability curves we have seen so far. Figure 2.12 depicts this small region for various values of r with $g = 0$ and $S = 0.1$. Note that each curve intersects the m axis at $m = 0$ and $m = r$.

Finally, the magnitudes of the maximum growth rates versus the viscosity ratio m and the corresponding wavenumbers versus m are shown in figures 2.13 and 2.14 respectively. In figure 2.13, two curves illustrate the cases where heavier fluids and lighter fluids are on the top. The surface tension in both cases is 0.1 and the value of g is 1.0. For $r < 1$, unlike the equal densities case, the maximum growth rates for m values closer to unity do not approach zero. Even in the presence of surface tension the magnitude of the growth rate at $m = 1$ is of the same order as the peak value.



— numerical, --- asymptotic

(1) $r=1.25$, (2) $r=1.0$, (3) $r=0.8$

Figure 2.11: Neutral stability curve for $g = 1.0$, $S = 0.1$ and various values of r

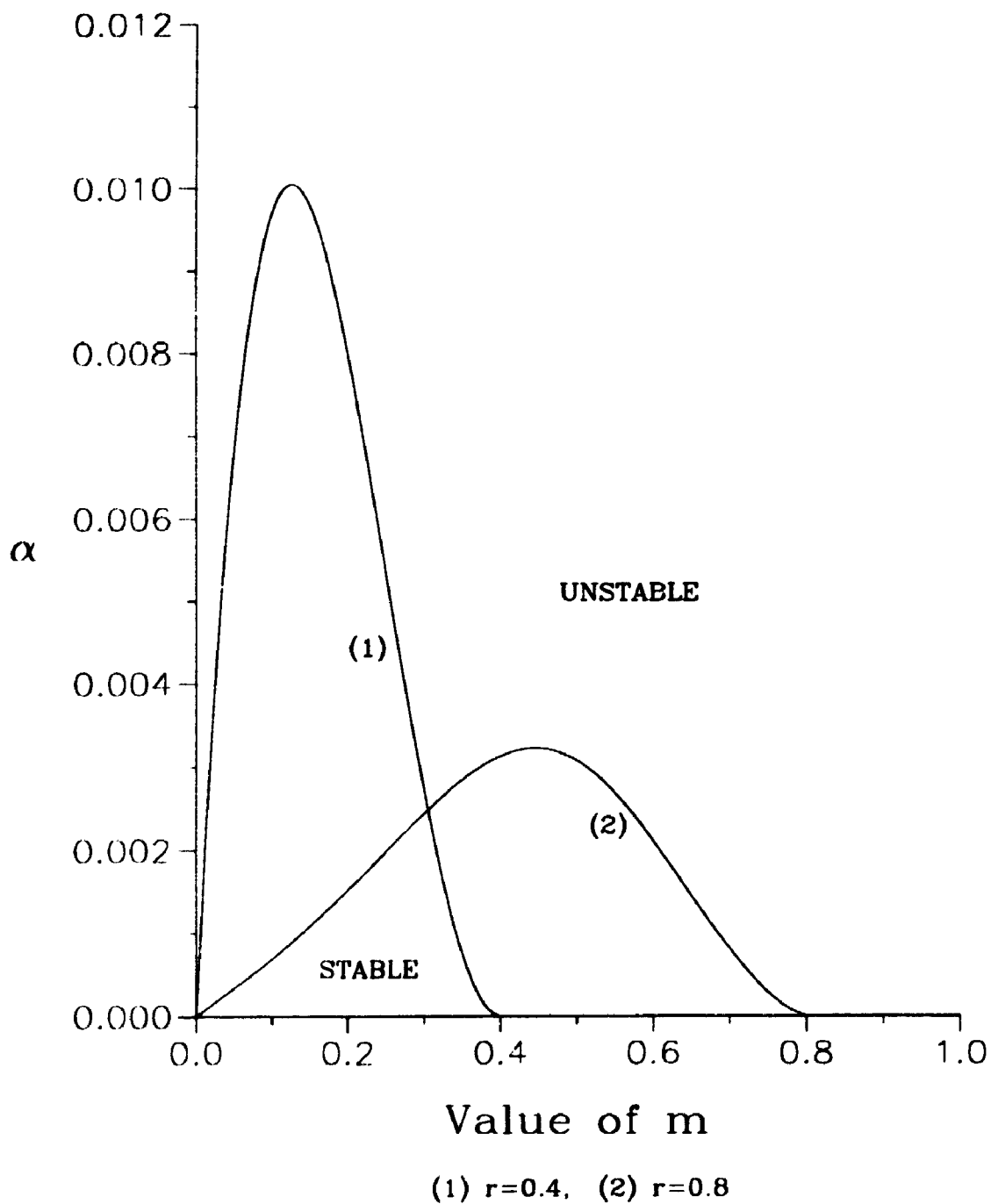
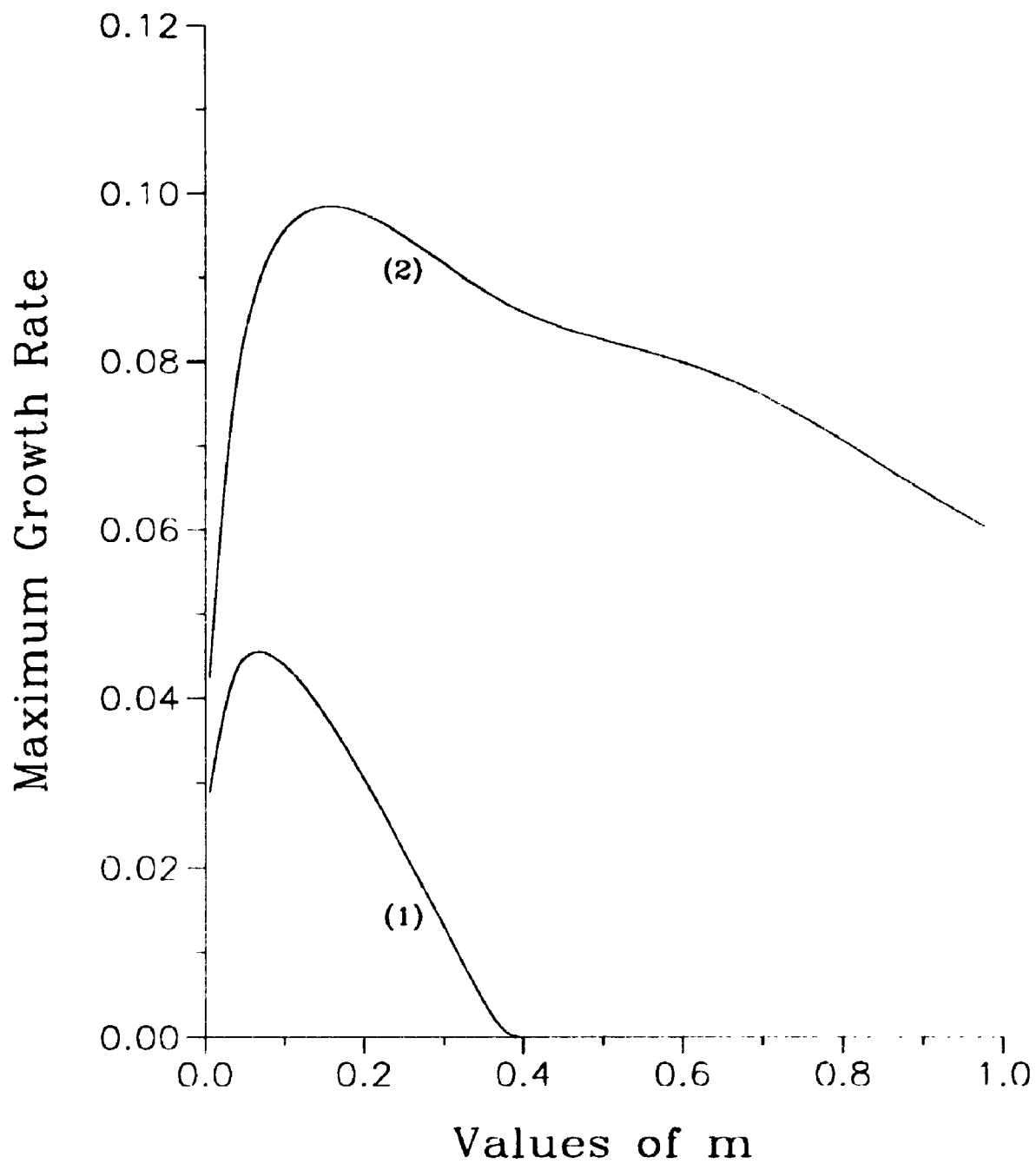


Figure 2.12: Marginal stability curves for small values of α .



(1) $r=1.25$, (2) $r=0.8$

Figure 2.13: Maximum growth rates for $r > 1$ and $r < 1$.

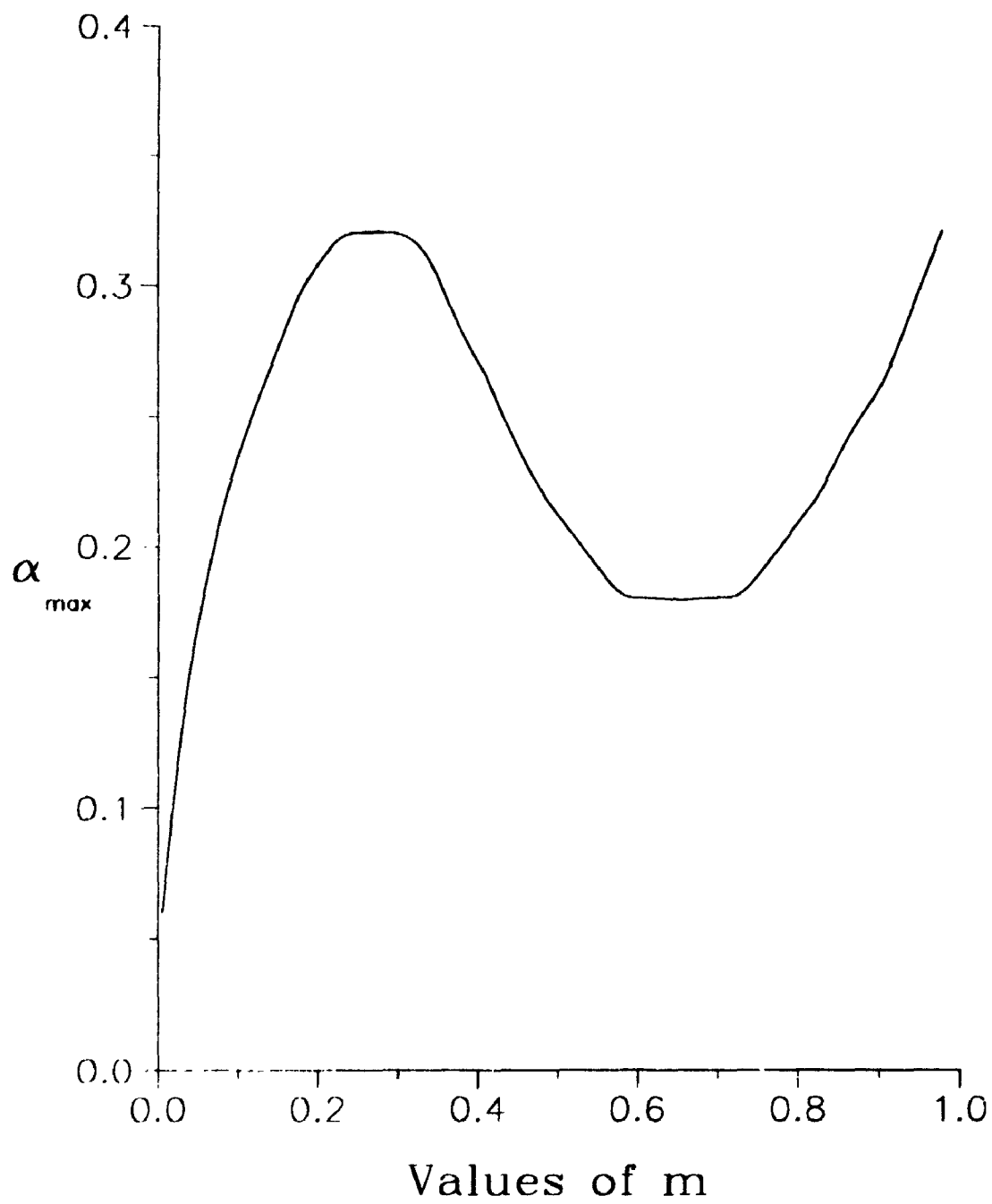


Figure 2.14: Values of α corresponding to maximum growth rates for $r = 0.8$

2.9 Conclusion

We reworked and extended the analysis of Hooper & Boyd [33], taking advantage of the advances that have been made in computer software since their work was published. The more comprehensive numerical results that we obtained show satisfactory agreement between our special cases and their work, and the points of disagreement were clarified. The re-working of the asymptotic analysis showed more significant qualitative changes. The starting assumption of HB for their asymptotic series was that the series would contain negative even powers only, whereas we demonstrated that the series contains other powers, particularly as the result of surface tension and gravity. The extensions to the numerical and asymptotic results allowed us to show that the agreement between the two is more extensive than one would suppose at first glance, allowing much of the qualitative behaviour of the numerical solutions to be understood without having to resort to large numbers of plots.

One particular qualitative generalization of HB requires reconsideration. Their abstract indicates that the instability occurs for short wavelengths. We agree that the large wavenumber limit is a significant one for the problem, being the one in which asymptotic results can be obtained. However, as soon as surface tension is added to the problem, the largest wavenumbers become stable, and in all cases the largest growth rates occur for moderate wavenumbers. The question then arises whether viscosity or inertia is the main factor in the instability. From our results it appears that as soon as surface tension is included in the problem, the viscosity difference is the main factor causing the instability whereas the density difference shifts the marginal curves by relatively minor amounts.

The more important effect of density difference is the introduction of gravity to the problem. The asymptotic analysis indicates that gravity is potentially the second most important contributor to the complex wave speed, although global effects on the basis of asymptotic results can be misleading. The numerical results confirm the importance of gravity in determining the marginal curves.

Chapter 3

Electrohydrodynamic Instability of Two Superposed Fluids in Normal Electric Fields

3.1 Introduction

In this chapter we consider the electrohydrodynamic extension of the shear flow instability problem discussed in the previous chapter. As before, the two fluids are separated by a plane interface and on each side of the interface there is an unbounded Couette flow. The fluids are assumed to have different viscosities, densities, basic velocities and electrical properties, and surface tension acts at the interface. In this electrohydrodynamic extension, the interface is initially stressed by applying uniform electric fields normal to the interface.

The introduction of the applied electric fields induces electromechanical effects related to the interaction of electric fields and free or polarization charges with the bulk of each fluid and their common interface. These effects come into play either through bulk coupling forces, or through interfacial coupling boundary conditions between the electric fields and the fluid flow quantities. In the model we develop in this chapter, the charge relaxation process dominates charge convection which implies that the electric field is not dependent on the fluid motion and the bulk forces of electrical origin are negligible. Therefore, the field coupling occurs at the interface

as specified by the appropriate boundary conditions.

Electrohydrodynamic instability at the interface between two fluids stressed by initially perpendicular electric fields has generated considerable interest due to its wide ranging scientific and engineering applications, including static and dynamic imaging [14], [25], atmospheric electrification [22], the orientation, confinement and levitation of liquids in zero gravity [8] and the separation of living and dead cells [13]. The linear electrohydrodynamic stability of the Rayleigh-Taylor instability of two inviscid dielectric superposed fluids subjected to a normal electric field has been studied by many authors including Taylor [77], Melcher [46] and Devitt [15]. In 1969, Melcher considered the viscous Rayleigh-Taylor problem and examined the dynamic interplay of the interfacial electric shear stresses and viscous stresses [49]. The electrohydrodynamic instability of a single charge-free surface separating two semi-infinite streaming inviscid fluids influenced by a normal electric field was investigated by Elshehawey [19] and Mohammed [53]. These problems are special cases of the shear flow electrohydrodynamic stability that is considered in this chapter.

As in chapter 2, the linear stability of the flow is analysed by deriving the exact dispersion relation in terms of the Airy functions and their integrals, and solving it numerically and asymptotically to find marginal stability curves. The stability of the system depends on ten parameters including the ratio of the viscosities, the ratio of the densities, the surface tension, gravity, the ratio of the permittivities, the two conductivities, the two initial electric fields and the velocity field of the upper fluid in the unperturbed motion.

In sections 3.2 and 3.3 we formulate the stability problem and develop the dispersion relation describing the stability of the flow. In the absence of the electric fields, the dispersion relation reduces to the equivalent of the dispersion relation found in the previous chapter.

In section 3.4, we consider two specific limiting cases representing configurations

with no shear stresses of electrical origin. The first limit represents the configuration in which the lower fluid is highly conducting relative to the upper fluid so that the fluid interface is perfectly conducting and supports a free charge. An example of this configuration is the air-water interface which has important meteorological applications. The second limit on the other hand represents a class of charge interactions of purely insulating dielectrics. Here, the interface does not support any free charge and, therefore, the conduction and interface coupling is entirely due to polarization charges. This type of interaction is sometimes referred to as a dielectrophoretic phenomenon and it has applications in the orientation of cryogenic liquid propellants. For both limiting cases, we examine the effects of the initial streaming on the growth rates and we investigate the existence of instabilities exhibiting purely exponential growth.

In sections 3.5 and 3.6 we consider two limiting cases in which the electromechanical effects are dominated by electrical surface shear forces. A wide range of electrohydrodynamic applications, including electro-optical image reproduction and space propulsion [27], involve the effects of electrical shear forces. In section 3.5, as in the dielectrophoretic configurations, the electric charge relaxation times of both fluids are longer relative to the time scales of the flow. However, here the electromechanical interactions are dominated by free charges which relax to the interface. In section 3.6 we consider the opposite case where the electric charge relaxation times are very short compared to the time scales of the flow so that the charge relaxation is essentially instantaneous. We find that, generally, the principle of exchange of stability, (ie. the onset of a static instability exhibiting purely exponential growth), does not hold in the presence of initial streaming of the fluids. The stability of the flow in this limit is dominated by the ratio of the conductivities of the fluids.

In section 3.7 we present a discussion of the effects of finite electrical charge relaxation times. These effects are likely to be important in cases involving surface

free charges. Moreover, since most real fluids have some finite relaxation times, the above limiting cases are approximations only. Although these approximations have been quite successful in modelling many real systems [47], finite relaxation time effects are believed to have important implications in the modelling of electrohydrodynamic interactions involving bulk coupling of the electric fields and the fluid flow. The stability of the flow for finite charge relaxation configurations is characterized by the ratio of the conductivities and the Hartmann number which is a measure of the relative effects of electric forces and mechanical forces due to viscosity and surface tension. For large Hartmann numbers, the threshold for static instability reduces to the threshold found for the infinite charge relaxation limit. For small Hartmann numbers, it reduces to the instantaneous charge relaxation limit. In general, a non-zero Hartmann number is destabilizing. However, the effects of the ratio of the conductivities are determined by the specific configurations. Finally, concluding remarks are presented in section 3.8.

3.2 Formulation of the Problem

We consider the two dimensional flow configuration sketched in figure 3.1 of two homogenous incompressible viscous fluids of constant viscosity μ_1 and μ_2 , densities ρ_1 and ρ_2 , permittivities ϵ_1^* and ϵ_2^* and conductivities σ_1^* and σ_2^* . In the unperturbed state, the interface $y^* = 0$ where x^* and y^* are the usual Cartesian coordinates, is stressed by uniform electric fields \hat{E}_1^* and \hat{E}_2^* in the \hat{y}^* direction. Note that, as in chapter 2, subscripts 1 and 2 refer to fluid properties and fluid flow quantities above and below the interface respectively. Gravity g^* acts in the negative \hat{y}^* direction. In the unperturbed state the flow has the velocity field

$$\mathbf{u}^*(x^*, y^*) = \begin{cases} (a_1 \tilde{\omega} y^*, 0) & \text{if } y^* > 0 \\ (a_2 \tilde{\omega} y^*, 0) & \text{if } y^* < 0 \end{cases} \quad (3.1)$$

where $a_1\tilde{\omega}$ and $a_2\tilde{\omega}$ are constant vorticities above and below the interface respectively and the vorticity coefficients a_1 and a_2 are nondimensional constants.

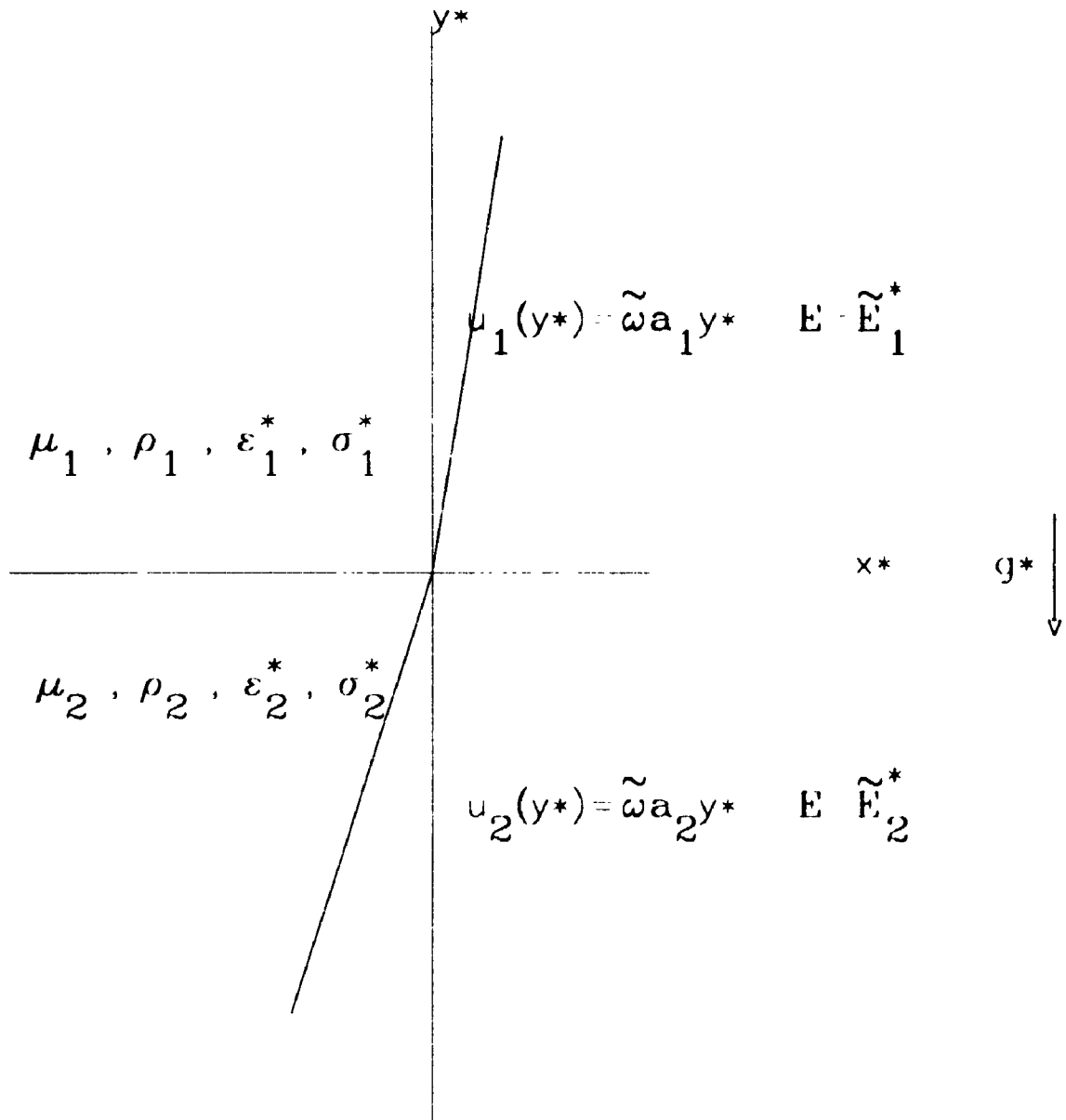


Figure 3.1: Schematic representation of the problem.

3.2.1 The Governing Equations

Since large currents are not present in this flow, the effects of magnetic inductions are negligible. Hence, the electric field \mathbf{E}^* is irrotational:

$$\nabla \times \mathbf{E}^* = 0. \quad (3.2)$$

The conservation of free charge requires that

$$\nabla \cdot \mathbf{J}^* + \frac{\partial q^*}{\partial t^*} = 0 \quad (3.3)$$

where \mathbf{J}^* is the free current density and q^* is the free charge density [71]. Since the permittivity ϵ^* is constant, the free charge density is given by

$$q^* = \epsilon^* \nabla \cdot \mathbf{E}^*. \quad (3.4)$$

The current density is the sum of the conduction, convection and diffusion currents. In this problem we neglect diffusion currents so that \mathbf{J}^* can be represented by

$$\mathbf{J}^* = \sigma^* \mathbf{E}^* + \mathbf{u}^* q^* \quad (3.5)$$

where σ^* is the electrical conductivity, which we assume to be constant, and \mathbf{u}^* is the fluid velocity vector [80]. This is known as Ohm's conduction law. Although not obeyed by all fluids, this simplest of all conduction laws has been used to successfully model a wide range of electrohydrodynamic phenomena [47], [48].

The conservation of momentum for the flow is then given by

$$\frac{\partial u^*}{\partial t^*} + u^* \frac{\partial u^*}{\partial x^*} + v^* \frac{\partial u^*}{\partial y^*} = -\frac{1}{\rho} \frac{\partial p^*}{\partial x^*} + F_{ex} + \nu \nabla^2 u^* \quad (3.6)$$

$$\frac{\partial v^*}{\partial t^*} + u^* \frac{\partial v^*}{\partial x^*} + v^* \frac{\partial v^*}{\partial y^*} = -\frac{1}{\rho} \frac{\partial p^*}{\partial y^*} - g^* + F_{ey} + \nu \nabla^2 v^*$$

and the conservation of mass is given by

$$\frac{\partial u^*}{\partial x^*} + \frac{\partial v^*}{\partial y^*} = 0 \quad (3.7)$$

where $u^*(x^*, y^*, t^*)$ is the actual fluid velocity parallel to the x^* axis, $v^*(x^*, y^*, t^*)$ is the actual velocity parallel to the y^* axis, $p^*(x^*, y^*, t^*)$ is the pressure, ν is the kinematic viscosity and $\mathbf{F}_c^* = (F_{cx}^*, F_{cy}^*)$ is the electric force density vector.

Combining equations 3.3, 3.4 and 3.7 we obtain the following equation for the conservation of electric charges in the presence of charge convection:

$$\frac{Dq^*}{Dt^*} + \frac{\sigma}{\epsilon} q^* = 0 \quad (3.8)$$

where the material derivative $\frac{D}{Dt^*} = \frac{\partial}{\partial t^*} + \mathbf{u}^* \cdot \nabla$. Hence, for every fluid particle there is a charge relaxation mechanism which forces the quantity q to relax to zero as $e^{-t/\tau}$ where $\tau = \frac{\epsilon}{\sigma}$ is the charge relaxation time associated with the relaxation of free charge density. Therefore, the free charge density in the bulk of the fluid is essentially zero regardless of the fluid motion[47].

The bulk coupling force \mathbf{F}_c^* is composed of the Coulomb force and dielectrophoric and electrorestrictive terms. It is commonly described by the general expression

$$\mathbf{F}_c^* = q^* \mathbf{E}^* - \frac{1}{2} E^{*2} \nabla \epsilon^* + \nabla \left(q^* \left(\frac{\partial \epsilon}{\partial q^*} \right)_\theta \frac{E^2}{2} \right) \quad (3.9)$$

where the subscript θ indicates an isothermal process[71].

Therefore, unless a net free charge is injected into the fluid, there is no free charge density in the bulk of the fluid so that the Coulomb force represented by the first term in the above expression is zero. Moreover, the last two terms also vanish since the fluids are assumed to be homogeneous. Consequently, the bulk coupling force \mathbf{F}_c^* is zero and the field coupling occurs only at the interface region as specified by the boundary conditions.

The electrohydrodynamic equations and the equations of motion are nondimensionalized with respect to the lower fluid as in chapter 2:

$$(\hat{x}, \hat{y}) = \left(\frac{\rho_2 \tilde{\omega}}{\mu_2} \right)^{1/2} (x^*, y^*)$$

$$(u, v) = \left(\frac{\rho_2}{\tilde{\omega} \mu_2} \right)^{1/2} (u^*, v^*)$$

$$p = \left(\frac{1}{\tilde{\omega} \mu_2} \right) p^*$$

$$g = \left(\frac{\rho_2}{\mu_2 \tilde{\omega}^3} \right)^{1/2} g^*$$

$$t = (\tilde{\omega}) t^*$$

$$E = \left(\frac{\epsilon_2^*}{\tilde{\omega} \mu_2} \right)^{1/2} E^*$$

$$\sigma = \left(\frac{1}{\tilde{\omega} \epsilon_2^*} \right) \sigma^*$$

$$\epsilon = \left(\frac{1}{\epsilon_2^*} \right) \epsilon^*.$$

Here, the nondimensionalization is performed with respect to $\tilde{\omega}$ in order to eliminate singularities at the no initial streaming limit.

We now impose small perturbations on the basic flow as follows:

$$\begin{aligned} u_i &= \hat{u}_i + u'(\hat{x}, \hat{y}, t) \\ v_i &= v'(\hat{x}, \hat{y}, t) \\ p_i &= \hat{p}_i + p'(\hat{x}, \hat{y}, t) \\ E_{xi} &= E'_{xi}(\hat{x}, \hat{y}, t) \\ E_{yi} &= \hat{E}_{yi} + E'_{yi}(\hat{x}, \hat{y}, t) \end{aligned} \tag{3.10}$$

where the tilde superscript is used to indicate quantities of the basic flow and the primed quantities denote small disturbances.

Then, by introducing equation 3.10 into equation 3.6, and by linearizing (i.e. neglecting quadratic and higher order terms in small primed quantities), we obtain a system of linear partial differential equations for the disturbances whose coefficients are only functions of \hat{y} . Therefore, the equations admit sinusoidal solutions which depend on \hat{x} and t of the following form

$$\begin{aligned}(\psi_i(\hat{x}, \hat{y}, t)) &= (\phi_i(\hat{y})) e^{i\alpha(\hat{x}-\hat{c}t)} \\(p'_i(\hat{x}, \hat{y}, t)) &= (p_i(\hat{y})) e^{i\alpha(\hat{x}-\hat{c}t)} \\(E_{r_i}(\hat{x}, \hat{y}, t)) &= (e_{r_i}(\hat{y})) e^{i\alpha(\hat{x}-\hat{c}t)} \\(E_{v_i}(\hat{x}, \hat{y}, t)) &= (e_{v_i}(\hat{y})) e^{i\alpha(\hat{x}-\hat{c}t)}\end{aligned}\tag{3.11}$$

where ψ_i are the stream functions and the real parts of these expressions are taken to obtain physical quantities. As in chapter 2, boundedness of the solutions as \hat{x} and \hat{y} go to ∞ requires the wavenumber α to be real. The wave speed $\hat{c} = \hat{c}_r + i\hat{c}_i$, represents the wave speed with an exponential growth rate \hat{c}_i .

In terms of the complex amplitudes of equations 3.11, the partial differential equations reduce to the following ordinary differential equations:

$$(D^2 - 1)^2 \phi_1 = \frac{i}{mr} \alpha^{-2} (a_1 y - c) (D^2 - 1) \phi_1\tag{3.12}$$

$$(D^2 - 1)^2 \phi_2 = i \alpha^{-2} (a_2 y - c) (D^2 - 1) \phi_2\tag{3.13}$$

$$(D^2 - 1) e_{x_i} = 0\tag{3.14}$$

$$e_{y_i} = -i D e_{x_i}\tag{3.15}$$

where $D = \frac{d}{dy}$ which indicates the derivative with respect to y , $r = \frac{\rho_2}{\rho_1}$ and the viscosity ratio $m = \frac{\mu_1}{\mu_2}$ is related to the vorticity coefficients a_1 and a_2 by the continuity of shear stress

$$m = \frac{a_2}{a_1}.\tag{3.16}$$

Note that the viscosity ratio m is the reciprocal of the viscosity ratio used in chapter 2. In order to obtain equations 3.12 to 3.15 we used the coordinate and phase speed rescaling given by

$$(x, y) = \alpha(\hat{x}, \hat{y}) \quad (3.17)$$

$$c = \alpha\hat{c}. \quad (3.18)$$

Equations 3.12 and 3.13 are equivalent to the Orr-Sommerfeld equations obtained in chapter 2. However, equations 3.14 and 3.15 are new additions obtained as a result of the introduction of electric fields. As pointed out earlier, the set of equations for the electric fields are not coupled with the equations for the stream function amplitude ϕ_i . The coupling occurs when the appropriate boundary conditions are applied.

3.2.2 Boundary Conditions

In addition to the requirement that all physical quantities must go to zero as y goes to ∞ for $i = 1$ and as y goes to $-\infty$ for $i = 2$, we must also impose interfacial boundary conditions. The kinematic condition requires that the fluids move with the common interface and that neither fluid crosses this interface. Therefore, the normal velocity of both fluids must equal the velocity of the interface whose location is described by

$$F(x, y, t) = \eta(x, t) - y = 0 \quad (3.19)$$

where the general distortion of the interface may be represented as a superposition of normal modes given by

$$\eta(x, t) = \epsilon e^{i(x-ct)} \quad (3.20)$$

where ϵ is a small parameter. The kinematic condition at the interface then implies that

$$\eta(x, t) = \frac{\phi_1(0)}{c} e^{i(x-ct)}. \quad (3.21)$$

Since both fluids move together with the interface, and since there is no slip between the fluids in the direction of flow, both the normal and the tangential velocities are continuous. The continuity of the normal velocity leads to

$$\phi_1(0) = \phi_2(0) = \phi(0). \quad (3.22)$$

Similarly, the continuity of the tangential velocities implies that

$$D\phi_1(0) - D\phi_2(0) = \frac{(a_2 - a_1)}{c} \phi(0). \quad (3.23)$$

The stress condition at the interface is a balance between the hydrodynamic pressure, the viscous stress, the surface tension and the electrical forces. It is given by [51]

$$\mathbf{n} (P_1 - P_2) = \mathbf{n} \cdot (T_1^m - T_2^m) + \mathbf{n} \cdot (T_1^e - T_2^e) \quad (3.24)$$

where \mathbf{n} is the unit normal to the interface, T^m is the stress tensor of mechanical origin and T^e is the stress tensor of electrical origin. In the absence of electric fields we have already resolved and linearized the normal and tangential components of this equation. We now incorporate the electric stress tensor which is given by [71]

$$T_{ij}^e = \epsilon E_i E_j - \frac{1}{2} \epsilon \delta_{ij} E_k E_k \quad (3.25)$$

where E_i are the components of the electric field. In the nondimensionalized form, the normal component of the stress condition at $y = \eta(x, t)$ can be written as

$$-p_1 + \frac{\rho_1}{\rho_2} g \hat{y} + 2m \frac{\partial v_1}{\partial \hat{y}} + p_2 - g \hat{y} - 2 \frac{\partial v_2}{\partial \hat{y}} = \frac{S}{R} + \frac{1}{2} (\epsilon E_{n1}^2 - E_{n2}^2) \quad (3.26)$$

where E_{n1} and E_{n2} are the normal components of the electric field, R is the nondimensionalized radius of curvature, S is a nondimensionalized surface tension given by

$$S = \left(\frac{\rho_2}{\tilde{\omega} \mu_2^3} \right)^{\frac{1}{2}} S^* \quad (3.27)$$

and ϵ is given by

$$\epsilon = \frac{\epsilon_1^*}{\epsilon_2^*}. \quad (3.28)$$

In the absence of the electric fields this equation is identical to the normal stress condition obtained in chapter 2. Therefore, by incorporating the linearized form of the electric force term above into the normal stress condition derived in chapter 2, we obtain the following coupling equation at $y = 0$

(3.29)

$$\begin{aligned}
 & i \alpha^{-2} \left(1 - \frac{1}{r}\right) (cD\phi_2(0) + a_2\phi_2(0)) \\
 & - i\alpha \left(S + \alpha^{-2} \left(1 - \frac{1}{r}\right) g\right) \left(\frac{D\phi_1(0) - D\phi_2(0)}{a_2 - a_1}\right) \\
 & = m (D^3 - 3D) \phi_1(0) - (D^3 - 3D) \phi_2(0) + \frac{i\epsilon \tilde{E}_1 e_{y1}}{\alpha} - \frac{i\tilde{E}_2 e_{y2}}{\alpha}.
 \end{aligned} \tag{3.30}$$

Similarly, the tangential component of the stress tensor can be linearized to obtain the following condition at $y = 0$

$$m \left(\frac{\partial u_1}{\partial \hat{y}} + \frac{\partial v_1}{\partial \hat{x}} \right) - \left(\frac{\partial u_2}{\partial \hat{y}} + \frac{\partial v_2}{\partial \hat{x}} \right) + \frac{\partial \eta}{\partial x} (\epsilon \tilde{E}_1^2 - \tilde{E}_1^2) + \epsilon \tilde{E}_1 e_{x1} - \tilde{E}_2 e_{x2} = 0. \tag{3.31}$$

In terms of the complex amplitudes, this reduces to

$$m(D^2\phi_1(0) + \phi_1(0)) - D^2\phi_2(0) + \phi_2(0) = \tilde{E}_2 e_{x2} - \epsilon \tilde{E}_1 e_{x1} + \frac{\phi_1(0)\alpha}{ic} (\epsilon \tilde{E}_1^2 - \tilde{E}_1^2) \tag{3.32}$$

which is another coupling equation.

Furthermore, the integration of equations 3.2 to 3.5 across the interface yields the following conditions

$$\mathbf{n} \times (\mathbf{E}_1 - \mathbf{E}_2) = 0 \tag{3.33}$$

$$\mathbf{n} \cdot (\sigma_1 \mathbf{E}_1 - \sigma_2 \mathbf{E}_2) + \nabla_{\Sigma} \cdot (q^* \mathbf{v}) + \frac{\partial q^*}{\partial t^*} = 0 \tag{3.34}$$

$$q^* = \mathbf{n} \cdot (\epsilon \mathbf{E}_1 - \mathbf{E}_2) \tag{3.35}$$

where $\nabla_{\Sigma} \cdot (q^* \mathbf{v})$ is the surface divergence of the current density $q^* \mathbf{v}$. These equations along with the stress conditions provide the coupling mechanism between the fluid

flow quantities and the electrical quantities. In linearized form they can be written as

$$e_{x1} - e_{x2} = \frac{\phi_1(0)\alpha P}{ic} \quad (3.36)$$

$$\sigma_1 e_{y1} - \sigma_2 e_{y2} + \alpha i Q D \phi_1 = \frac{\partial e_{y2}}{\partial t} - \epsilon \frac{\partial e_{y1}}{\partial t} \quad (3.37)$$

where

$$P = \tilde{E}_1 - \tilde{E}_2 \quad (3.38)$$

and

$$Q = \epsilon \tilde{E}_1 - \tilde{E}_2. \quad (3.39)$$

3.3 The Dispersion Relation

As discussed in chapter 2, equations 3.12 and 3.13 can be solved exactly in terms of the Airy functions [16]. In order to solve the eigenvalue problem given in the last section we make the following changes of variables:

$$\begin{aligned} z_1 &= m^{-1/3} a_1^{1/3} r^{-1/3} \alpha^{-2/3} e^{-i\pi/2} \left(y - \frac{c}{a_1} - i\alpha^2 r m a_1 - 1 \right) \\ z_2 &= \alpha^{-2/3} a_2^{1/3} e^{-i\pi/2} \left(y - \frac{c}{a_2} - i\alpha^2 a_2^{-1} \right) \\ \xi_i(z_i) &= (1 - D^2) \phi_i(y). \end{aligned} \quad (3.25)$$

Hence, ξ_i represents the complex amplitude of the disturbance vorticity. Then, in terms of ξ_i , equations 3.12 and 3.13 become

$$\frac{d^2 \xi_1}{dz_1^2} - z_1 \xi_1 = 0 \quad (3.40)$$

$$\frac{d^2 \xi_2}{dz_2^2} - z_2 \xi_2 = 0. \quad (3.41)$$

These equations are in the form of the Airy equation and therefore their solutions are given by

$$\xi_1 = b_1 Ai(z_1) + c_1 Ai(z_1 e^{\theta_1}) \quad (3.42)$$

$$\xi_2 = b_2 Ai(z_2) + c_2 Ai(z_2 e^{\theta_2}) \quad (3.43)$$

where Ai denotes the Airy function and $\theta_i = 2\pi/3$ or $-2\pi/3$ [1]. Then, the boundary conditions at ∞ imply that the vorticities must tend to zero as $y \rightarrow \infty$ or as $y \rightarrow -\infty$, so that $b_1 = b_2 = 0$, $\theta_1 = 2\pi/3$ and $\theta_2 = -2\pi/3$. Therefore,

$$\xi_1 = c_1 A_1(y) \quad (3.44)$$

$$\xi_2 = c_2 A_2(y) \quad (3.45)$$

where

$$A_1(y) = Ai\left(z_1 e^{\frac{2\pi}{3}}\right) = Ai\left(m^{-1/3} a_1^{1/3} r^{-1/3} \alpha^{-2/3} \left(y - \frac{c}{a_1} - i\alpha^2 r m a_1^{-1}\right) e^{i\pi/6}\right)$$

$$A_2(y) = Ai\left(z_2 e^{-\frac{2\pi}{3}}\right) = Ai\left(a_2^{1/3} \alpha^{-2/3} \left(y - \frac{c}{a_2} - i\alpha^2 a_2^{-1}\right) e^{5i\pi/6}\right).$$

Consequently, we obtain the following equations for ϕ_1 and ϕ_2 :

$$(D^2 - 1)\phi_1 = c_1 A_1(y) \quad (3.46)$$

$$(D^2 - 1)\phi_2 = c_2 A_2(y). \quad (3.47)$$

After solving these second order linear differential equations with the boundary conditions at infinity we obtain the following expressions for the stream functions:

$$\phi_1 = c_3 e^{-y} + c_1 \left(e^{-y} \int_0^y e^s A_1(s) ds + e^y \int_y^\infty e^{-s} A_1(s) ds \right) \quad (3.48)$$

$$\phi_2 = c_4 e^y + c_2 \left(e^y \int_0^y e^{-s} A_2(s) ds + e^{-y} \int_y^{-\infty} e^s A_2(s) ds \right) \quad (3.49)$$

where c_3 and c_4 are constants.

Similarly, by solving 3.14 and 3.15 with conditions at ∞ we obtain

$$e_{x1} = c_5 e^{-y} \quad (3.50)$$

$$e_{x2} = c_6 e^y \quad (3.51)$$

$$e_{y1} = i c_5 e^{-y} \quad (3.52)$$

$$c_{y_2} = -ic_6 e^y. \quad (3.53)$$

Finally, applying the remaining six boundary conditions given by the equations (3.19) through (3.24), we obtain six linear equations for the six unknown constants c_1, c_2, c_3, c_4, c_5 and c_6 . The linear homogenous system of equations can then be written as

$$\mathbf{A}\mathbf{h} = 0 \quad (3.54)$$

where $\mathbf{h}^T = (c_3, c_4, c_1, c_2, c_5, c_6)$ and where the matrix \mathbf{A} is given by

$$\mathbf{A} = \begin{pmatrix} 1 & -1 & J_1 & J_2 & 0 & 0 \\ -1 + \frac{a_1}{c} & -1 - \frac{a_2}{c} & \left(1 + \frac{a_1}{c}\right) J_1 & \left(-1 + \frac{a_2}{c}\right) J_2 & 0 & 0 \\ \phi_{3,1} & -2 & \phi_{3,3} & (-2J_2 + 2A_2) & \frac{\epsilon \tilde{E}_1}{\alpha} & \frac{-\tilde{E}_2}{\alpha} \\ \phi_{4,1} & \phi_{4,2} & \phi_{4,3} & \phi_{4,4} & \frac{\epsilon \tilde{E}_1}{\alpha} & \frac{\tilde{E}_2}{\alpha} \\ \frac{\alpha P i}{c} & 0 & \frac{\alpha P J_1 i}{c} & 0 & 1 & -1 \\ -i\alpha Q & 0 & i\alpha J_1 Q & 0 & c\alpha + i\sigma_1 & c + i\sigma_2 \end{pmatrix}.$$

Here

$$\begin{aligned}
\phi_{3,1} &= 2m + \frac{i(\epsilon \tilde{E}_1^2 - \tilde{E}_2^2)}{c} \\
\phi_{3,3} &= m(2J_1 - 2A_1) + \frac{i(\epsilon \tilde{E}_1^2 - \tilde{E}_2^2)}{c} \\
\phi_{4,1} &= 2m - \frac{i\alpha}{a_2 - a_1} \left(S + \alpha^{-2} \left(1 - \frac{1}{r} \right) g \right) \\
\phi_{4,2} &= 2 - \frac{i\alpha}{a_2 - a_1} \left(S + \alpha^{-2} \left(1 - \frac{1}{r} \right) g \right) + i\alpha^{-2} \left(1 - \frac{1}{r} \right) (c - a_2) J_2 \\
\phi_{4,3} &= -2m(J_1 + A'_1) + \frac{i\alpha J_1}{a_2 - a_1} \left(S + \alpha^{-2} \left(1 - \frac{1}{r} \right) g \right) \\
\phi_{4,4} &= 2(J_2 - A'_2) - \frac{i\alpha J_2}{a_2 - a_1} \left(S + \alpha^{-2} \left(1 - \frac{1}{r} \right) g \right) + i\alpha^{-2} \left(1 - \frac{1}{r} \right) (a_2 + c)
\end{aligned} \tag{3.41}$$

and

$$\begin{aligned}
J_1 &= \int_0^\infty e^{-s} A_1(s) ds \\
J_2 &= \int_0^\infty e^{-s} A_2(-s) ds \\
A_1 &= A_1(0) \\
A_2 &= A_2(0) \\
A'_1 &= \left. \frac{dA_1(y)}{dy} \right|_{y=0} \\
A'_2 &= \left. \frac{dA_2(y)}{dy} \right|_{y=0}.
\end{aligned} \tag{3.42}$$

For a non-trivial solution of equation 3.40 we require the determinant of \mathbf{A} to vanish. This gives the following dispersion relation relating the eigenvalues c and the nondimensional quantities $\alpha, m, r, g, S, \epsilon, \sigma_1, \sigma_2, \tilde{E}_1$ and \tilde{E}_2 :

$$F(\alpha, c, a_1, m, r, g, S, \epsilon, \sigma_1, \sigma_2, \tilde{E}_1, \tilde{E}_2) = 0 \tag{3.55}$$

where

$$F = F_1 + \frac{F_2}{c} + \frac{PF_3 + iQF_4}{c(\epsilon + 1) + i(\sigma_1 + \sigma_2)} + \frac{(\epsilon \tilde{E}_1^2 - \tilde{E}_2^2)}{c} F_5 \quad (3.56)$$

and

$$\begin{aligned} F_1 = & 2(m-1)J_1(A_2 + A'_2) + 2m(A'_1A_2 - A'_2A_1) + 2m(m-1)(A'_1 - A_1)J_2 \\ & + 4(1-m)^2J_1J_2 + i(1 - \frac{1}{r})\alpha^{-2}((2(m-1)J_1J_2 + (c+a_2)A_2J_1 \\ & + (a_1-c)A_1J_2)) \end{aligned}$$

$$\begin{aligned} F_2 = & 2(a_2 - a_1)m(J_1A_2 + A_1J_2) - i\alpha(S + \alpha^{-2}(1 - \frac{1}{r})g)(mJ_2A_1 + J_1A_2) \\ & + m(a_2 - a_1)A'_1A_2 - m(a_2 - a_1)A'_2A_1 \end{aligned}$$

$$\begin{aligned} F_3 = & (A_2J_1 + mA_1J_2) \left(\frac{\dot{E}_2\sigma_1 - \sigma_2\dot{E}_1}{c} + i\epsilon P \right) + (mA'_1J_2 + A'_2J_1 \\ & + 2(m-1)J_1J_2 + i\epsilon\alpha^{-2}(1 - \frac{1}{r})J_1J_2) \left(\frac{\epsilon\tilde{E}_1\sigma_2 + \tilde{E}_2\sigma_1}{c} - i\epsilon(\tilde{E}_1 + \tilde{E}_2) \right) \end{aligned}$$

$$\begin{aligned} F_4 = & \left(\left(1 + \frac{a_2 - a_1}{c} \right) J_1A_2 + 2(m-1)J_1J_2 - mJ_2A_1 \right) (\epsilon\dot{E}_1 + \dot{E}_2) \\ & - Q \left(\left(1 + \frac{a_2 - a_1}{c} \right) A'_2J_1 + \frac{i\alpha S + \alpha^{-1}(1 - \frac{1}{r})g}{c} J_1J_2 - \frac{2(a_2 - a_1)}{c} J_1J_2 \right. \\ & \left. - mA'_1J_2 - ia_1\alpha^{-2}(1 - \frac{1}{r})J_1J_2 - i\frac{\epsilon\tilde{E}_1^2 + \tilde{E}_2^2}{c} J_1J_2 \right) \end{aligned}$$

$$F_5 = i(A'_2J_1 + mA'_1J_2 + 2(m-1)J_1J_2) - \alpha^{-2}(1 - \frac{1}{r})J_1J_2c.$$

Note that, in the limit of no electric fields, this equation reduces to the dispersion relation discussed in chapter 2 and, in the limit of no initial streaming, it reduces to the dispersion relation discussed in reference [49].

To analyze the stability of this problem we investigate the dependence of the eigenvalues c on the various stability parameters. Since the effects of m , r , g and S have been studied in the previous chapter, we will examine the solutions of this dispersion relation and investigate the stability of the flow with respect to the electrical stability

parameters such as ϵ, σ_i and \hat{E}_i in the following sections.

3.4 Free Charge (EH-If) and Polarization Charge (EH-Ip) Configurations

In this section we consider two configurations, each representing a specific type of charge interaction phenomena, in which there are no shear stresses of electrical origin. Regardless of interfacial deformations, the surface forces of electrical origin always act perpendicular to the interface in these important classes of interactions. The physical mechanisms of the interactions are discussed in reference [46].

The free charge configurations (EH-If) represent the limiting cases in which the fluid interface is perfectly conducting and supports a free charge Q which may be induced on a conducting film at the interface by externally applied electric fields. In practice, this configuration represents cases in which one fluid has much greater conductivity than the other. If the lower fluid is highly conducting relative to the upper fluid, then the electric field is confined to region 1 and $\hat{E}_2 = 0$. An important example of this case is the air-water interface which has attracted so much interest due to its meteorological applications [22]. In this limit, the dispersion relation reduces to

$$F_1 + \frac{F_2}{c} + \frac{c\hat{E}_1^2(A_2J_1 + mA_1J_2)}{c}. \quad (3.57)$$

In contrast, in the polarization charge configuration (EH-Ip), sometimes termed dielectrophoretic phenomenon [60], there is no free charge on the interface ($Q=0$). Therefore, there are no effects of free charge and hence of conduction and the coupling is entirely due to polarization. Furthermore, both fluids are perfectly insulating so that the fluid motions occur in relatively shorter time scales compared to the electric charge relaxation times which are given by

$$\tau_1 = \frac{\epsilon}{\sigma_1}$$

$$\tau_2 = \frac{1}{\sigma_2}. \quad (3.58)$$

In our stability analysis where we assumed an instability dynamics of the form $e^{i(x-ct)}$, this limit requires that $\tau c \gg 1$. As in the (EH-If) case, the interface represented by this configuration does not support any tangential electric stress. In addition to its application in the separation of living and dead cells [13] and in understanding ferrohydrodynamic phenomena in ferrofluids [66], this class of polarization interaction has important applications because of its possibilities for solving orientation problems of cryogenic liquid propellants in the zero-gravity environment of space [8]. The electric field is used to replace the influence of gravity. The dispersion relation in this case reduces to

$$k_1 + \frac{k_2}{c} + \frac{i\tilde{E}_1\tilde{E}_2(1-\epsilon)^2(A_2J_1 + mA_1J_2)}{(\epsilon+1)c}. \quad (3.59)$$

Equations 3.57 and 3.59 are analogous to equations (20) and (22) respectively in reference [49]. The latter equations were obtained by assuming that there is no initial streaming of the fluids. In general, the dispersion relations cannot be solved analytically. However, as in chapter 2, we can obtain an asymptotic expression for c as $\alpha \rightarrow \infty$. Following the asymptotic methods described in chapter 2 we assume that

$$c = c_0\alpha + c_1 + c_2\alpha^{-1} + o(\alpha^{-1}). \quad (3.60)$$

Then the Airy functions and their integrals can be approximated by

$$\begin{aligned} \frac{A'_1}{A_1} &= -1 + \frac{ic_0}{2mr\alpha} + \frac{(4rc_1i - c_0^2 - 2a_1ri)}{8mr^2\alpha^2} \\ \frac{A'_2}{A_2} &= 1 - \frac{ic_0}{2\alpha} - \frac{(4c_1i - c_0^2 + 2a_2i)}{8\alpha^2} \\ \frac{J_1}{A_1} &= \frac{1}{2} + \frac{ic_0}{8r\alpha} + \frac{(2rc_1i - c_0^2 - 2a_1ri)}{16mr^2\alpha^2} \\ \frac{J_2}{A_2} &= \frac{1}{2} + \frac{ic_0}{8\alpha} + \frac{(2c_1i - c_0^2 + 2a_2i)}{16\alpha^2}. \end{aligned} \quad (3.61)$$

Substituting these approximations in the dispersion relations we obtain the following

expressions for the coefficients c_i

$$c_0 = -\frac{iS}{2(1+m)} \quad (3.62)$$

$$c_1 = i\frac{\Gamma^\epsilon}{2(1+m)} - \frac{3}{16}\frac{i(1+r^{-1})S^2}{(1+m)^3} \quad (3.63)$$

$$c_2 = -g\frac{(1-r^{-1})i}{2(1+m)} + \frac{3}{8}\frac{(1+r^{-1})i\Gamma^\epsilon S}{(1+m)^3} + \frac{(-5a_1 - 3ma_1 + 3ra_2 + 5ma_2r)S}{8r(1+m)^3} \\ - \frac{i(r^2 + 20mr^2 + 20m + m^2 + 34rm)S^3}{128m(1+m)^5r^2} \quad (3.64)$$

where

$$\Gamma^\epsilon = \begin{cases} \epsilon \dot{E}_1^2 & \text{for the EH-Ir case} \\ \frac{\dot{E}_1 \dot{E}_2 (1-\epsilon)^2}{(\epsilon+1)} & \text{for the EH-Ip case.} \end{cases} \quad (3.65)$$

In the absence of the electric fields, the above expression for the eigenvalue c is equivalent to what was obtained in chapter 2. Clearly, the effect of the electric field represented by the quantity Γ^ϵ is to destabilize the interface. If the heavier fluid is on the bottom such that gravity stabilizes the system as the electric field is raised, then there is a critical value when the interface first becomes unstable. For the EH-Ip configuration Γ^ϵ vanishes when $\epsilon = 1$. This is to be expected, since polarization is characterized by the presence of permittivity gradients at the interface. In this order of approximation, the term consisting of the initial streaming coefficients a_1 and a_2 is purely real so that, in the short wavelength limit, the initial streaming does not have any effect on the stability of the flow. If these coefficients are large, then we must obtain higher order terms in order to determine the effects of the initial streaming for short wavelength instabilities.

Similarly, in the long wavelength limit, asymptotic analyses yield

$$c = -\frac{(r-1)g}{ra_2 - a_1} - \frac{(a_1 + a_2)^2 (r-1)^2 \sqrt{mr} (i-1) \alpha}{\sqrt{2} (ra_2 - a_1)^{\frac{3}{2}} (1+r)^{\frac{1}{2}} (\sqrt{m} + \sqrt{r})} + o(\alpha). \quad (3.66)$$

Therefore, in the long wavelength limit, the growth rate of the instabilities is determined by inertia terms only. In general, the electric field does not affect the stability

behaviour of the flow.

3.4.1 The Principle of Exchange of Stabilities

As discussed in chapter 2, for a given set of stability parameters, the temporal evolution of each disturbance mode is governed by the sign of the imaginary part of c , c_i . If $c_i < 0$ for all wavenumbers, the disturbances decay exponentially and the flow is classified as stable. On the other hand, if $c_i > 0$ for any wavenumber, then the flow is classified as unstable. The marginal state then separates the stable and the unstable modes of disturbances. In the marginal states, two different behaviours are observed depending on whether c_r is zero or not. If the marginal state is represented by $c = 0$, then it is characterized by static instability and the disturbances grow monotonically. Here, we say that the *the principle of exchange of stability* is valid. If the marginal state corresponds to $c = c_r$ where c_r is non-zero, then the instability will develop in the form of oscillations of increasing amplitude. This is called *over stability*.

We now consider the possibility that the marginal states of the above limiting cases of our problem are characterized by static instability. Therefore, as $c \rightarrow 0$ in equations 3.57 and 3.59 we obtain the following conditions for the incipience of static instability for the (EH-II) charge configuration

$$\alpha^2 - \frac{\epsilon \dot{E}_1^2}{S} \alpha + \alpha^{*2} + i(a_2 - a_1) \frac{a_{12}}{S} \alpha = 0 \quad (3.67)$$

where

$$a_{12} = \frac{m(2J_1 A_2 + 2A_1 J_2 + A_1' A_2 - A_2' A_1)}{(A_2 J_1 + m A_1 J_2)} \quad (3.68)$$

and

$$\alpha^{*2} = \frac{(1 - \frac{1}{r})g}{S}. \quad (3.69)$$

Similarly, for the (EH-Ip) configuration we obtain the following condition

$$\alpha^2 - \frac{\dot{E}_1 \dot{E}_2 (1 - \epsilon)^2}{(\epsilon + 1)S} \alpha + \alpha^{*2} + i(a_2 - a_1) \frac{a_{12}}{S} \alpha = 0 \quad (3.70)$$

where the Airy functions are evaluated with $c = 0$ in their argument.

In the absence of initial streaming, $a_1 = a_2 = 0$ so the a_{12} term in the above equation does not make any contribution. In this case, the minimum electric fields required for the incipience of instability obtained from equations 3.67 and 3.70 are

$$\hat{E}_1^* = \left(\frac{2\alpha^* S}{\epsilon} \right)^{\frac{1}{2}} \quad (3.71)$$

for the (EH-If) case and

$$P^* = \left(\frac{2\alpha^* S(1 + \epsilon)}{\epsilon} \right)^{\frac{1}{2}} \quad (3.72)$$

for the (EH-Ip) case. When the electric field is raised to these critical values, the first unstable mode occurs at the critical wavenumber α^* . This is consistent with the result found by [49].

However, in the presence of initial streaming, the a_{12} term does not vanish and the principle of exchange of stability is valid only if $\text{Real}(a_{12}) \rightarrow 0$. If the incipience of instability occurs at large values of α , then by utilizing the asymptotic expressions 3.61 we obtain the following condition for the exchange of stabilities

$$\alpha^3 - \Gamma^* \alpha^2 + \alpha^{*2} \alpha - a_1^2 V = 0 \quad (3.73)$$

where

$$V = \frac{(1 - m)(1 - m^2 r)}{S(1 + m)r}. \quad (3.74)$$

If $\frac{a_1}{\alpha^*}$ is small, then the incipience of static instability occurs at

$$\hat{\alpha} = \alpha^* - \frac{a_1^2 V}{\alpha^{*2}} + o\left(\left(\frac{a_1}{\alpha^*}\right)^2\right) \quad (3.75)$$

and the corresponding critical electric fields will be

$$\hat{E}_1 = \hat{E}_1^* - \frac{\hat{E}_1^* (\alpha^* - \hat{\alpha})}{4\alpha^*} \quad (3.76)$$

for the (EH-If) case and

$$\hat{P}^* = P^* - \frac{P^* (\alpha^* - \hat{\alpha})}{4\alpha^*} \quad (3.77)$$

for the (EH-1p) case. Therefore, if V is positive, then the critical electric fields required for the incipience of static instability are reduced by the initial streaming and the instability occurs at a lower wavenumber $\hat{\alpha}$.

Figures 3.2 and 3.3 are examples of the marginal stability curves for the (EH-1f) and (EH-1p) configurations respectively. In both cases, $\alpha^* = \sqrt{20}$, $m = 0.5$, $a_1 - a_2 = 0.5$, and $V = 0.83$. In the absence of the applied electric fields the flow is stable. The curves are computed using the numerical procedures described in the last chapter. Since α^* is large, the effect of the initial streaming is small as discussed above. This is demonstrated in figure 3.2 where, as the electric field is increased, equation 3.75 predicts instability to occur at $\frac{\alpha}{\alpha^*} = 0.991$. The critical values of the electric fields corresponding to this wavenumber are 0.861, 0.944 and 1.056 for $\epsilon = 1.2$, $\epsilon = 1.0$ and $\epsilon = 0.8$ respectively. Even in the presence of such moderate initial streaming, the agreement between the computed critical values and the predicted values is quite remarkable. Similarly, in figure 3.3, the critical electric fields 1.417 and 1.280 corresponding to $\epsilon = 0.8$ and $\epsilon = 1.2$ respectively, predicted by equation 3.77, are in close agreement with the computed curve. Furthermore, for values of α exceeding 1.0, the numerically computed curves match the hyperbolas described by equations 3.67 and 3.70.

Finally, the destabilizing effects of the initial streaming for positive V are demonstrated in figure 3.4. As $a_1 - a_2$ increases, the configurations become more and more unstable until the flow becomes unstable even in the absence of the electric field. Figure 3.4 depicts $a_1 - a_2$ and the electric field required for a marginal state for the disturbance of wavenumber α^* . As the initial streaming increases, the electric field required for destabilizing α^* goes to zero. Furthermore, figure 3.5 demonstrates that, as $a_1 - a_2$ increases, the real part of c corresponding to the marginal state at α^* becomes non-zero. Consequently, there is no exchange of stability and 3.67 and 3.70 are not valid.

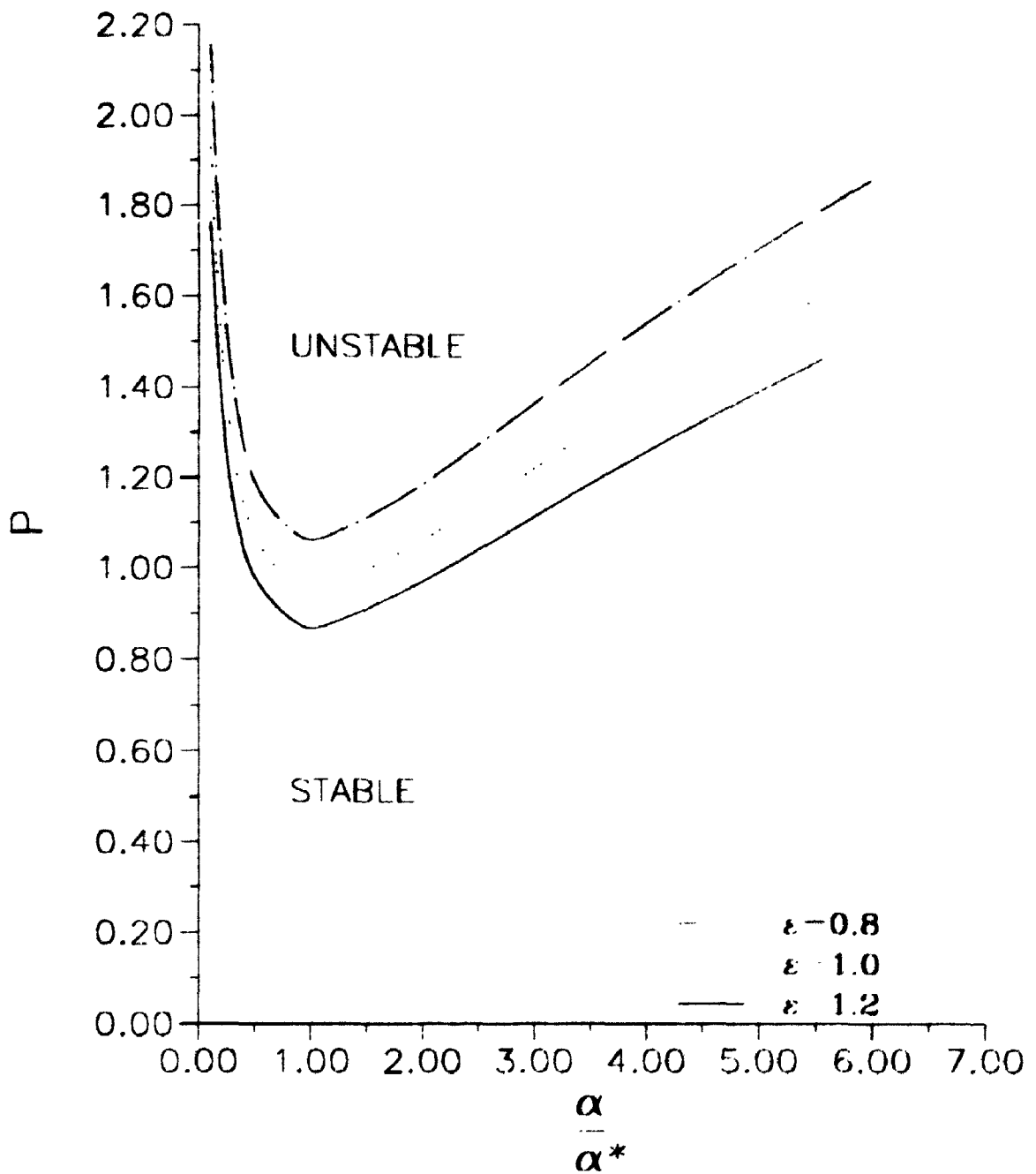


Figure 3.2: Marginal stability curves for the EH-If configuration with $\alpha^* = 4.47$, $a_1 - a_2 = 0.5$ and $V = 0.83$

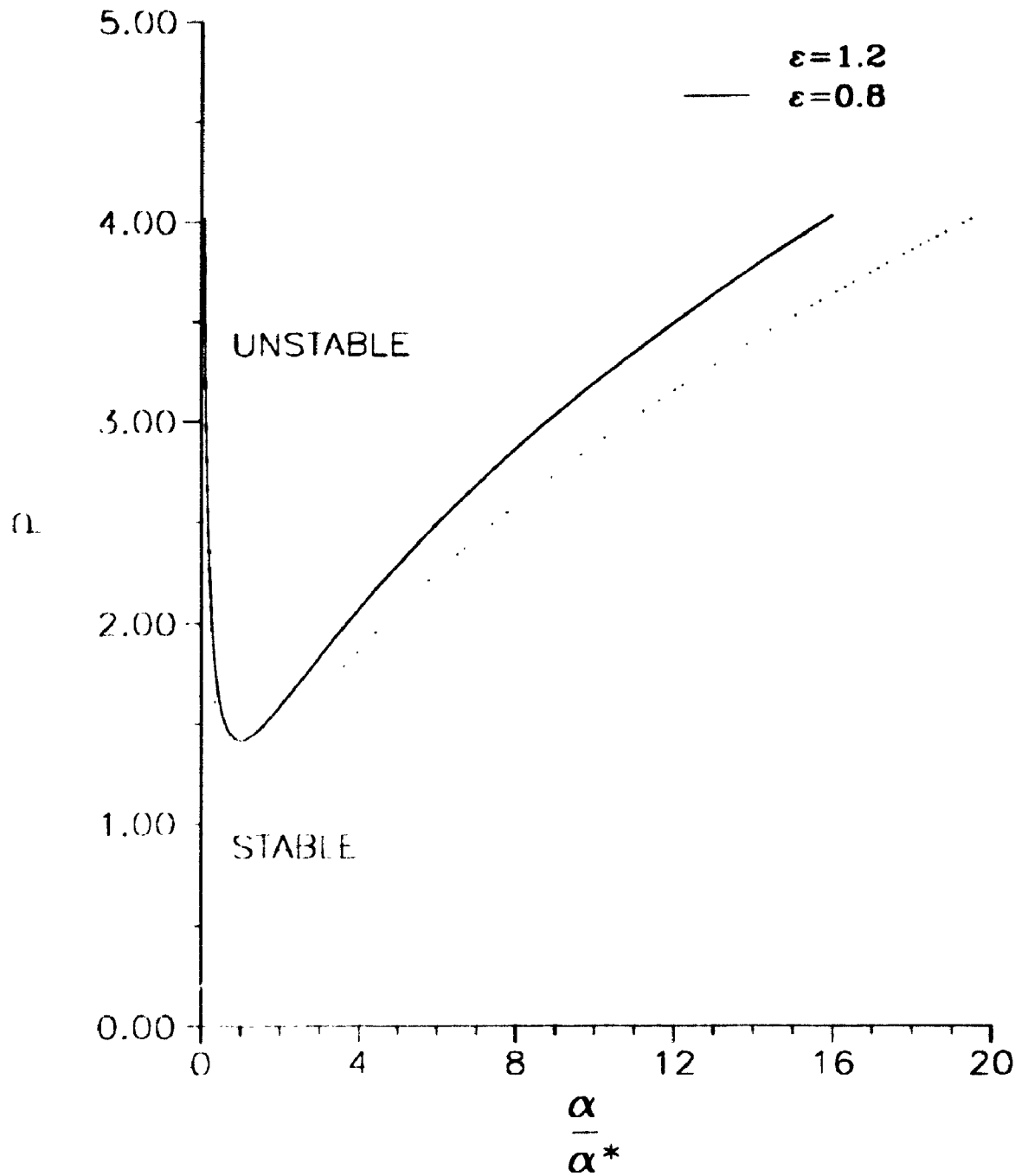


Figure 3.3: Marginal stability curves for the EH-1p configuration with $\alpha^* = 4.47$, $a_1 - a_2 = 0.5$ and $V = 0.83$

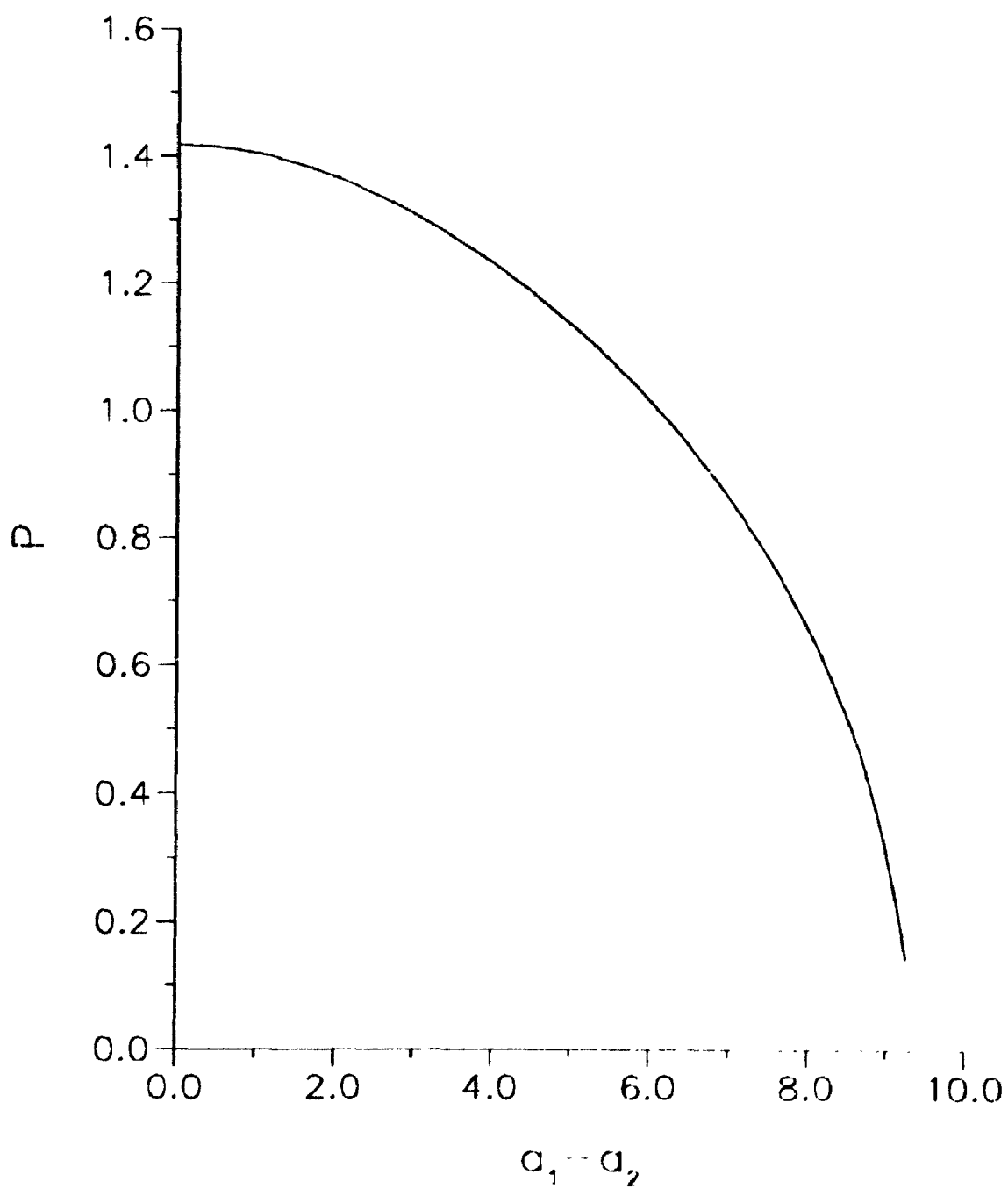


Figure 3.4: Electric field required to destabilize $\alpha^* = 4.47$ as a function of $a_1 - a_2$

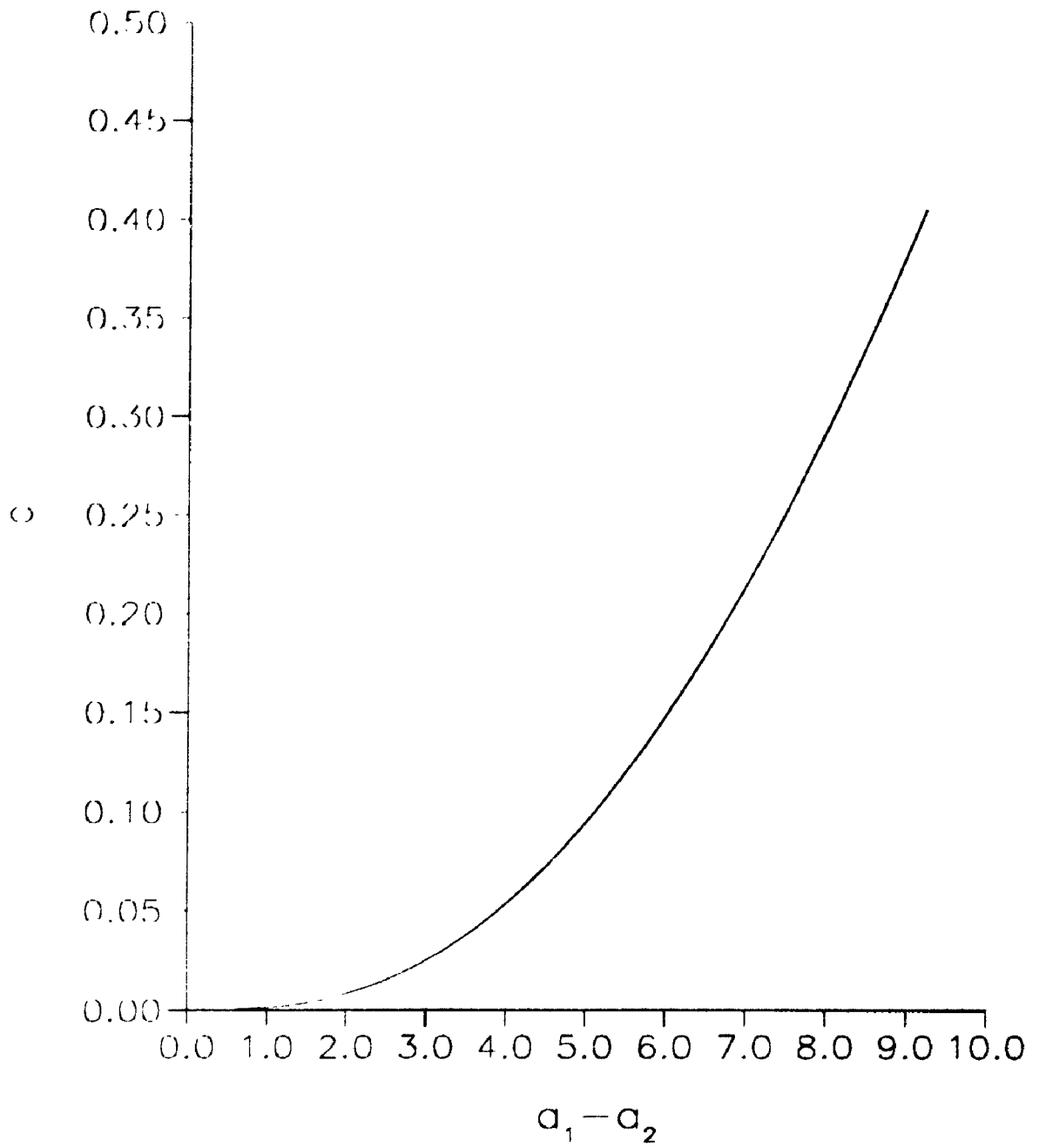


Figure 3.5: Real part of c for marginal stability at $\alpha^* = 4.47$ as a function of $a_1 - a_2$

3.5 Infinite Electric Charge Relaxation Limit

Here we consider the limit in which the relaxation times of both fluids are very long compared to the time scales of the flow and in which the equilibrium surface charge Q is non-zero. Unlike the limiting cases discussed in the previous section, here interfacial electrical stresses are present and dominate the surface interactions. A wide range of applications including static and dynamic image reproduction and space propulsion, involve electrical relaxation and electrical shear effects [27]. In this limit, the dispersion relation reduces to

$$F = F_1 + \frac{F_2}{c} + \frac{P\hat{F}_3 + iQF_4}{c(\epsilon + 1)} + \frac{(\epsilon\hat{E}_1^2 - \hat{E}_2^2)}{c}F_5 \quad (3.78)$$

where \hat{F}_3 is the same as F_3 with $\sigma_1 = 0$ and $\sigma_2 = 0$. In the limit where $c \rightarrow 0$, the above expression further reduces to

$$\alpha^2 - \frac{\epsilon\hat{E}_1^2 + \hat{E}_2^2}{S}\alpha + \alpha^{*2} + i(a_2 - a_1)\frac{b_{12}}{S}\alpha = 0 \quad (3.79)$$

where

$$b_{12} = \epsilon\hat{E}_1 + \hat{E}_2 - (A'_2 - 2J_2)Q. \quad (3.80)$$

Therefore, in general, an exchange of stabilities is not possible in the presence of initial streaming.

If there is no initial streaming of the fluids, then the principle exchange of stability holds and the marginal stability curves are given by

$$\alpha^2 - \frac{\epsilon\hat{E}_1^2 + \hat{E}_2^2}{S}\alpha + \alpha^{*2} = 0. \quad (3.81)$$

Therefore, the minimum electric fields for the incipience of instability must satisfy the relation

$$\epsilon\hat{E}_1^2 + \hat{E}_2^2 = 2\alpha^*S. \quad (3.82)$$

In terms of P and Q this condition is given by

$$\epsilon P^2 + Q^2 - \frac{4\epsilon PQ}{1 + \epsilon} = \frac{2\alpha^*S(1 - \epsilon)^2}{1 + \epsilon} \quad (3.83)$$

which is equivalent to the expression (32) of [49]. For any value of ϵ , equation 3.83 represents a rotated ellipse on the $P - Q$ plane. For values of P and Q inside this ellipse the flow is always stable. However, P and Q values outside the ellipse represent unstable configurations.

For a configuration with $\alpha^* = \sqrt{20}$, $S = 0.1$, $a_1 - a_2 = 0.05$, $\epsilon = 0.8$ and an equilibrium surface charge of 0.14, equation 3.83 yields the minimum value of P required for the onset of static instability to be about 0.32. Figure 3.6 depicts the marginal stability curves for two different values of Q . The curves are computed using the numerical procedure and they are consistent with the predicted analytical values for the critical values of α and P for the incipience of static instability.

As discussed above, however, in the presence of initial motion the induced instability is not necessarily static and the predicted critical values are not valid. Figure 3.7 demonstrates this case where we have the same configuration as in figure 3.6 but where $a_1 - a_2 = 1.25$ instead of 0.05. The critical values of α and P are $0.21\alpha^*$ and 0.203 respectively which are considerably smaller than the predicted values of α^* and 0.32 respectively in the no initial streaming limit.

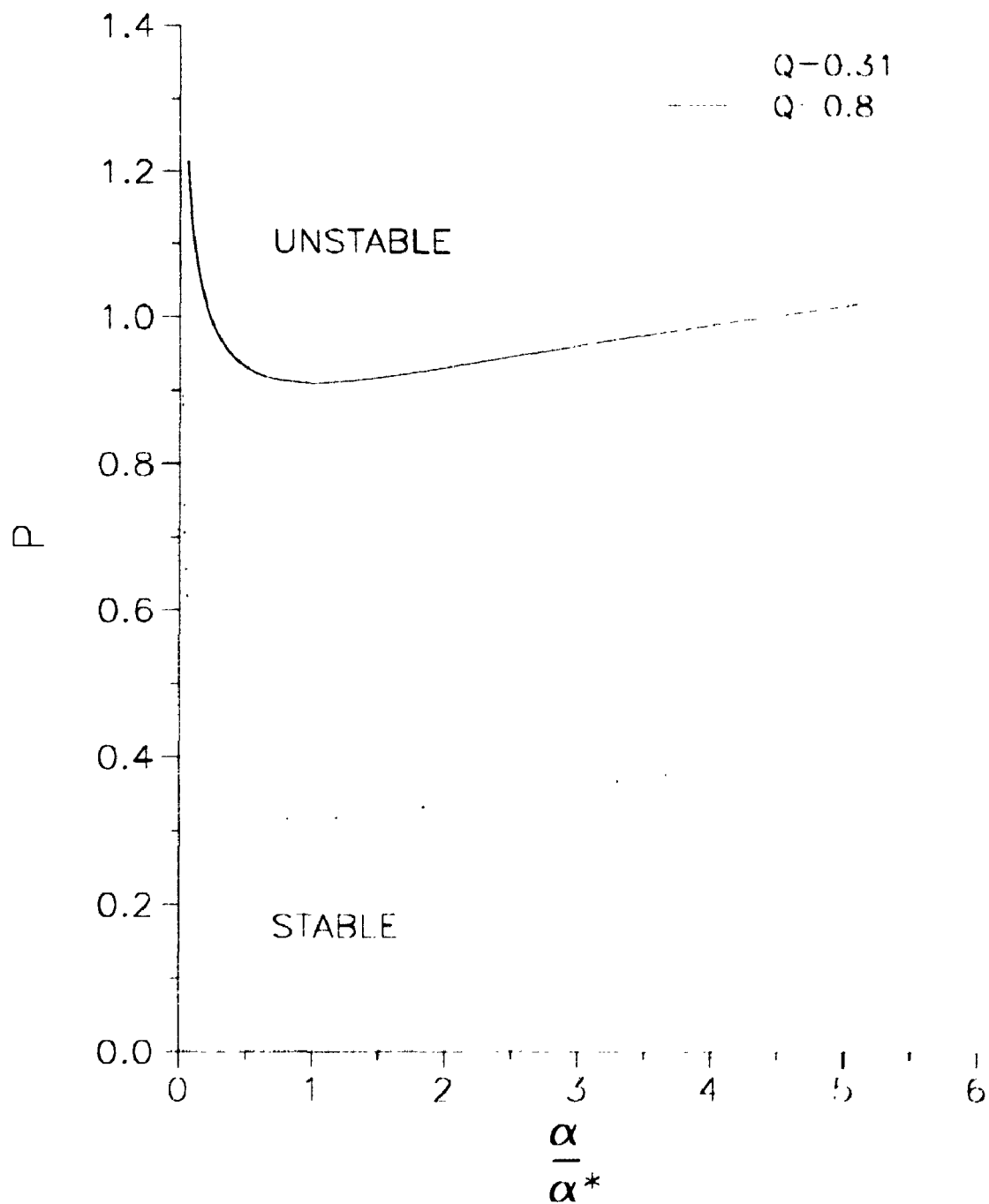


Figure 3.6: Marginal stability curves for the infinite charge relaxation limit with $a_1 - a_2 = 0.05$

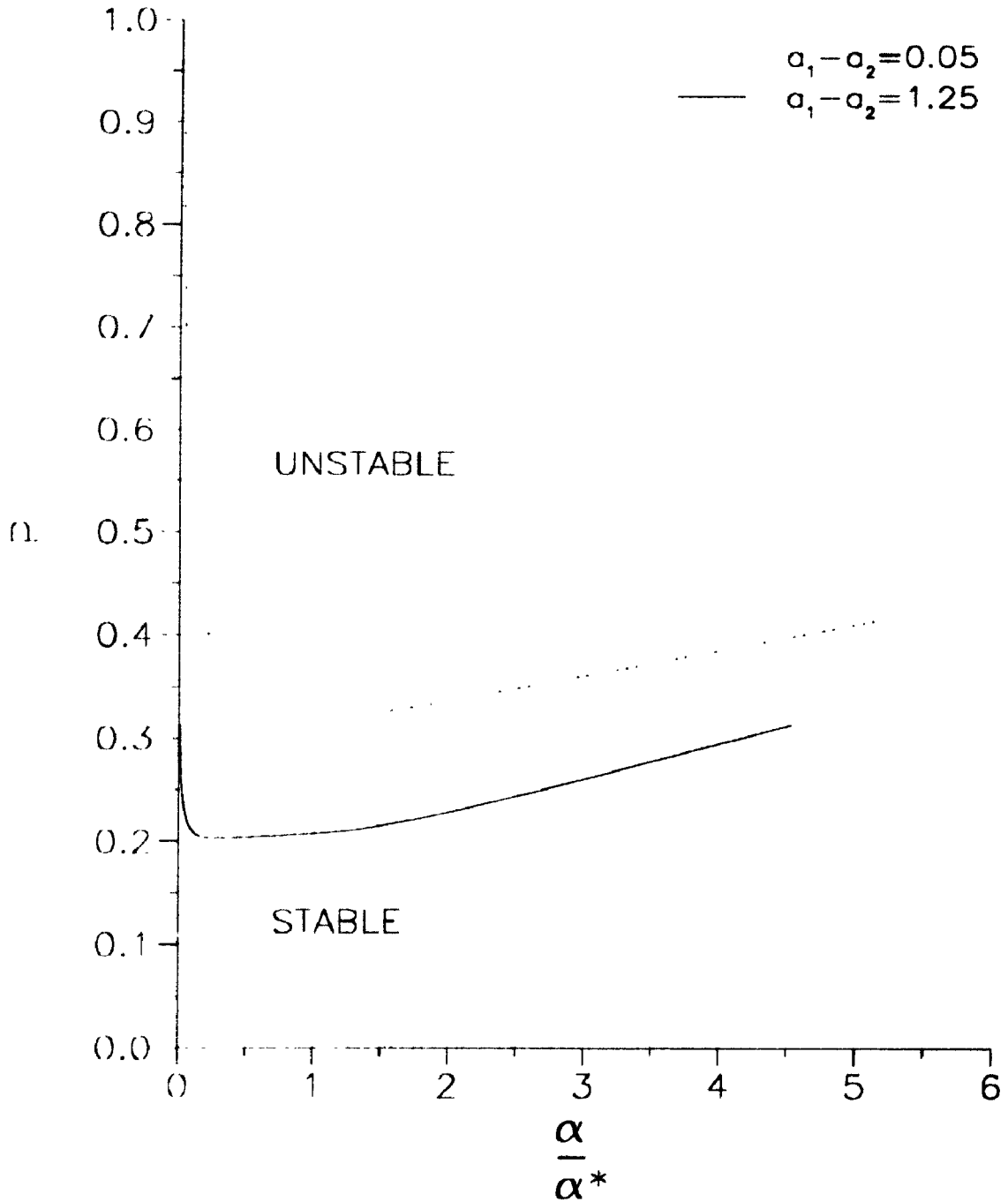


Figure 3.7: Marginal stability curves for the infinite charge relaxation limit with $q=0.31$

3.6 Instantaneous Charge Relaxation Limit

In this section we consider another limiting case involving shear stresses of electrical origin. In contrast to the limiting case discussed in the previous section, here the electric charge relaxation times of both fluids are very short compared to the mechanical time scales of the flow, so that $\tau_1 c \ll 1$ and $\tau_2 c \ll 1$. Therefore, this configuration represents interfaces between fluids that are highly conducting, for example, an electrolyte and mercury. In this limit, the dispersion relation becomes

$$F = F_1 + \frac{F_2}{c} - i \frac{P \hat{F}_3 + iQ \hat{F}_4}{c(\sigma_1 + \sigma_2)} + \frac{(\epsilon \hat{E}_1^2 - \hat{E}_2^2)}{c} F_5 \quad (3.84)$$

where

$$\begin{aligned} \hat{F}_3 &= (A_2 J_1 + m A_1 J_2)(\hat{E}_2 \sigma_1 - \sigma_2 \epsilon \hat{E}_1) + (m A'_1 J_2 + A'_2 J_1 \\ &\quad + 2(m-1)J_1 J_2)(\epsilon \hat{E}_1 \sigma_2 + \hat{E}_2 \sigma_1) \\ \hat{F}_4 &= (a_2 - a_1) \left(J_1 A_2 (\epsilon \hat{E}_1 + \hat{E}_2) + (A'_2 J_1 - J_1 J_2) Q \right) \\ &\quad - Q \left(i \alpha S + \alpha^{-1} \left(1 - \frac{1}{r} \right) g \right) J_1 J_2 - iQ (\epsilon \hat{E}_1^2 + \hat{E}_2^2). \end{aligned}$$

For the short wavelength limits, the asymptotic expressions for the Airy functions and their integrals, given by equation 3.61, can be substituted in the above dispersion relation to give the following approximation for the eigenvalue c :

$$c = b_0 \alpha + b_1 + b_2 \alpha^{-1} + o(\alpha^{-1}) \quad (3.85)$$

where

$$\begin{aligned} b_0 &= -\frac{iS}{2(1+m)} \\ b_1 &= i \frac{(\hat{E}_1 \epsilon k - \hat{E}_2)P}{2(1+m)(1+k)} - \frac{3i(1+r^{-1})S^2}{16(1+m)^3} \\ b_2 &= -g \frac{(1-r^{-1})i}{2(1+m)} + \frac{3i(1+r^{-1})(\hat{E}_1^2 \epsilon k - \hat{E}_2^2)S}{8(1+m)^3(1+k)} - \frac{i(1-r^{-1})(\hat{E}_1^2 \epsilon - \hat{E}_2^2 k)S}{16(1+m)^3(1+k)} \\ &\quad - \frac{i(r^3 + 20mr^2 + 20m + m^2 + 34rm)S^3}{128m(1+m)^5 r^2} - \frac{(5a_1 + 3ma_1 - 3ra_2 - 5ma_2 r)S}{8r(1+m)^3} \\ &\quad - \frac{1}{16} i \hat{E}_1 \hat{E}_2 \frac{(\epsilon k(7 + 5r^{-1}) + (5 + 7r^{-1}))S}{(1+m)^3(1+k)} \end{aligned}$$

and

$$k = \frac{\sigma_2}{\sigma_1}. \quad (3.86)$$

From this expression, we deduce that the growth rate for the short wavelength instability depends on the ratio of the conductivities of the two fluids. If the lower fluid has a much greater conductivity relative to the conductivity of the upper fluid, then the above expression reduces to equation 3.60 with Γ^c corresponding to the (EH-If) limit. On the other hand, if the fluids have nearly equal relaxation times so that there is no equilibrium charge, then the above expression reduces to equation 3.60 with Γ^c corresponding to the (EH-1p) configuration. Therefore, in the instantaneous relaxation limit the nature of the charge interaction and the stability of the flow are closely related to the conduction and relaxation of the electric charges.

By letting $c \rightarrow 0$ in the dispersion relation, we determine the following condition for the onset of static instability:

$$\alpha^2 + \alpha^{*2} - B\alpha/S \left((\sigma_1 + \sigma_2)(mJ_2A_1 + J_1A_2) + Q^2J_1J_2 \right) = 0 \quad (3.87)$$

where

$$B = \left(P\dot{E}_3 + Q^2(\epsilon\dot{E}_1^2 + \dot{E}_2^2) + i(a_2 - a_1) \left(J_1A_2(\epsilon\dot{E}_1 + \dot{E}_2)Q + (A_2'J_1 - J_1J_2)Q^2 + m(2J_1A_2 + 2A_1J_2 + A_1'A_2 - A_2'A_1)(\sigma_1 + \sigma_2) \right) \right).$$

Again, if $a_2 - a_1$ is not small, then there is no exchange of stabilities. However, if the initial streaming is small, then incipience of instability occurs at α^* and the critical electric fields satisfy

$$2\alpha^* = \frac{B^*\alpha}{S((\sigma_1 + \sigma_2)(mJ_2A_1 + J_1A_2) + Q^2J_1J_2)}. \quad (3.88)$$

For large values of α^* , equation 3.87 reduces to the following simple condition for the incipience of static instability:

$$\alpha^2 - \frac{(\dot{E}_1\epsilon k - \dot{E}_2)P}{S(1+k)}\alpha + \alpha^{*2} = 0. \quad (3.89)$$

demonstrated both theoretically and experimentally that electric and surface tension stresses could balance for a liquid in the shape of a cone of a half angle of 49.30 at a particular voltage depending on the surface tension and on the electrode configuration. In recent years, further analytical and experimental investigations of liquid drops in electric fields were carried out by many authors including Kim and Turnbull [40], Elghazaly and Castle [18] and Cerkanowicz [9]. In 1988, Inculet and Kromann [34] experimentally studied the breakup of large water droplets in an electric field in the presence of gravity by suspending an alcohol doped water droplet in a dielectric oil. The droplet elongated and developed a Taylor cone on one or both sides of the droplet and ejected a filament. When the droplet was symmetrically positioned between the electrodes, Taylor cones formed at both ends. However, if the droplet was lightly displaced from the centre, only one cone formed at the end closer to the electrode.

In comparison to the experimental and analytical investigations, the numerical simulations of liquid drops in electric fields have been limited. This is due primarily to the numerical and computational difficulties in solving the full nonlinear equations of motion where the location of the free boundary is not known a priori. Basaran and Scriven developed a finite element algorithm to investigate the profiles of electrified conducting drops and bubbles [6]. Theodossious, Nelson and Odel developed a numerical simulation for the motion of dielectric fluids [78]. In 1989 Inculet, Floryan and Haywood developed and utilized a numerical simulator based on a finite volume technique and an adaptive grid algorithm to predict the experimentally observed elongation of a large liquid droplet by a uniform electric field [35]. The droplet was placed between two parallel electrodes and the experiment was carried out in microgravity conditions produced with parabolic KC-135 NASA aircraft flights. Unfortunately, the numerical technique was unable to predict the evolution of the droplet beyond the elongation.

In 1990, similar experiments were carried out to investigate the behaviour of sessile

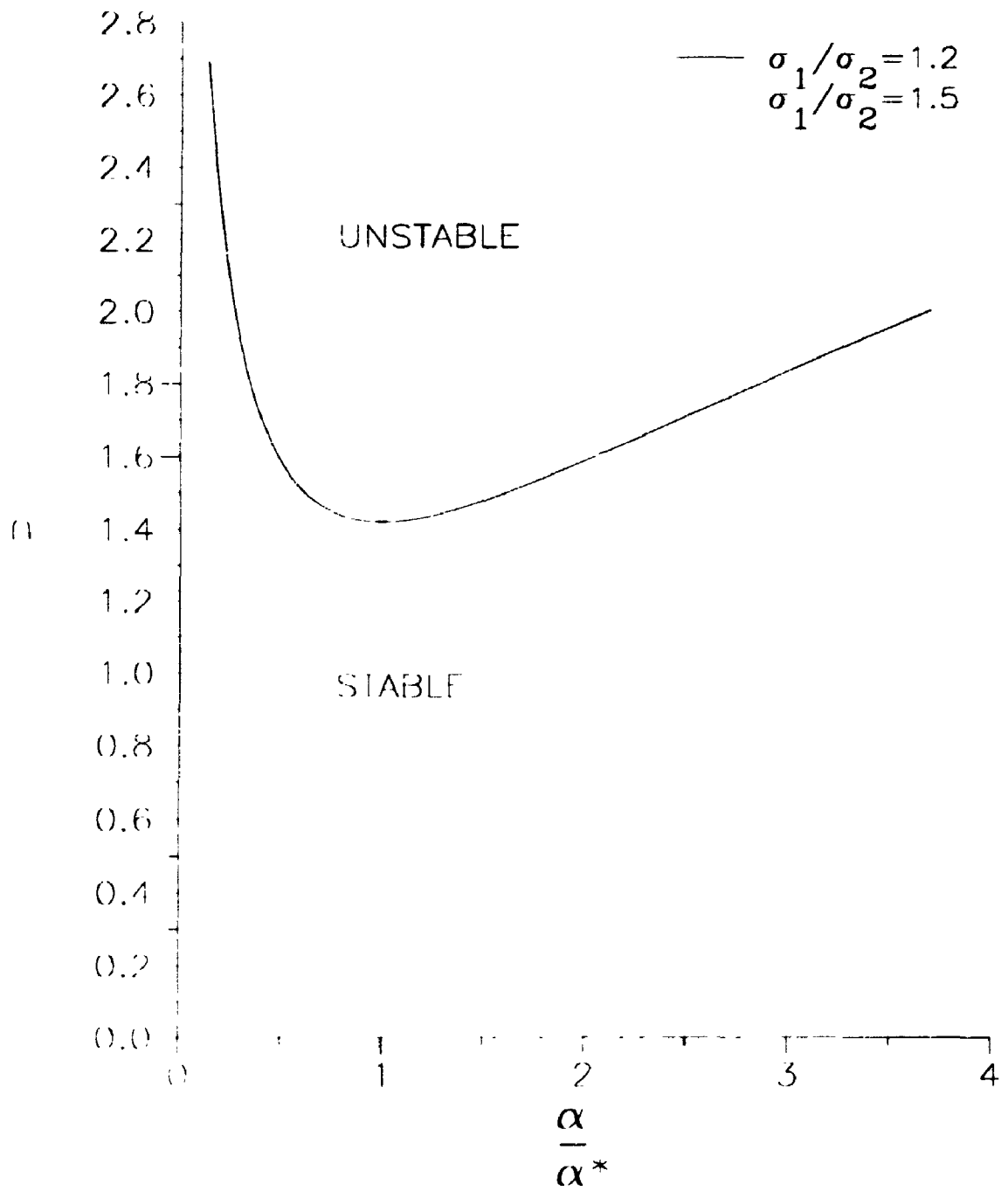


Figure 3.8: Marginal stability curve for the case of instantaneous relaxation limit, $Q = 0.5$ and $a_1 - a_2 = 0.05$

3.7 Finite Relaxation Time Effects

The limiting cases we have considered so far involve either very small or very large electric charge relaxation times compared to the characteristic dynamic time scales of the flow. In this section we look at configurations in which the fluids have finite electric charge relaxation times that are comparable to the characteristic time scale of the flow. These configurations are important since, for most real systems, the limiting cases we have considered are approximations only. Even though these approximations have been quite successful in modelling many real systems [47], finite relaxation effects are likely to be important in configurations where equilibrium charges are present. Furthermore, it is believed that finite relaxation time effects have important implications for fluid interactions involving bulk coupling of the fluids [51].

In this finite relaxation configuration the possibility of incipience of static instability (ie. the principle exchange of stability is valid) is determined by

$$\begin{aligned} & (\alpha^2 + \alpha^{*2})(H_e^2 S + 1) - H_e^2(\epsilon \tilde{E}_1^2 + \tilde{E}_2^2)\alpha - \frac{(\dot{E}_1 \epsilon k - \dot{E}_2)P}{S(1+k)}\alpha \\ & - \frac{P(\dot{E}_1 \epsilon k + \dot{E}_2) - (\epsilon \tilde{E}_1^2 + \tilde{E}_2^2)(1+k)}{1+k} f_5 \alpha \\ & + i(a_2 - a_1) \frac{a_{12}(\sigma_1 + \sigma_2) + QJ_1 b_{12}}{S(mJ_2 + J_1)(\sigma_1 + \sigma_2)} \alpha = 0 \end{aligned}$$

where a_{12} and b_{12} are given by 3.68 and 3.80 respectively and

$$f_5 = \frac{A_2' J_1 + m A_1' J_2 - 2(1-m)J_1 J_2}{mJ_2 + J_1} \quad (3.92)$$

$$H_e^2 = \frac{Q^2 J_1 J_2}{(mJ_1 + J_2)(\sigma_1 + \sigma_2)}. \quad (3.93)$$

The quantity H_e is called the electric Hartmann number and it is a measure of the relative effects of the electric forces and the mechanical forces[51]¹.

Clearly, in the presence of initial streaming the imaginary part of the above equation is nonzero and therefore, the onset of instability will not be static in general. In

¹This is analogous to the Hartmann number of magnetohydrodynamics.

the short wavelength limit and where there is relatively small initial streaming, the condition for the static instability reduces to

$$(\alpha^2 + \alpha^{*2})(H_{cl}^2 S + 1) - H_{cl}^2(\epsilon \tilde{E}_1^2 + \tilde{E}_2^2)\alpha - \frac{(\tilde{E}_1 \epsilon k - \tilde{E}_2)P}{S(1+k)}\alpha = 0 \quad (3.94)$$

where

$$H_{cl}^2 = \frac{Q^2}{2(m+1)(\sigma_1 + \sigma_2)}. \quad (3.95)$$

Therefore, as the electric field is raised the first unstable mode will occur at α^* again.

The critical electric field must be such that

$$2\alpha^* (1 + H_{cl}^2) = H_{cl}^2(\epsilon \tilde{E}_1^2 + \tilde{E}_2^2) + \frac{(\tilde{E}_1 \epsilon k - \tilde{E}_2)P}{S(1+k)} = 0. \quad (3.96)$$

Therefore, the general stability behaviour of the flow is characterized by the Hartmann number. If the Hartmann number is large compared to unity, then equation 3.94 reduces to equation 3.81 which is the condition for the onset of static instability for the infinite charge relaxation limit. On the other hand, if the Hartmann number is small in comparison to unity, then equation 3.94 reduces to equation 3.89 which is the condition for the onset of static instability for the instantaneous charge relaxation limit.

If the Hartmann number is finite, then the stability is generally determined by the conductivity ratio k , the permittivity ratio ϵ and the Hartmann number. While H_{cl} is always destabilizing, the effects of the conductivity ratio are determined by the quantity $(\tilde{E}_1 \epsilon k - \tilde{E}_2)P$. If this quantity is negative, then k is stabilizing. Otherwise it is destabilizing.

3.8 Concluding Remarks

We examined the electrohydrodynamic stability of a shear flow which is subjected to perpendicular electric fields. We investigated various limiting cases and developed conditions for the incipience of static instability (characterized in the marginal state by $c = 0$). As the initial motion parameter $a_1 \rightarrow 0$, our results agreed with previous work [47]. In the long wavelength limit the electric field does not affect the stability behaviour. Short wavelength analysis, however, demonstrated that the electric field effects are of secondary importance compared to the effects of surface tension. In the presence of initial motion, static stability is not generally possible except in the limit of short wavelengths. Finally, we considered the effect of finite relaxation times. We found that the electric field effects are characterized by the Hartmann number and the ratio of the conductivities. For large Hartmann numbers the threshold for static instability reduces to the threshold found for the infinite charge relaxation limit and for small Hartmann numbers it reduces to the instantaneous charge relaxation limit. While a non-zero Hartmann number causes instability, the effects of the ratio of the conductivities are determined by the specific configurations.

Chapter 4

Interfacial Deformation of Liquid Droplets by Applied Electric Fields at Zero Gravity

4.1 Introduction

In this chapter we consider an electrohydrodynamic problem in which a large viscous droplet is subjected to an applied electric field in a zero gravity environment. When drops and bubbles are subjected to electric fields, electric shear-induced convections are usually present [76]. These convections are physically similar in nature to the convections that occur in the shear flow electrohydrodynamics problem discussed in chapter 3. Due to the applied electric field, an electric charge is induced on the surface of the droplet, resulting in an outwardly directed force to the surface. This outward pressure directly counteracts the surface tension and, under suitable conditions, it forces the liquid up into a cone from which small charged droplets are ejected. The emission of the charged droplets depends on the viscosity, the surface tension, the mass density, the permittivity and the electrical conductivity of the fluid.

In addition to being of theoretical interest, this problem has widespread applications in several areas including electrostatic precipitators for air pollution control [82], electrostatic painting, insecticide spraying of crops and ink-jet printing [73], [32]. In the case of water droplets, the deformation and break up of the interface

is believed to be an important factor in the production of thunder storms [75]. In zero-gravity conditions, droplet dynamic problems are important in order to obtain a better understanding of containerless processing technology in space [50].

In chapter 2 and in chapter 3, we studied two problems related to the interfacial instability of shear flows. By utilizing linear stability analyses, we identified specific parameters which governed the instability and we determined the critical conditions at which these parameters destabilize the interface. While these conditions are important in understanding the mechanism of the interfacial instability and evolution, one must solve the full nonlinear equations of motion in order to fully describe the interfacial dynamics and the deformation process. Therefore, in order to study the the viscous droplet dynamic problem considered in the present chapter, we solve the full nonlinear equations of motion using computational techniques.

The interaction of electric fields with fluids and the presence of a cone on the surface of a liquid in an electric field was recorded as early as 1600 by William Gilbert. He noted that when an electrified rod was brought near a drop of water which was sitting on a dry surface, the droplet formed into a conical shape. In 1882, Lord Rayleigh derived the critical amount of the charge (Rayleigh Limit) that was required to destabilize an isolated conductive spherical droplet, and observed that the resulting instability was a fine jet that broke up into a series of small stable charged droplets [65]. The validity of Rayleigh's observation was later confirmed by Hendricks and others [28]. In 1914, Zeleny photographed and studied the reaction of a meniscus held at the end of an electrified glass capillary tube with a diameter of less than a millimeter [85]. The meniscus oscillated at a lower voltage and, eventually, with increased voltage, the droplet disintegrated after forming a conical end and issuing a thin jet. Zeleny later showed that the square of the potential at which instability begins is proportional to the surface tension of the liquid and the radius of the droplet formed [86]. Taylor gave further explanation to these observations in 1964 [75]. He

demonstrated both theoretically and experimentally that electric and surface tension stresses could balance for a liquid in the shape of a cone of a half angle of 49.30 at a particular voltage depending on the surface tension and on the electrode configuration. In recent years, further analytical and experimental investigations of liquid drops in electric fields were carried out by many authors including Kim and Turnbull [40], Elghazaly and Castle [18] and Cerkanowicz [9]. In 1988, Inculet and Kromann [34] experimentally studied the breakup of large water droplets in an electric field in the presence of gravity by suspending an alcohol doped water droplet in a dielectric oil. The droplet elongated and developed a Taylor cone on one or both sides of the droplet and ejected a filament. When the droplet was symmetrically positioned between the electrodes, Taylor cones formed at both ends. However, if the droplet was lightly displaced from the centre, only one cone formed at the end closer to the electrode.

In comparison to the experimental and analytical investigations, the numerical simulations of liquid drops in electric fields have been limited. This is due primarily to the numerical and computational difficulties in solving the full nonlinear equations of motion where the location of the free boundary is not known a priori. Basaran and Scriven developed a finite element algorithm to investigate the profiles of electrified conducting drops and bubbles [6]. Theodossious, Nelson and Odel developed a numerical simulation for the motion of dielectric fluids [78]. In 1989 Inculet, Floryan and Haywood developed and utilized a numerical simulator based on a finite volume technique and an adaptive grid algorithm to predict the experimentally observed elongation of a large liquid droplet by a uniform electric field [35]. The droplet was placed between two parallel electrodes and the experiment was carried out in microgravity conditions produced with parabolic KC-135 NASA aircraft flights. Unfortunately, the numerical technique was unable to predict the evolution of the droplet beyond the elongation.

In 1990, similar experiments were carried out to investigate the behaviour of sessile

droplets under the influence of applied electric fields [36]. A large liquid droplet generated in microgravity conditions was placed on the bottom electrode of a parallel electrode system. Once the electric field was applied, the evolution of the droplet was recorded on a high speed camera. The experiment shows that when the applied electric field is above a critical value, then the droplet elongates into a cone from which small charged droplets are ejected.

The aim of this chapter is to model and develop a computational procedure in order to simulate the elongation and break up processes of the droplets observed during this experiment. As stated above, one of the main difficulties encountered while simulating these types of problems involving interfacial deformations is in tracking the moving interface which is not known a priori. Among the various computational techniques available for solving problems with interfacial dynamics, volume tracking methods have shown great promise for numerical simulations of large surface deformations. In this chapter we modify and employ a finite difference algorithm called NASA-VOF2D [79] which is based on a volume tracking technique called *volume of fluid* (VOF)[30], [31]. The NASA-VOF2D algorithm which descended from the *Marker And Cell* (MAC) method [23], [21] solves two dimensional transient fluid flow problems with free boundaries. In this algorithm, the location of the interface is identified in terms of a volume fraction parameter F , which represents the fractional volume of the surface cell that is filled with fluid. Therefore, F is unity in cells filled with fluid, zero in empty cells and takes intermediate values in the interface cells. A special *donor-acceptor* method is utilized to advect the volume fraction field and to reconstruct the fluid interface [56].

In the next section we discuss the mathematical model describing the dynamical behaviour of the droplet. As in the previous chapter, the coupling between the electric quantities and the fluid flow quantities in this droplet model occurs at the interface only. There is no bulk force of electrical origin and gravity is neglected. Furthermore,

the axisymmetric assumption simplifies the complicated three dimensional problem. The numerical simulation used to study and predict the behaviour of the droplets is discussed in section 4.3 and a discussion of the numerical results is presented in section 4.4. While our results are consistent with the qualitative behaviour of the droplet break up when compared to the experimental data, there is a need for a more realistic three dimensional model in order to obtain quantitative agreement as well.

4.2 Formulation of the Problem

Consider a single spherical incompressible liquid droplet of density ρ and kinematic viscosity ν placed on the surface of the lower electrode of a parallel plane electrode system as shown in figure 4.1. Gravity is assumed to be zero and hence all gravitational effects are assumed to be negligible. We suppose that the problem is two dimensional and axisymmetrical with respect to the z-axis from the droplet centre normal to the electrodes. Furthermore, we assume that the droplet is a perfect conductor and, therefore, that there is no bulk coupling between the electrostatic variables and the fluid flow variables since the free electric charges in a conductor reside on the surface of the conductor. Hence, the electrostatic equations are solved separately and coupled by the appropriate stress condition at the interface.

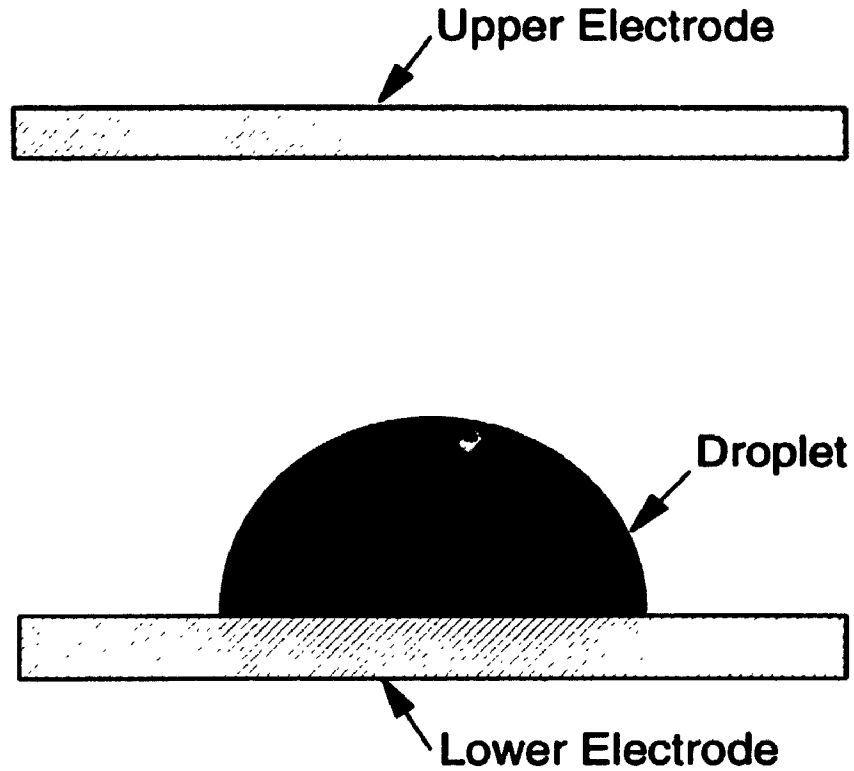


Figure 4.1: Schematic representation of the the physical problem

4.2.1 Governing Equations

Within the bulk of the fluid the conservation of mass and the conservation of momentum must be satisfied. The mass conservation equation is the continuity equation, which for incompressible fluids is given by

$$\nabla \cdot \mathbf{v} = 0 \quad (4.1)$$

where $\mathbf{v} = (u, v)$ is the velocity vector field. Similarly, the equations expressing the conservation of momentum are the Navier-Stokes equations

$$\frac{\partial \mathbf{v}}{\partial t} + \mathbf{v} \cdot \nabla \mathbf{v} = -\frac{\mathbf{F}}{\rho} - \frac{\nabla P}{\rho} + \nu \nabla^2 \mathbf{v} \quad (4.2)$$

where \mathbf{F} is the total body force and p is the pressure. In this model, there are no external forces in the bulk of the fluid so that \mathbf{F} is identically zero. Therefore, for an

axisymmetric cylindrical flow the conservation of mass becomes

$$\frac{\partial u}{\partial r} + \frac{u}{r} + \frac{\partial v}{\partial z} = 0 \quad (4.3)$$

and the conservation of momentum becomes

$$\frac{\partial u}{\partial t} + u \frac{\partial u}{\partial r} + v \frac{\partial u}{\partial z} = -\frac{1}{\rho} \frac{\partial p}{\partial r} + \nu \left(\frac{\partial^2 u}{\partial r^2} + \frac{1}{r} \frac{\partial u}{\partial r} - \frac{u}{r^2} + \frac{\partial^2 u}{\partial z^2} \right) \quad (4.4)$$

$$\frac{\partial v}{\partial t} + u \frac{\partial v}{\partial r} + v \frac{\partial v}{\partial z} = -\frac{1}{\rho} \frac{\partial p}{\partial z} + \nu \left(\frac{\partial^2 v}{\partial r^2} + \frac{1}{r} \frac{\partial v}{\partial r} + \frac{\partial^2 v}{\partial z^2} \right) \quad (4.5)$$

where r and z are the radial and axial coordinates respectively, and u and v are the velocity components in the r and z direction respectively.

Along with the above equations we must also solve the relevant electrodynamic equations. Since our model is based on perfect conductivity, the electrodynamic equation is the Laplace equation for the electric potential ϕ

$$\frac{\partial^2 \phi}{\partial r^2} + \frac{1}{r} \frac{\partial \phi}{\partial r} + \frac{\partial^2 \phi}{\partial z^2} = 0 \quad (4.6)$$

which must be solved in the region outside the bulk of the droplet where we neglect the mechanical effects of air. The electric field components are then computed by taking the negative of the gradient of the potential ϕ . They are given by

$$E_r = -\frac{\partial \phi}{\partial r} \quad (4.7)$$

and

$$E_z = -\frac{\partial \phi}{\partial z} \quad (4.8)$$

where (E_r, E_z) is the electric field.

4.2.2 Boundary Conditions

Let the profile of droplet surface be described by

$$\eta(t, r, z) = 0. \quad (4.9)$$

Then the initial profile of the droplet surface at $t = t_0$ is

$$\eta(t = t_0, r, z) = 0. \quad (4.10)$$

The kinematic condition at the surface of the droplet can be stated as

$$[(\mathbf{v} - \mathbf{v}_s) \cdot \mathbf{n}]_{\Gamma_d} = 0 \quad (4.11)$$

where \mathbf{v}_s is the velocity of the droplet's surface, Γ_d represents the surface of the droplet and $\mathbf{n} = (n_r, n_z)$ is the unit vector normal to the surface of the droplet. This condition represents the conservation of mass and it can be obtained by integrating the continuity equation across the interface. In terms of the droplet profile this condition can be written as

$$\frac{D\eta}{Dt} = \frac{\partial\eta}{\partial t} + u \frac{\partial\eta}{\partial r} + v \frac{\partial\eta}{\partial z} = 0. \quad (4.12)$$

At the interface, the stresses must be continuous. As shown in the previous chapter, this surface condition can be decomposed into normal and tangential stress conditions. The continuity of the normal stresses is given by

$$P - P_0 = \mu \left(\frac{\partial v_i}{\partial x_j} + \frac{\partial v_j}{\partial x_i} \right) n_i n_j + \gamma \left(\frac{1}{R_1} + \frac{1}{R_2} \right) - \epsilon_0 \frac{E_n^2}{2} \quad (4.13)$$

where γ is the constant surface tension, μ is the viscosity, E_n is the normal component of the electric field, ϵ_0 is the permittivity of free space and $\frac{1}{R_1} + \frac{1}{R_2}$ is the mean radius of curvature where R_1 and R_2 are the local principal radii of curvature. The first term in equation 4.13 represents the stress due to viscosity, the second term represents the pressure jump across the interface due to surface tension, and the last term is produced by the electric field. Similarly, the continuity of the tangential stresses is given by

$$\left(\frac{\partial v_i}{\partial x_j} + \frac{\partial v_j}{\partial x_i} \right) t_i n_j = 0 \quad (4.14)$$

where $\mathbf{t} = (t_1, t_2)$ is the unit tangential vector.

We also have wall conditions for the velocities and for the potential ϕ . The boundary conditions for v result from the no-slip and no-penetration conditions which require the vanishing of the tangential and normal components of the velocity respectively. A constant contact angle is given at the triple point where the droplet interface intersects with the solid electrodes. This condition is usually determined from experiments.

One of the boundary conditions for ϕ results from the assumption that the droplet is a perfect conductor so that its surface is equipotential. Therefore, on Γ_b , which represents all the points on the lower electrode and the droplet surface, we require

$$[\phi]_{\Gamma_b} = \phi_b \quad (4.15)$$

where ϕ_b is the constant potential of the lower electrode. Similarly, on the upper electrode we require

$$[\phi]_{\Gamma_t} = \phi_t \quad (4.16)$$

where ϕ_t is the constant potential at the upper electrode. Finally, the following Neumann boundary condition is imposed along the lines of symmetry

$$\nabla\phi \cdot \mathbf{n} = 0. \quad (4.17)$$

These surface and wall boundary conditions along with the equations of motion given by equations 4.3 to 4.5 define the mathematical model. In the next section we discuss the numerical method used for solving these sets of equations.

4.3 Description of the Numerical Procedure

4.3.1 The Fluid Flow Model

The core of the fluid flow model is solved using the NASA-VOF2D program which solves the fluid flow equations for the velocity and pressure directly with an Eulerian

representation of the mesh [79] . It discretizes both the space and time variables of the continuity and momentum equations utilizing the finite difference technique. In this section, a qualitative description of the NASA-VOF2D program is presented. A more detailed examination of the program is provided in the documentation of Torrey *et. al.*[79]. The NASA-VOF2D program is essentially an extended version of the SOLA-VOF algorithm, and further discussion of the program may be found in reference [55].

As illustrated in figure 4.2, a typical computational mesh divides the region of interest into rectangular meshes. Each cell has sizes δr_i for the i^{th} column and δz_j for the j^{th} row. As depicted in figure 4.3, the radial velocity components $u_{i-\frac{1}{2},j}$ and $u_{i+\frac{1}{2},j}$ are located on the left and right cell faces respectively, and the axial velocity components $v_{i,j-\frac{1}{2}}$ and $v_{i,j+\frac{1}{2}}$ are located on the bottom and on the top cell faces respectively. The pressure variable P and the volume of fluid variable F are both located at the centre of the cell. The positioning of the field variables in this manner simplifies boundary condition application and assists in the conservation of mass[81]. The variable F assigned to each cell indicates the fractional amount of fluid occupying that cell. A value of one for F corresponds to a cell filled with fluid. A value of zero corresponds to a completely empty cell . A value between zero and one corresponds to a free surface.

The solution of the problem for advancing one time step δt proceeds in the following manner. First, by employing the previous values of the velocity field and the pressure, we update the velocities by an explicit finite difference approximation of the momentum equations given by 4.4 and 4.5. The updated velocities do not satisfy the continuity equation given by 4.3. Therefore, to satisfy the continuity equation, the pressure in each cell is adjusted in an iterative procedure. This iteration is continued until the new velocity components satisfy the continuity equation within a defined convergence criterion. Finally, the volume of fluid function F is updated and the

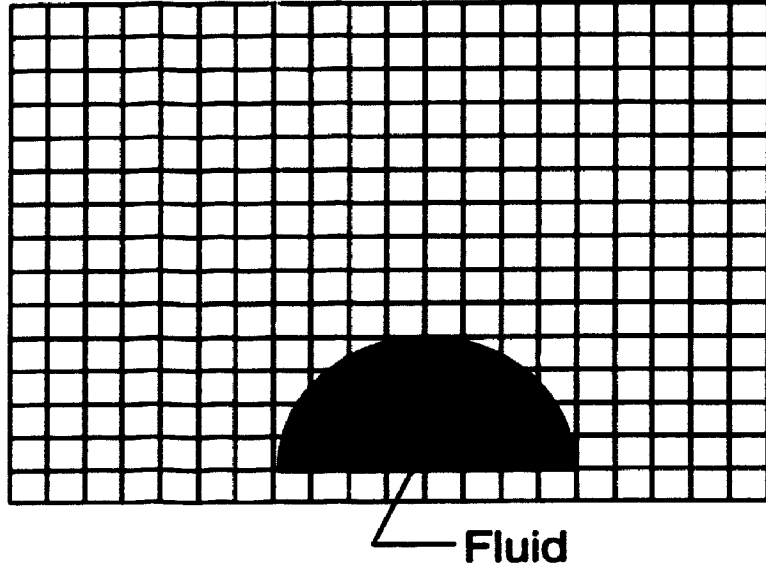


Figure 4.2: A typical computational mesh

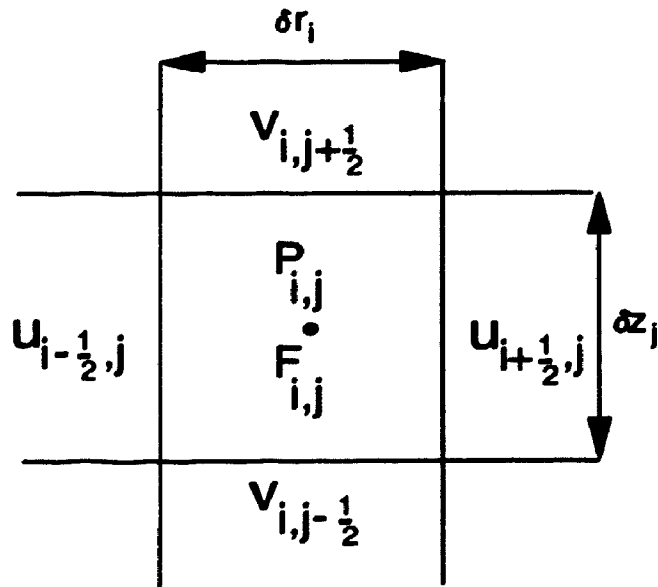


Figure 4.3: Location of variables in a typical mesh cell

entire procedure is repeated up to any desired interval of time. During each stage, suitable wall and interface boundary conditions must be imposed.

Therefore, as a first step, we find an explicit finite difference approximation to the momentum equations. The only terms in the momentum equations that are discretized with respect to time are $\frac{\partial u}{\partial t}$ and $\frac{\partial v}{\partial t}$. Their finite difference approximations at the right face of the cell (i, j) are given by

$$\left(\frac{\partial u}{\partial t}\right)_{i+\frac{1}{2},j} = \frac{u_{i+\frac{1}{2},j}^{n+1} - u_{i+\frac{1}{2},j}^n}{\delta t} \quad (4.18)$$

$$\left(\frac{\partial v}{\partial t}\right)_{i,j+\frac{1}{2}} = \frac{v_{i,j+\frac{1}{2}}^{n+1} - v_{i,j+\frac{1}{2}}^n}{\delta t} \quad (4.19)$$

where the superscript $n + 1$ corresponds to the updated velocities. The variables without a superscript represent the previous or the old values. The remaining terms represent partial derivatives with respect to the space coordinates.

We also have the viscous acceleration terms in the momentum equation and they are given by

$$VISR = \nu \left(\frac{\partial^2 u}{\partial r^2} + \frac{1}{r} \frac{\partial u}{\partial r} - \frac{u}{r^2} + \frac{\partial^2 u}{\partial z^2} \right) \quad (4.20)$$

$$VISZ = \nu \left(\frac{\partial^2 v}{\partial r^2} + \frac{1}{r} \frac{\partial v}{\partial r} + \frac{\partial^2 v}{\partial z^2} \right). \quad (4.21)$$

The first order partial derivatives are defined by

$$\left(\frac{\partial u}{\partial r}\right)_{i,j} = \frac{u_{i+\frac{1}{2},j} - u_{i-\frac{1}{2},j}}{r_{i+\frac{1}{2}} - r_{i-\frac{1}{2}}} \quad (4.22)$$

and

$$\left(\frac{\partial u}{\partial z}\right)_{i+\frac{1}{2},j+\frac{1}{2}} = \frac{u_{i+\frac{1}{2},j+1} - u_{i+\frac{1}{2},j}}{z_{j+1} - z_j} \quad (4.23)$$

where $r_{i-\frac{1}{2}}$ and $r_{i+\frac{1}{2}}$ are the coordinate positions of the left and right cell sides respectively. Similar equations may be obtained for the first derivatives at $(i+1, j)$ and $(i+\frac{1}{2}, j-\frac{1}{2})$.

The approximation of $VISR$ at the right side of the mesh cell is then given by

$$VISR_{i+\frac{1}{2},j} = \nu \left[\frac{\left(\frac{\partial u}{\partial r}\right)_{i+1,j} - \left(\frac{\partial u}{\partial r}\right)_{i,j}}{r_{i+1} - r_i} + 2 \frac{\left(\frac{\partial u}{\partial z}\right)_{i+\frac{1}{2},j+\frac{1}{2}} - \left(\frac{\partial u}{\partial z}\right)_{i+\frac{1}{2},j-\frac{1}{2}}}{z_{j+1} - z_{j-1}} + \frac{\delta r_{i+1} \left(\frac{\partial u}{\partial r}\right)_{i,j} + \delta r_i \left(\frac{\partial u}{\partial r}\right)_{i+1,j}}{r_{i+\frac{1}{2}} (\delta r_{i+1} + \delta r_i)} - \frac{u_{i+\frac{1}{2},j}}{r_{i+\frac{1}{2}}^2} \right]. \quad (4.24)$$

The factor 2 in the second term is required in order to compensate for the extra distance associated with the use of cell-centered coordinate positions z_{j+1} and z_{j-1} . Similar expressions can be written for $VISZ$ at the top side of the mesh cell.

Finally, we approximate the convective terms which are the products of the velocities and their derivatives. These are approximated using a combination of forward difference approximation and central difference approximation using the method which is described in reference [55]. For example, the flux of u in the r direction $FUR = u \frac{\partial u}{\partial r}$ is approximated at the right side of the cell mesh by

$$FUR_{i+\frac{1}{2},j} = \left(u \frac{\partial u}{\partial r}\right)_{i+\frac{1}{2},j} = \frac{u_{i+\frac{1}{2},j}}{\delta r_\alpha} \left[\delta r_i \left(\frac{\partial u}{\partial r}\right)_{i+1,j} + \delta r_{i+1} \left(\frac{\partial u}{\partial r}\right)_{i,j} + \alpha \operatorname{sgn}(u_{i+\frac{1}{2},j}) \left(\delta r_{i+1} \left(\frac{\partial u}{\partial r}\right)_{i,j} + \delta r_i \left(\frac{\partial u}{\partial r}\right)_{i+1,j} \right) \right] \quad (4.25)$$

where

$$\delta r_\alpha = \delta r_i + \delta r_{i+1} + \alpha \operatorname{sgn}(u_{i+\frac{1}{2},j}) (\delta r_i + \delta r_{i+1}) \quad (4.26)$$

and δr_i is the width of the cell i . The variable α is the donor-cell fraction and sgn is the sign function. When $\alpha = 0$, this expression reduces to a central-difference second order accurate approximation. When $\alpha = 1$, this expression reduces to a forward

first order accurate approximation. Initially, the upper limit $\alpha = 1$ is used and then reduced to $0.25 < \alpha < 0.5$ for later runs. An analogous expression can be written for the flux of u in the z direction $FUZ_{i+\frac{1}{2},j}$.

Substituting the above expressions into equation 4.4 we obtain the following explicit finite difference approximation for the provisional value of the radial velocity component u :

$$u_{i+\frac{1}{2},j}^{n+1} = u_{i+\frac{1}{2},j}^n - \delta t \left(\frac{P_{i+1,j}^{n+1} - P_{i,j}^{n+1}}{\rho(r_{i+1} - r_i)} + FUR_{i+\frac{1}{2},j} + FUZ_{i+\frac{1}{2},j} - VISX_{i+\frac{1}{2},j} \right). \quad (4.27)$$

Similar expressions may be written to approximate the provisional values of the axial velocity component v .

These provisional values do not yet satisfy the continuity equation given by 4.3. Thus, we must adjust the pressure and the velocities in order to satisfy the conservation of mass. To determine the required pressure adjustment we let the new pressure $P_{i,j}^k$ be the old pressure $P_{i,j}^{k-1}$ and a correction factor δP

$$P_{i,j}^k = P_{i,j}^{k-1} + \delta P \quad (4.28)$$

where k is the current number of iteration of the pressure and velocities values at the time cycle $(n + 1)$. If we substitute equation 4.28 into the finite difference approximation 4.27, we find an adjusted expression for the right side velocity $u_{i+\frac{1}{2},j}$

$$u_{i+\frac{1}{2},j}^k = u_{i+\frac{1}{2},j}^{k-1} + \frac{\delta t \delta P}{\rho(r_{i+1} - r_i)}. \quad (4.29)$$

Here, the second terms on the right are the required velocity correction factors that reflect the adjusted pressure. Similar expressions can be found for the top, left and bottom side velocities.

The finite difference approximation of the continuity equation is given by

$$D_{i,j}^{n+1} = \frac{u_{i+\frac{1}{2},j}^{n+1} - u_{i-\frac{1}{2},j}^{n+1}}{\delta r_i} + \frac{v_{i,j+\frac{1}{2}}^{n+1} - v_{i,j-\frac{1}{2}}^{n+1}}{\delta z_j} + \frac{u_{i+\frac{1}{2},j}^{n+1} + u_{i-\frac{1}{2},j}^{n+1}}{2r_i} = 0. \quad (4.30)$$

If we substitute the adjusted velocities into this equation, we find an equation for the increments pressure δP . Then, solving for δP , we obtain the following expression:

$$\delta P = -\frac{\rho D_{i,j}^{n+1}}{\beta_{i,j}^{n+1}} \quad (4.31)$$

where

$$\beta_{i,j}^{n+1} = \frac{2\delta t}{\delta r_i \delta z_j} \left[\frac{\delta z_j}{\delta r_{i+1} + \delta r_i} + \frac{\delta z_j}{\delta r_{i-1} + \delta r_i} + \frac{\delta r_i}{\delta z_{j+1} + \delta z_j} + \frac{\delta r_i}{\delta z_{j-1} + \delta z_j} \right]. \quad (4.32)$$

This incremental pressure is calculated for each cell and immediately put into the velocity correction equations, such as equation 4.29, in order to update the provisional velocities. Once all the fluid cells have been updated, the maximum value of $D_{i,j}^{n+1}$ is compared to a small predetermined value. Note that $D_{i,j}^{n+1}$ is the residual of the continuity equation and, consequently, if it is not sufficiently less than this predetermined value, then we repeat the iteration all over again. On the other hand, if $D_{i,j}^{n+1}$ turns out to be within the desired accuracy requirement for each cell, then these velocities and pressure will be taken as the updated values.

Since we have a pressure boundary condition at the interface, this procedure is modified for interface cells. For these cells, the pressure $P_{i,j}$ is computed by a linear interpolation or extrapolation between the surface pressure P_s calculated from surface tension and electrostatic forces and a neighbouring pressure P_n inside the fluid in a direction closest to the normal to the interface. Hence, we set

$$S_{i,j}^{n+1} = (1 - \xi_d) P_n + \xi_d P_s - P_{i,j} \quad (4.33)$$

where $\xi_d = \frac{d_c}{d_s}$ is the ratio of the distance between the cell centers and the distance between the free surface and the centre of the interpolation cell (see figure 4.4). Therefore, using the new P_n and the old $P_{i,j}$, we compute a new $P_{i,j}$ iteratively until all the $S_{i,j}$'s are within some defined accuracy requirement.

Finally, we use the updated velocities and pressures to determine the new location of the fluid interface. This is done using the VOF function $F(r, z, t)$ mentioned earlier.

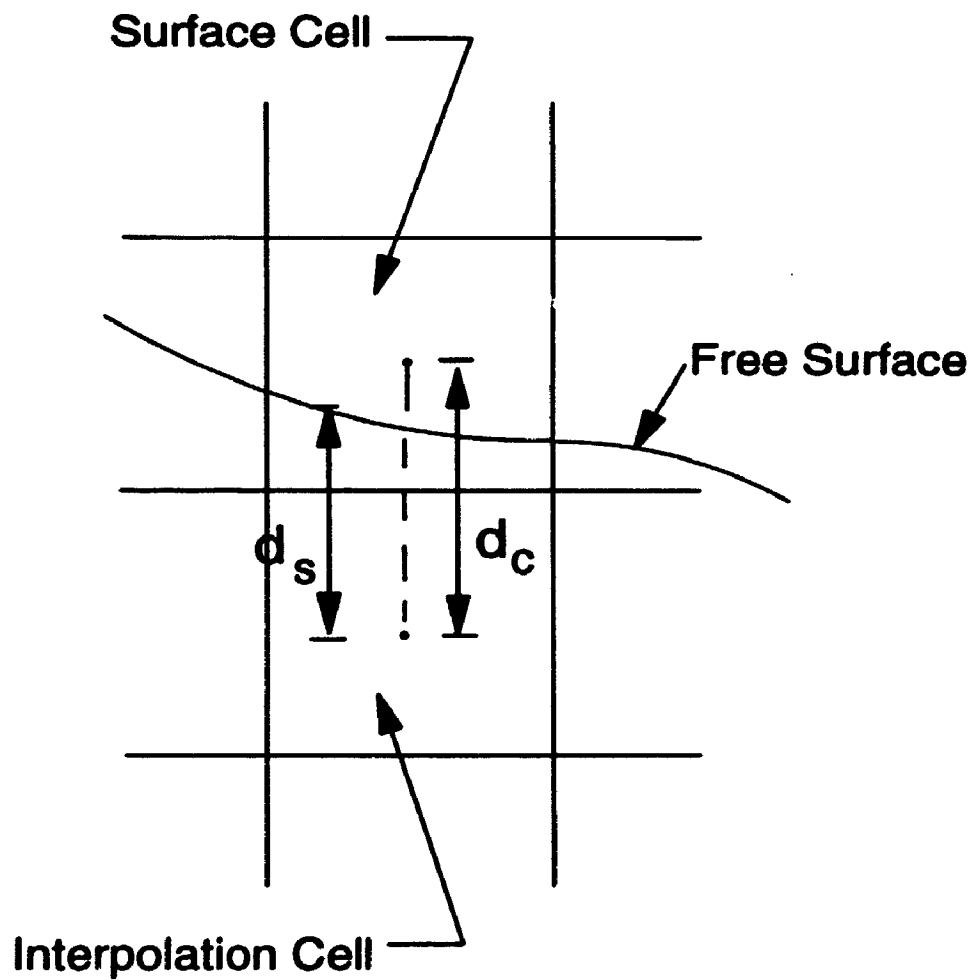


Figure 4.4: Definition of d_s and d_c for the surface pressure interpolation.

The time dependence of F is governed by

$$\frac{DF}{Dt} = \frac{\partial F}{\partial t} + u \frac{\partial F}{\partial r} + v \frac{\partial F}{\partial z} = 0. \quad (4.34)$$

This equation states that F moves with the fluid. In our Eulerian mesh, the flux of F moving with the fluid through a cell must be computed. However, standard finite difference approximations would lead to a smearing of the F function and the interfaces would lose their definition. In order to preserve the discontinuous nature of the F function, its value at each of the four cell boundaries is first determined to be either a donor or an acceptor of fluid depending on the sign of the corresponding velocity components. For example, if $u_{i+\frac{1}{2},j}$ is positive, then cell i is the donor and cell $i+1$ is the acceptor of fluid, at this one cell side. By incorporating this directional indicator with the value of F at each interface cell and by paying close attention to the maximum value of fluid contained in the donor cell, a value of each interfacial F can be determined from an explicit finite difference formula for F . The details of this procedure are given in [56], [31].

Let us now discuss the calculation of the surface tension effect that must be incorporated into the surface pressure P_s . The surface tension term in P_s is given by

$$P_s^{st} = -\gamma H \quad (4.35)$$

where the mean curvature H is given by

$$\frac{1}{R_{rz}} + \frac{1}{R_{cyl}}. \quad (4.36)$$

R_{rz} is the principal radius of curvature in the plane and R_{cyl} is the principal radius of curvature associated with the azimuthal direction of the cylindrical coordinates. In order to determine H , we must know the exact orientation of the interface. This is done by introducing surface height functions $Z(r)$ and $R(z)$ based on the value of F in the surface cell and its eight neighbours. For example, $Z(r)$ for the (i, j) cell, is given by

$$Z_i = Z(r_i) = F_{i,j-1} \delta z_{j-1} + F_{i,j} \delta z_j + F_{i,j+1} \delta z_{j+1}. \quad (4.37)$$

Therefore, the slope of the fluid interface at cell (i, j) can be approximated by the expression

$$\left(\frac{dZ}{dr}\right)_{i,j} = \frac{\frac{(Z_{i+1} - Z_i) \delta r_{i-\frac{1}{2}}}{\delta r_{i+\frac{1}{2}}} + \frac{(Z_i - Z_{i-1}) \delta r_{i+\frac{1}{2}}}{\delta r_{i-\frac{1}{2}}}}{\delta r_{i-\frac{1}{2}} + \delta r_{i+\frac{1}{2}}} \quad (4.38)$$

where

$$\delta r_{i+\frac{1}{2}} = \frac{\delta r_i + \delta r_{i+1}}{2} \quad (4.39)$$

and so forth. By interchanging the roles of r and z , a similar equation can be derived for $\frac{dR}{dz}$ at each cell (i, j) . If $\left|\frac{dZ}{dr}\right|$ is smaller than $\left|\frac{dR}{dz}\right|$, the boundary is more nearly horizontal than vertical, otherwise it is more nearly vertical. The derivative with the smallest magnitude gives the best approximation of the slope because the corresponding R and Z approximations are more accurate in that case.

The surface tension force f acting across the faces of the computational cell is given by

$$f = \gamma \oint_{\mathcal{C}} \mathbf{n} \times d\mathbf{L} \quad (4.40)$$

where $d\mathbf{L}$ is the differential element directed along a counter-clock-wise path on the fluid interface. Then the surface pressure P_s^{sr} due to R_{rz} will be

$$P_s^{sr} = -\gamma \frac{\sin\beta_r + \sin\beta_l}{\delta r_i} \quad (4.41)$$

where β_r is the angle that the normal of the fluid surface makes with the z axis (counter-clock-wise angle) at the right cell side and β_l is the angle that the normal of the fluid surface makes with the z axis at the left cell side. The β angles are determined from the relations

$$\tan\beta_r = \frac{AVFR - AVFCR}{\delta r_{i+\frac{1}{2}}} \quad (4.42)$$

and

$$\tan\beta_l = \frac{AVFCR - AVFL}{\delta r_{i-\frac{1}{2}}} \quad (4.43)$$

where $AVFR$, $AVFCR$ and $AVFL$ are average fluid height values in the right, centre and left cells respectively. Then, the $\sin\beta$ required for the surface pressure can be easily determined from the trigonometric identity

$$\sin\beta = \frac{\tan\beta}{\sqrt{1 + \tan^2\beta}} \quad (4.44)$$

The surface pressure contribution P_s^{sc} of R_{cyl} is

$$P_s^{sc} = -\gamma \frac{\cos\theta}{W_i} \quad (4.45)$$

for a nearly horizontal surface and

$$P_s^{sc} = -\gamma \frac{\cos\theta}{r_{cyl}} \quad (4.46)$$

for a nearly vertical surface. Here, θ is the angle between the interface tangent and the radial axis when the interface is mainly horizontal, and θ is the angle the interface tangent makes with the axial axis if the interface is mainly vertical. W_i is the distance in the r-direction from the axis of symmetry to the centre of the cell (i, j) , and r_{cyl} is given by

$$r_{cyl} = \begin{cases} -r_{i-\frac{1}{2}} + F_{i,j}\delta r_i & \text{if fluid is to the right of the interface} \\ r_{i+\frac{1}{2}} - F_{i,j}\delta r_i & \text{if fluid is to the left of the interface.} \end{cases} \quad (4.47)$$

Therefore, the surface pressure P_s^s due to the surface tension is the sum of the two contributions P_s^{sr} and P_s^{sc} .

$$P_s^s = P_s^{sr} + P_s^{sc} \quad (4.48)$$

The total surface pressure P_s is then given by

$$P_s = P_s^s + P_s^e \quad (4.49)$$

where P_s^e is the surface pressure due to the applied electric fields which are calculated in the next section.

4.3.2 The Electrostatic Model

For the electrostatic field model we must solve Laplace's equation which is given by 4.6 for the electric potential ϕ within the region of study. To do this we make the following change of variable

$$\sqrt{x} = \frac{r}{2} \quad (4.50)$$

which transforms the Laplace's equation into

$$x \frac{\partial^2 \phi}{\partial x^2} + \frac{\partial \phi}{\partial x} + \frac{\partial^2 \phi}{\partial z^2} = 0. \quad (4.51)$$

This equation has two advantages. First, it eliminates the numerical difficulties encountered in the usual Laplace's operator as r goes to zero [2]. Second, with this change of variables, the spacing in the radial direction used for the fluid flow model, is transformed to a finer spacing in x near the axis of symmetry and this gives a more accurate boundary condition approximation at $r = 0$, and a more accurate field calculation at the tip of the droplet.

There are various numerical methods available for solving Laplace's equation including finite difference, finite elements, Monte Carlo and boundary integral methods. In this thesis, we employ the finite difference techniques because they are easy to implement and incorporate with the fluid flow model which is also based on the finite difference method. To find a finite difference approximation to 4.51, we use the same rectangular mesh used for the fluid flow problem as shown in figure 4.5. The coordinates of the node points are denoted by the mesh (i, j) whose distance from the neighbouring left, right, bottom and top mesh points are labelled as h_l , h_r , h_b and h_t respectively. For surface cells, the values of the h s are calculated using the VOF variable F . The neighbouring mesh point for a surface cell is taken to be a point on the interface. For example, if cell (i, j) is a surface cell where cell $(i, j - 1)$ is a fluid cell, then the $(i, j - 1)$ mesh point will be the point of intersection of the vertical line passing through (i, j) with the interface as depicted in figure 4.6. Accordingly, h_b will

be the distance between these points. For all the empty cells, the h s are simply the spacing between the neighbouring cells. Because of the perfect conductivity assumption, the value of the potential for all surface cells and full cells is simply the lower electrode potential which is ϕ_b .

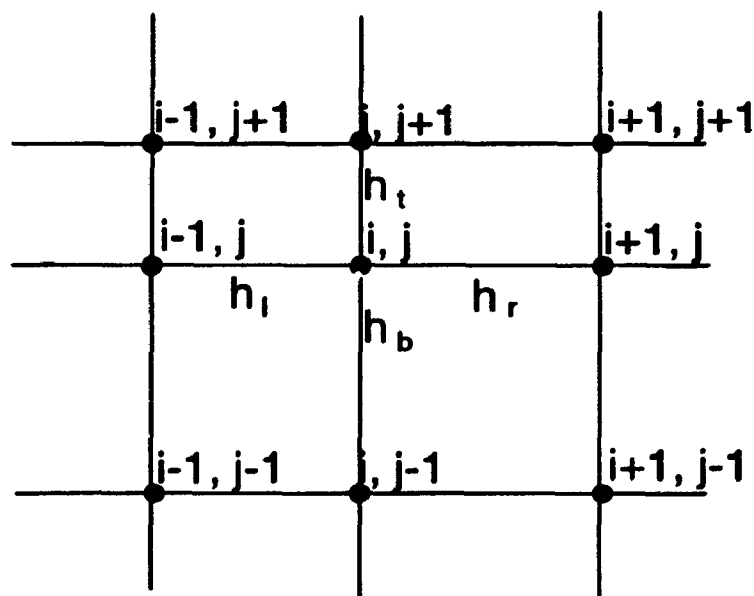


Figure 4.5: The rectangular mesh used to solve the electrostatic problem

If the cell (i, j) is a surface cell or a cell on an electrode, then we call the node corresponding to this cell a *metal node*; otherwise we call it a *non metal node*. Using this definition, we obtain the following finite difference approximation of equation 4.51 [26]

$$a_{i,j}\phi_{i+1,j} + b_{i,j}\phi_{i-1,j} + c_{i,j+1}\phi_{i,j+1} + d_{i,j}\phi_{i,j-1} - e_{i,j}\phi_{i,j} = f_{i,j} \quad (4.52)$$

where, for non metal nodes,

$$\begin{aligned} a_{i,j} &= \frac{x_i}{h_r(h_r + h_l)} + \frac{1}{2(h_l + h_r)} \\ b_{i,j} &= \frac{x_i}{h_l(h_r + h_l)} - \frac{1}{2(h_l + h_r)} \end{aligned} \quad (4.53)$$

$$\begin{aligned}
 c_{i,j} &= \frac{1}{h_t(h_t + h_b)} \\
 d_{i,j} &= \frac{1}{h_b(h_t + h_b)} \\
 e_{i,j} &= \frac{x_i}{h_r(h_r + h_l)} + \frac{x_i}{h_l(h_r + h_l)} + \frac{1}{h_t(h_t + h_b)} + \frac{1}{h_b(h_t + h_b)} \\
 f_{i,j} &= 0.
 \end{aligned}$$

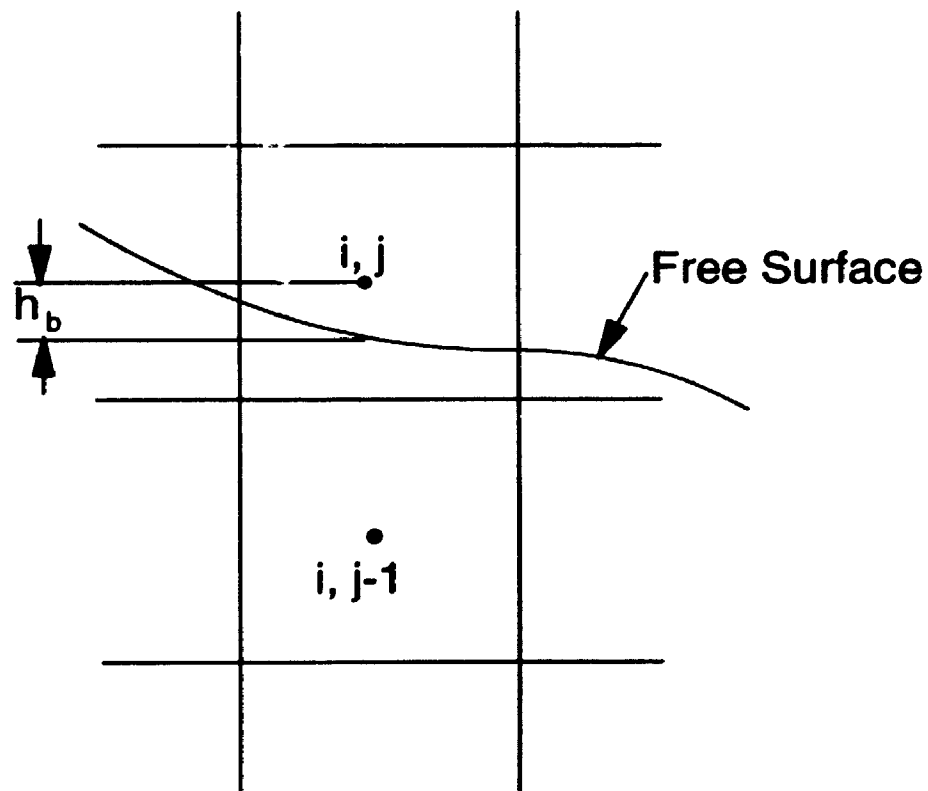


Figure 4.6: Definition of the h 's for the surface cells

If the cell (i, j) or any of its neighbours are metal nodes, then the coefficients $a_{i,j}$ to $f_{i,j}$ must be modified. For example, if the bottom neighbour is a metal node, then

we set

$$d_{i,j} = 0 \quad (4.54)$$

$$f_{i,j} = -\frac{\phi_{i,j-1}}{h_b(h_t + h_b)}. \quad (4.55)$$

Since cell $(i, j - 1)$ is a metal node in this case, $\phi_{i,j-1}$ is known and has a fixed value. Similarly, a metal node neighbour on the left will modify $b_{i,j}$ and $f_{i,j}$, and so on.

Equation 4.52 represents a linear system of equations. There are several direct and iterative methods for solving such systems. Direct solutions generally require excessive computational efforts and computer memory to solve large numbers of equations. Iterative methods are therefore the preferred. They are less time consuming and easier to implement than direct methods. In this thesis we employ an iterative technique referred to as *successive over relaxation* (SOR) [84]¹. In this technique the potential at each node is updated by scanning the set of mesh points in a prearranged manner. The updated potential at a node influences the next mesh point calculation. After each node has been updated, the entire mesh is scanned again until the solution converges within a preassigned tolerance. During the iteration process the boundary conditions at the electrodes and at the interface will propagate their influence throughout the mesh until a solution is obtained [7]. This is done by multiplying the potential residual $\zeta_{i,j}$, by a constant factor ω and adding it to the old potential at each mesh point (i, j) . That is

$$\phi_{i,j}^{new} = \phi_{i,j}^{old} - \omega \frac{\zeta_{i,j}}{e_{i,j}} \quad (4.56)$$

where $\zeta_{i,j}$ is the residual and is given by

$$\zeta_{i,j} = a_{i,j}\phi_{i+1,j} + b_{i,j}\phi_{i-1,j} + c_{i,j+1}\phi_{i,j+1} + d_{i,j}\phi_{i,j-1} - e_{i,j}\phi_{i,j} - f_{i,j}. \quad (4.57)$$

The constant ω is called the over relaxation parameter. If $\omega = 1$ in equation 4.56, then this reduces to the usual Gauss Seidel iteration procedure. In successive over

¹Southwell named this technique by analogy to the relaxation of strains in stressed, jointed frameworks [70]

relaxation method the value of ω is between 1 and 2. Therefore, the SOR procedure effectively accelerates the rate of convergence by adding a greater change of potential to the old potential than in the Gauss Seidel procedure. The optimum value of ω is highly problem dependent. It can be evaluated analytically only for the simplest configuration. In practice it is determined by trial and error. However, a numerical estimate can be obtained from the expression

$$\omega^{opt} = \lim_{n \rightarrow \infty} \left(\frac{\zeta_{max}^{n+1}}{\zeta_{max}^n} \right) \quad (4.58)$$

where ζ_{max} is the maximum residual of the nodes. For a rectangular mesh spacing, an approximate value of this optimum ω can also be evaluated from

$$\omega^{opt} = \frac{2}{1 + \sqrt{1 - \rho_{jacob}^2}} \quad (4.59)$$

where ρ_{jacob} is the spectral radius for the Jacobi method and is given by

$$\rho_{jacob} = \frac{\cos \frac{\pi}{I} + \beta^2 \cos \frac{\pi}{J}}{1 + \beta^2} \quad (4.60)$$

where $\beta = \frac{\delta r_z}{\delta z_j}$ is the grid aspect ratio and I and J represent the total number of grid points in the r and z directions respectively. Thus, we repeat the iterations with the optimum ω^{opt} until ζ_{max} is within some defined error ϵ . In our problem, ϵ is of the order of 10^{-6} .

The coupling of the electrostatic model and the fluid flow model occurs at the interface through the electric field. The electric field is defined as the gradient of the potential so that

$$E_r = -\frac{\partial \phi}{\partial r} \quad (4.61)$$

$$E_z = -\frac{\partial \phi}{\partial z}. \quad (4.62)$$

Therefore, the derivatives of the potential in both the r and z directions are required. There are various methods of numerical differentiations. Among them are central differencing, extrapolation techniques and polynomial techniques. After a thorough

numerical experimentation on the problem, a high order polynomial approximation is employed. A third order polynomial in r and z is used to locally to describe the potential at any point [68]. Therefore, in the r direction we let

$$\phi(r) = a_0 + a_1r + a_2r^2 + a_3r^3. \quad (4.63)$$

Then

$$E_r(r) = -a_1 - 2a_2r - 3a_3r^2 \quad (4.64)$$

and, using this expression for the potentials of the four nodes located at $r_1, r_2, r_3,$ and r_4 respectively, we find four equations for a_0, a_1, a_2 and a_3 . Then substituting for the a 's we obtain

$$E_r(r) = \phi_{12} + \phi_{123}(2r - r_1 - r_2) + \phi_{1234}(3r^2 - 2r_1r - 2r_2r - 2r_3r + r_1r_2 + r_1r_3 + r_2r_3) \quad (4.65)$$

where

$$\begin{aligned} \phi_{12} &= \frac{\phi_2 - \phi_1}{r_2 - r_1} \\ \phi_{123} &= \frac{\frac{\phi_3 - \phi_2}{r_3 - r_2} - \frac{\phi_2 - \phi_1}{r_2 - r_1}}{r_3 - r_1} \\ \phi_{1234} &= \frac{\frac{\frac{\phi_4 - \phi_3}{r_4 - r_3} - \frac{\phi_3 - \phi_2}{r_3 - r_2}}{r_4 - r_2} - \frac{\frac{\phi_3 - \phi_2}{r_3 - r_2} - \frac{\phi_2 - \phi_1}{r_2 - r_1}}{r_3 - r_1}}{r_4 - r_1} \end{aligned} \quad (4.66)$$

where ϕ_i is the potential at r_i . This expression can also be used for finding $E_z(z)$ by replacing the r 's with the z 's. If the electric field is required at a non-nodal location, then the potential is determined by interpolating the nearby potentials at the nodal points.

Experience with the problem shows that the selection of the four points for the derivative is crucial. It is found that only one metal node must be used to obtain best results. More than one consecutive metal node tends to distort the value of the electric field near metal node boundaries. For example, in figure 4.7 we use nodes 2, 3, 4 and 5 instead of 1, 2, 3, and 4.

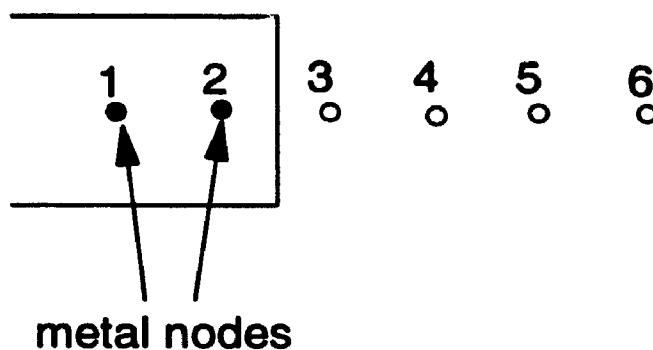


Figure 4.7: Selection of metal nodes

Once E_r and E_z are calculated using the above procedure, we must compute the normal component of the electric field. The pressure discontinuity at the interface due to the electric field as given by equation 4.13 is

$$P_s^e = -\epsilon_0 \frac{E_n^2}{2}. \quad (4.67)$$

The normal unit vector to the interface can be described by its slope if the surface is nearly horizontal, or by its inverse slope if the surface is nearly vertical. For example if the neighbouring interpolation cell is below the surface cell (i, j) , then the normal electric field component for a nearly horizontal surface will be

$$E_n = \frac{mE_r - E_z}{\sqrt{1 + m^2}} \quad (4.68)$$

where m is the slope. Similarly, for a nearly vertical slope

$$E_n = \frac{E_r - m'E_z}{\sqrt{1 + m'^2}} \quad (4.69)$$

where m' is the inverse slope. Similar expressions can be found for other arrangements of the surface cell and neighbouring cells.

Now we substitute the computed E_n into equation 4.67 and enter it into equation 4.49 to obtain the total surface pressure P_s .

4.4 The Initial Equilibrium Shape

The equilibrium shape of droplet A which is in contact with surrounding fluid B is governed by the Young-Laplace equation. This is the basic equation of capillarity [5]

$$\Delta P = \gamma \left(\frac{1}{R_1} + \frac{1}{R_2} \right). \quad (4.70)$$

This equation relates the interfacial tension to the pressure difference between the fluids at each point along the interface.² The pressure difference ΔP may be obtained from the hydrostatic equation

$$\Delta P = (\rho_1 - \rho_2)gz + \frac{2\gamma}{b} \quad (4.71)$$

where b is the principal radius of curvature at the origin O for our cylindrical coordinates (r, z) . The first term in equation 4.71 represents the hydrostatic pressure and the second term represents the reference pressure which is chosen at the apex for the sake of convenience. The principal radii of curvature for the axisymmetric droplet is

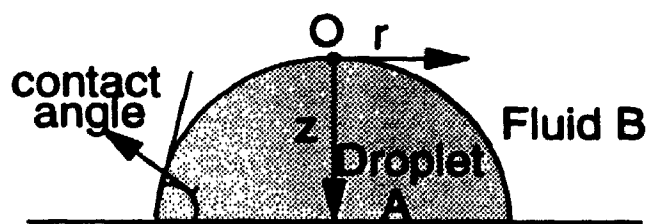


Figure 4.8: Equilibrium profile of a sessile droplet.

²This relation is the basis of most experimental methods for measuring the interfacial surface tension γ of liquids.

given by [3]

$$\begin{aligned}\frac{1}{R_1} &= \frac{\frac{d^2 z}{dr^2}}{\left(1 + \left(\frac{dz}{dr}\right)^2\right)^{\frac{3}{2}}} \\ \frac{1}{R_2} &= \frac{\frac{dz}{dr}}{r \left(1 + \left(\frac{dz}{dr}\right)^2\right)^{\frac{1}{2}}}\end{aligned}\quad (4.72)$$

so that equation 4.71 becomes

$$\gamma \left\{ \frac{\frac{d^2 z}{dr^2}}{\left(1 + \left(\frac{dz}{dr}\right)^2\right)^{\frac{3}{2}}} + \frac{\frac{dz}{dr}}{r \left(1 + \left(\frac{dz}{dr}\right)^2\right)^{\frac{1}{2}}} \right\} = (\rho_1 - \rho_2)gz + \frac{2\gamma}{b}. \quad (4.73)$$

This second order ordinary differential equation and the boundary conditions $z(0) = 0$ and $z'(0) = 0$ define the equilibrium shape of the droplet where prime denotes the differentiation with respect to r . Unfortunately, this cannot be solved analytically except in certain limiting cases. Usually, a numerical method such as the Runge-Kutta technique is implemented. In the absence of gravity, however, the equation can be written in the simple form

$$\frac{d}{dr} \left(\frac{rz'}{(1+z'^2)^{\frac{1}{2}}} \right) = \frac{2r\gamma}{b} \quad (4.74)$$

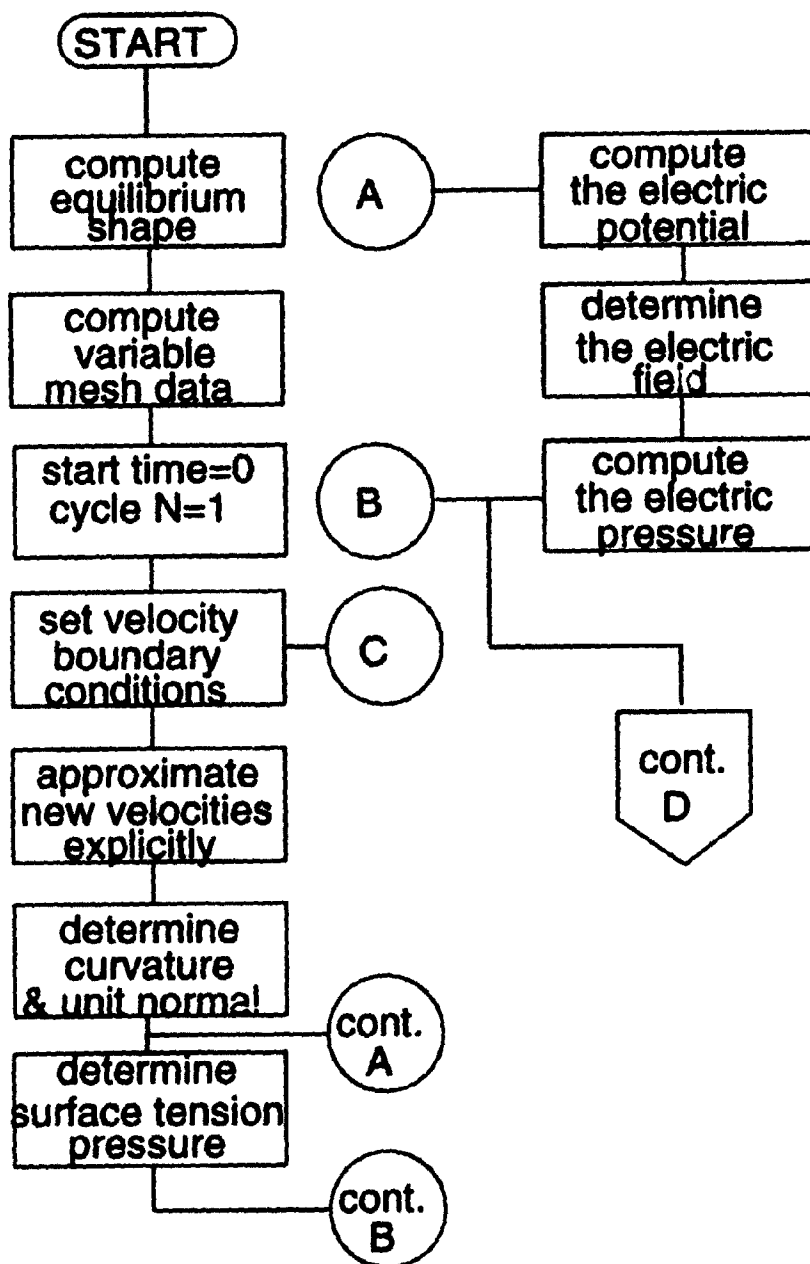
which may be easily integrated to obtain the following circular arc:

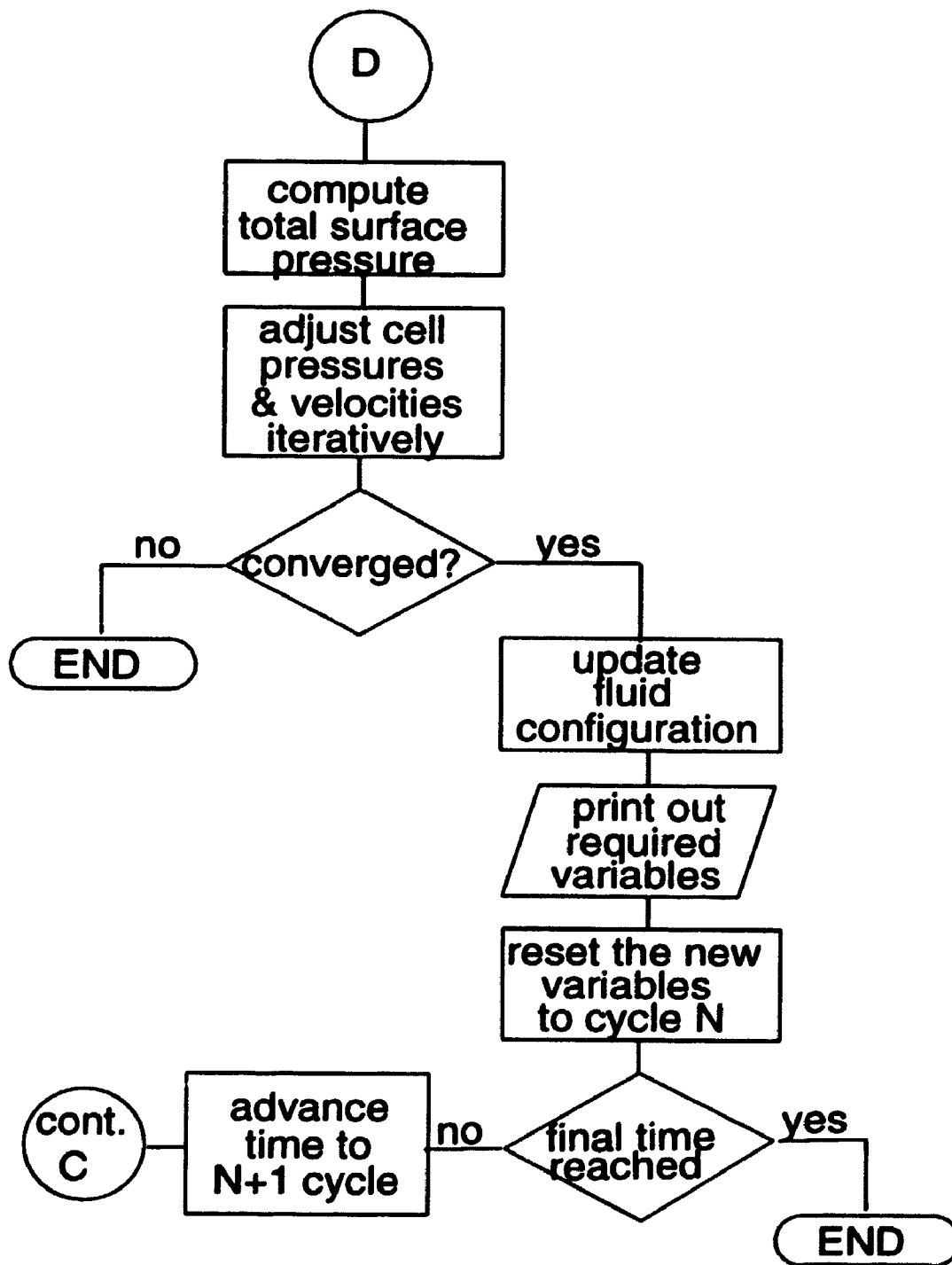
$$(c - z)^2 + r^2 = \left(\frac{b}{\gamma}\right)^2. \quad (4.75)$$

The constant c is determined by the contact angle λ which is generally a material property of the fluids and solids which are present. If this angle is 90 degrees, then the shape of the droplet is a hemisphere and it's radius is dependent on the total volume of the droplet.

4.5 Flow Chart of the Numerical Model

The flow chart below illustrates the calling sequence of the various computational steps. It summarizes the procedures involved in advancing one time step.





4.6 Numerical Results

In order to investigate the validity of our numerical procedure, we carry out numerical computations on a water droplet with a volume of 3 cm^3 . The droplet is placed on the lower electrode of a parallel electrode system which is kept at a potential difference of 30,000 volts. The difference between the electrodes is 7.5 cm. These parameters are chosen for the purpose of making direct comparisons with the the experimental data, described below.

The typical flow parameters for water at the ambient temperature are

$$\rho = 1000 \text{ kg/m}^3$$

$$\nu = 9.7 \times 10^{-7} \text{ m}^2/\text{sec}$$

$$\gamma = 7.2 \times 10^{-2} \text{ N/m.}$$

The initial equilibrium shape of the droplet is computed using the sessile droplet model developed in section 4.4. The result in figure 4.9 shows that the contact angle between the fluid interface and the lower electrode is 82 degrees. By employing the equilibrium configuration as our initial condition, we carry out numerical computations to simulate the evolution of the droplet up to 54 milliseconds utilizing the numerical algorithm developed in this chapter.

The computations are carried out on the Cyber 962. We employ a 100×100 mesh for the computational area between the two electrodes. The time step is $\delta t = 0.1$ milliseconds. This small time step is used in order to guarantee convergence. The evolution of the droplet is shown by plotting the surface plot coordinates for various times. Figures 4.10 to 4.18 depict the various stages of the droplet's evolution. The equally spaced square mesh background is plotted to give a dimensional reference for our analysis and comparison with the experimental data. The size of each grid is 0.25 millimeters which is the size used for the background frame during the experiment. The initial droplet profile has a maximum horizontal diameter of 2.76 cm. at the

bottom axis and a maximum vertical radius of 1.14 cm. at the vertical axis.

Once the electric field is applied, the droplet elongates at the tip following the direction of the electric field and forms into a cone shape. This is depicted in figure 4.10 where $t = 25.6$ milliseconds. Figure 4.11 shows the droplet profile at 28.3 milliseconds where the first breakup is about to occur. At this stage, the droplet's maximum vertical radius has elongated to 1.36 cm. The volume of the droplet is conserved, however, since the contact line between the lower electrode and the droplet surface is moving inward. The maximum horizontal diameter is 2.66 cm. Less than 0.3 milliseconds later, the first droplet breaks off as shown in figure 4.12 at $t = 28.5$ milliseconds. The emitted droplet occupies only two grid spaces and it's estimated volume is approximately 0.3 cubic millimeters. As shown in figure 4.13, the emitted droplet travels a distance of approximately 1 cm in less than 8 milliseconds. As the droplet approaches the upper electrode, it accelerates rapidly. Since the model does not incorporate space charge and other phenomena associated with the breakup, the computations carried out after the first breakup may not be accurate. The second breakup occurs at 40 milliseconds as shown in figure 4.14. This is 11.5 milliseconds after the first breakup. Figure 4.15 illustrates the subsequent evolution at 51 milliseconds. The conical shape at the tip of the droplet in figure 4.16 at $t = 52$ milliseconds indicates the imminent emission of a third droplet. This breakup occurs at 52.5 milliseconds; 12.5 milliseconds after the second breakup. The profile of the droplet after the third break up is depicted in figure 4.16 at $t = 54$ milliseconds. Here, the contact line has moved inward to a maximum horizontal radius of 2.5 cm.

4.7 Comparison of the Model With Experimental Results

In 1991, microgravity experiments were carried out jointly by the Applied Electrostatic Research Centre of the University of Western Ontario and the Canadian Space

Agency. The microgravity conditions were produced with NASA KC 135 aircraft flights. The experiment apparatus shown in appendix C consisted of a parallel electrode system, a high-speed camera, a charge/current measuring unit and a data acquisition system. A detailed description of the apparatus and of the experimental methodology is reported in reference [36].

Large liquid droplets were generated and placed between two parallel plane electrodes separated by a distance of 7.5 cm. The maximum potential difference between the electrodes was 60,000 volts. When the electric field was applied, the droplet elongated, formed into a cone and emitted small droplets. The evolution of each droplet was recorded with a high speed camera at a rate of 2000 frames per second. The charge transfer from the sessile droplet to the smaller, emitted droplets was recorded using a charge/current measurement unit. Samples of the pictures taken during these experiments are provided in appendix C.

Prior to the application of the electric field, the droplet's surface made a contact angle of 82 degrees with the lower electrode. After the electric field was applied, the contact line, which is the intersection between the droplet surface and the lower electrode, moved continuously and the contact angle did not remain constant. The sessile droplet then formed into a cone shape and emitted a droplet of 0.3 cm^3 at $t = 650$ milliseconds. The data collected from the charge/current measurement unit shows that there were several intermittent charge losses well before the droplet was emitted. Once this initial break-up occurred, the pictures reveal that the flow was not axisymmetric.

Recall that our numerical results predicted that droplets would be emitted at $t = 28.5, 40$ and 52.5 milliseconds and that the droplets would be quite small; 0.3 cubic millimeters. The critical breakup time observed during the experiment was considerably longer and the the size of the emitted droplet was considerably larger than these predictions. The reason that the experiment was unable to record the existence

of droplet emission before $t = 650$ milliseconds is that the droplets emitted prior to that time were too small to be detected. In reality, these ejected droplets are tiny dots travelling at high speed. This conclusion is supported by the data collected from the charge/current measurement unit. The intermittent charge fluctuations of the sessile droplet observed during the experiment can be attributed to the loss of charge as the small droplets were emitted prior to $t = 650$ milliseconds. Unfortunately, due to the lack of analyzed charge data, this conclusion cannot yet be quantitatively verified. Therefore, further experimental studies which employ more accurate charge/current instrumentation are suggested in order to evaluate and compare the observed charge losses at the breakup.

4.8 Future Improvements and Considerations

Both the experimental and numerical results suggest that further studies are required in a number of areas to successfully model the behaviour of the droplets.

It is clear that the dynamic behaviour of the contact angle and the contact line is an important factor in the deformation process. The dynamic contact line introduces additional modelling difficulties which arise because it describes the intersection of a solid with the interface of the fluids. In our problem, the zero shear-stress boundary condition applies at the air-water interface while the no-slip boundary condition applies at the water-solid interface. Both of these conditions must be satisfied at the contact line. Studies of dynamic contact lines show that this essentially leads to an infinite velocity gradient [44]. This apparent contradiction is due to the fact that, in the immediate neighbourhood of the contact line region, the continuum approach breaks down. Consequently, the molecular activities in that region such as absorption, relaxation and re-orientation become important [67]. Further experimental and numerical investigations are therefore recommended.

Since the experiments were carried out in microgravity conditions, the zero gravity

assumption made in our model should be modified to incorporate the effects of residual accelerations present during the flight. The sources of these residual accelerations include the earth's gravity gradient, the atmospheric drag on the spacecraft and the spacecraft altitude motions arising from machine vibration and crew movement during the experiment [37]. The effects of these accelerations are not yet completely understood. However, recent studies suggest that they may be important in experiments involving bubbles and drops [37]. Attempts have been made to model microgravity experiments involving bubbles using a sinusoidal function vibration of gravity environment [29]. However, further investigation is required in order to examine the effect of these residual accelerations on our experiment.

The droplet deformation, as recorded in the experiment, is eventually characterized by the full, three-dimensional equations of motion. Therefore, our axisymmetric assumption becomes invalid at this point, and we must consider the full, three-dimensional Navier Stokes equations. Since three-dimensional solutions of free surface problems are still not fully developed, this poses an interesting research problem for future study.

Finally, it is recommended that this model be extended to include non-conducting liquids. For these fluids, further investigation is required in order to take into account the effect of charge relaxation as discussed in chapter 3. In practical situations, we can assume that any liquid which can be effectively charged through induction will have sufficiently high conductivity to satisfy this model.

4.9 Concluding Remarks

The dynamic behaviour of a viscous droplet in zero gravity and under the influence of applied electric fields was investigated by numerically computing the axisymmetric Navier Stokes equations which were subjected to initial and boundary conditions. The initial condition of the droplet profile was determined by solving the Young-

Laplace equation of capillarity and the core of the fluid flow model was adapted from the NASA-VOF2D algorithm developed by Torrey *et. al.* [79]. The electrostatic equations were solved using finite difference techniques.

The model was successful in predicting the dynamic deformation process of the droplet including its breakup. Although the numerically observed breakups were too small to be detected experimentally, our computational results were supported by the charge loss measurements of the sessile droplet carried out during the experiment.

Potential difficulties involving contact line problems, residual acceleration and the charge relaxation process were identified. Further investigation of these difficulties by extending the model to simulate the full, three-dimensional problem is recommended.

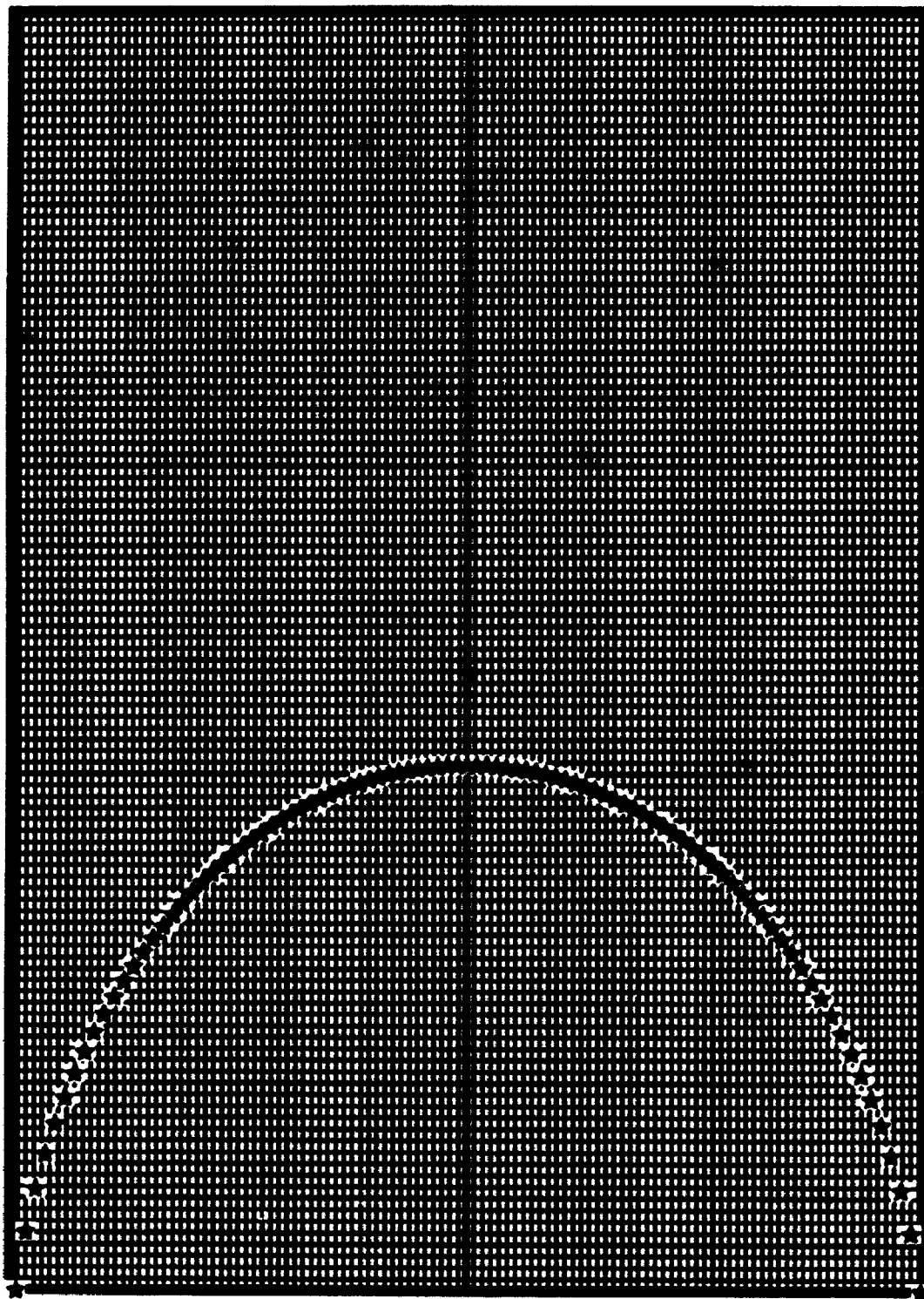


Figure 4.9: Equilibrium droplet profile at $t = 0$ milliseconds. The contact angle is 82 degrees.

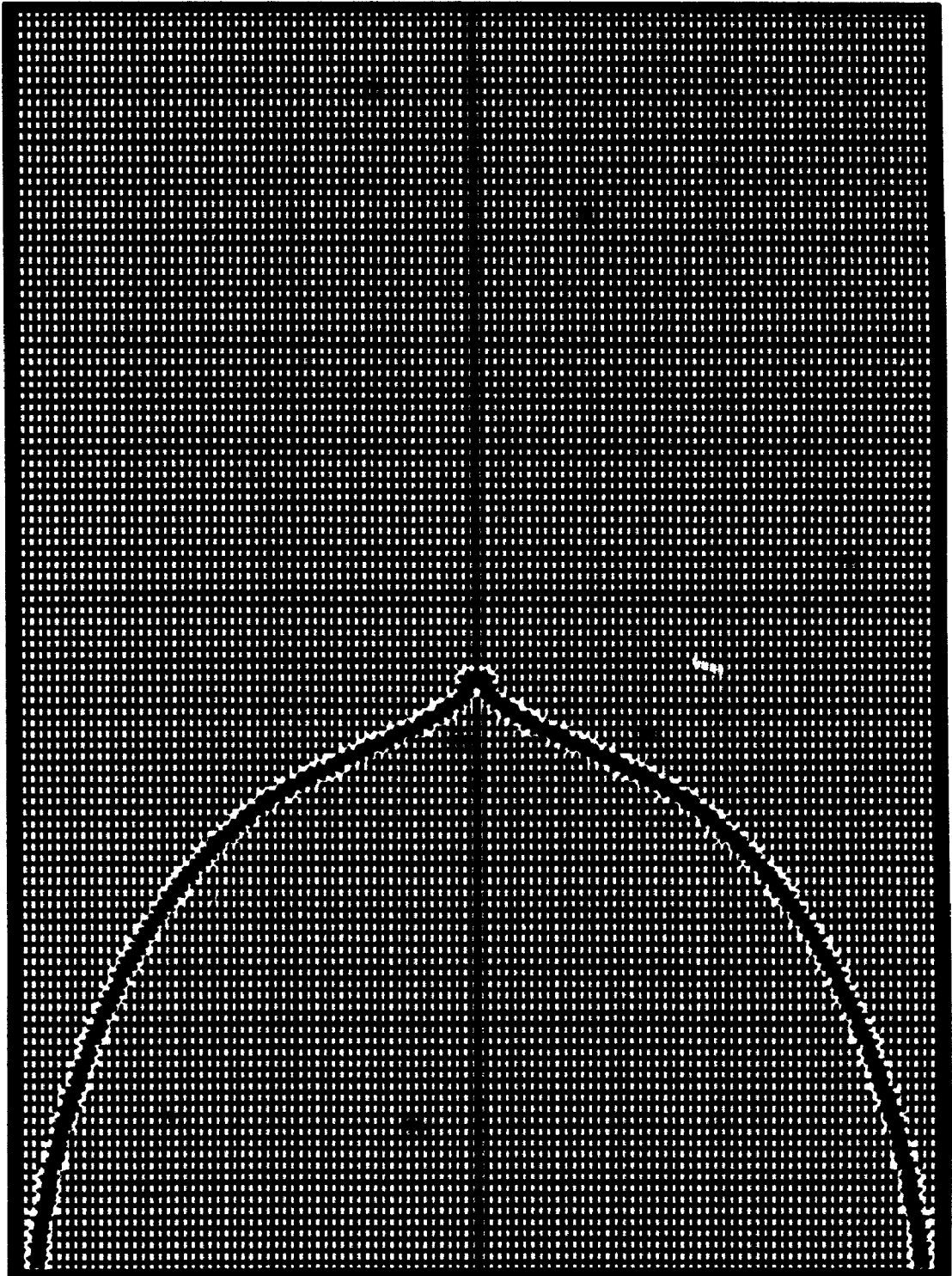


Figure 4.10: Droplet profile at $t = 25.6$ milliseconds.

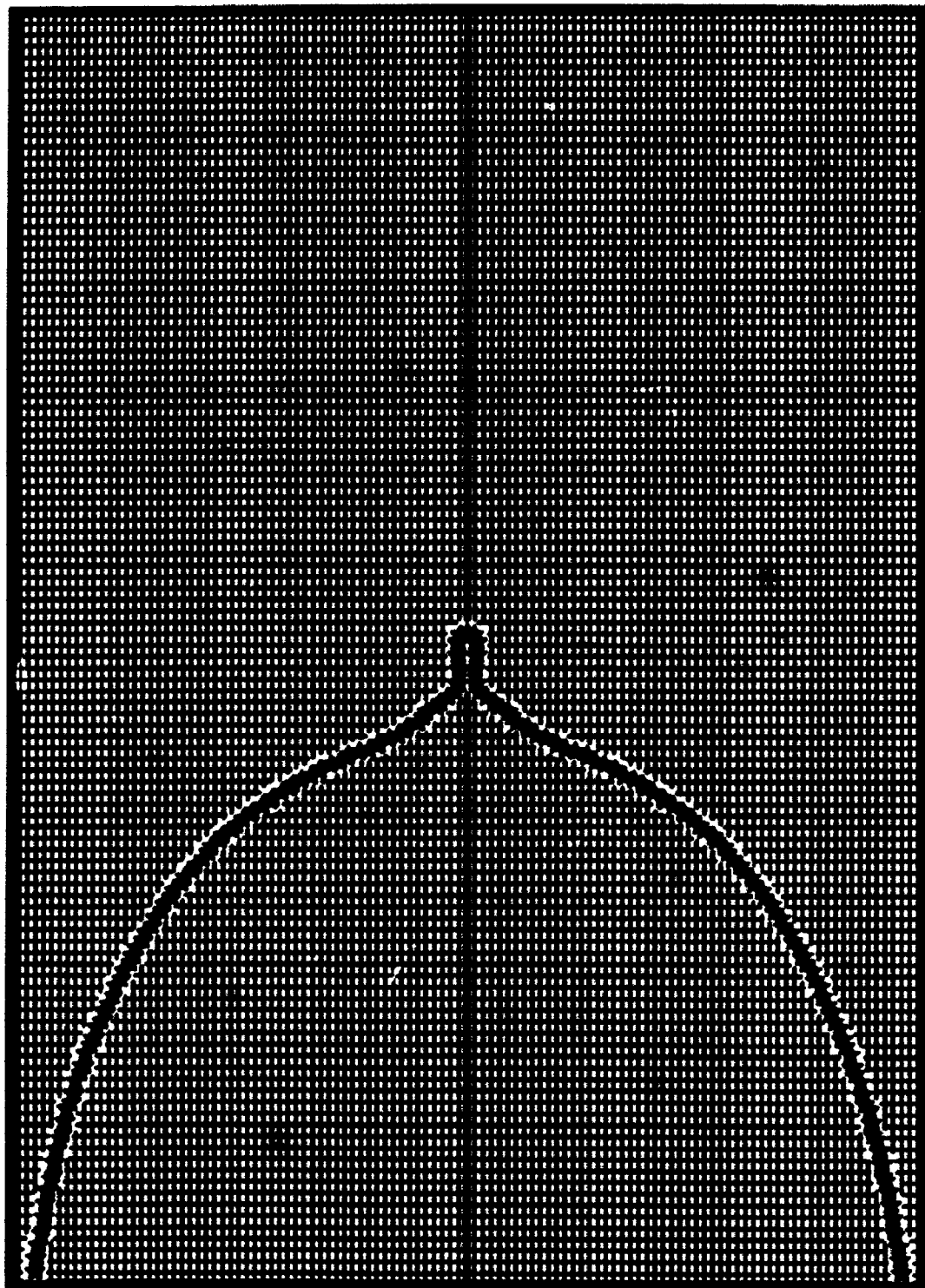


Figure 4.11: Droplet profile at $t = 28.3$ milliseconds.

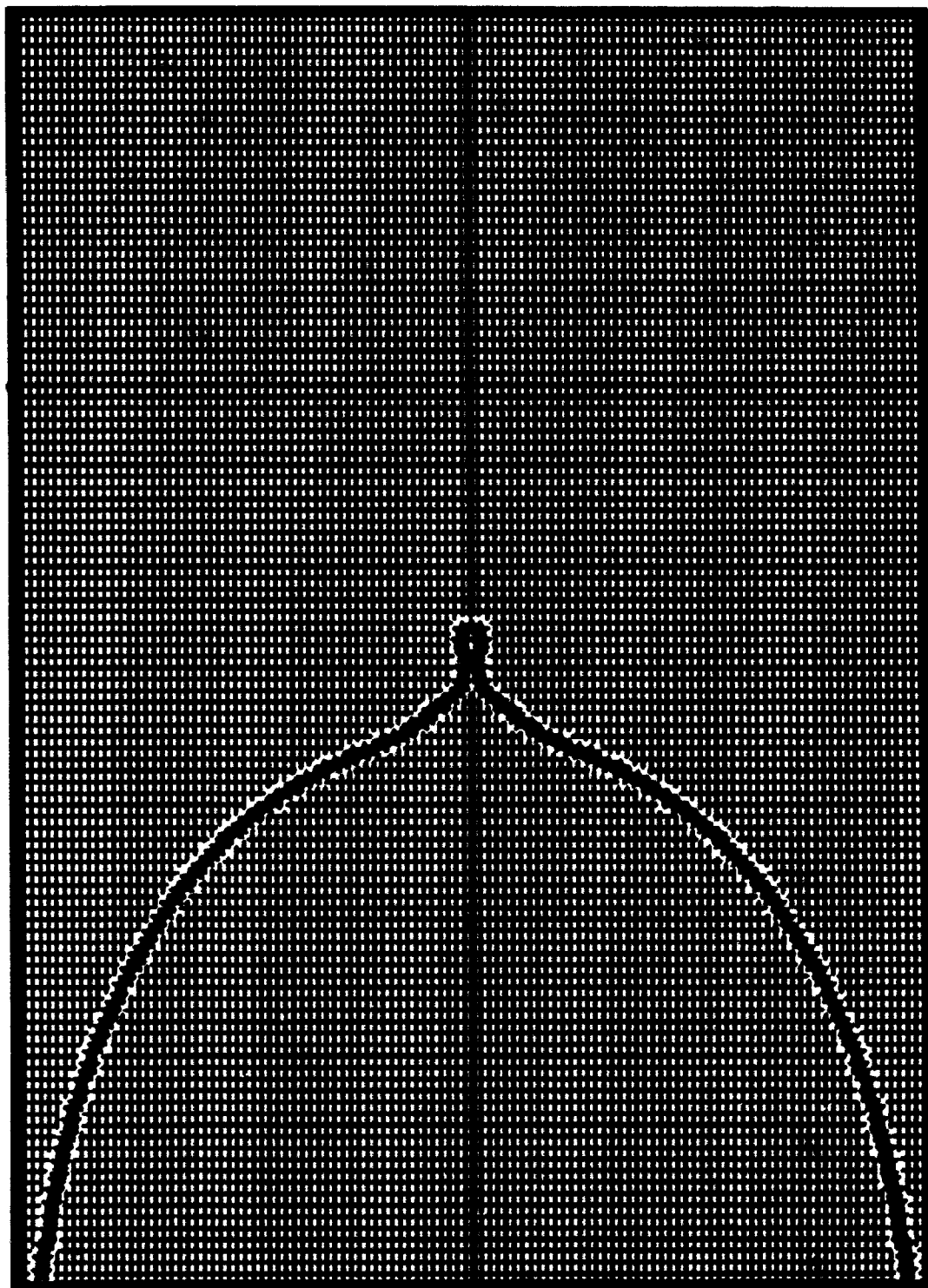


Figure 4.12: Droplet profile at $t = 28.5$ milliseconds. First breakup occurs.

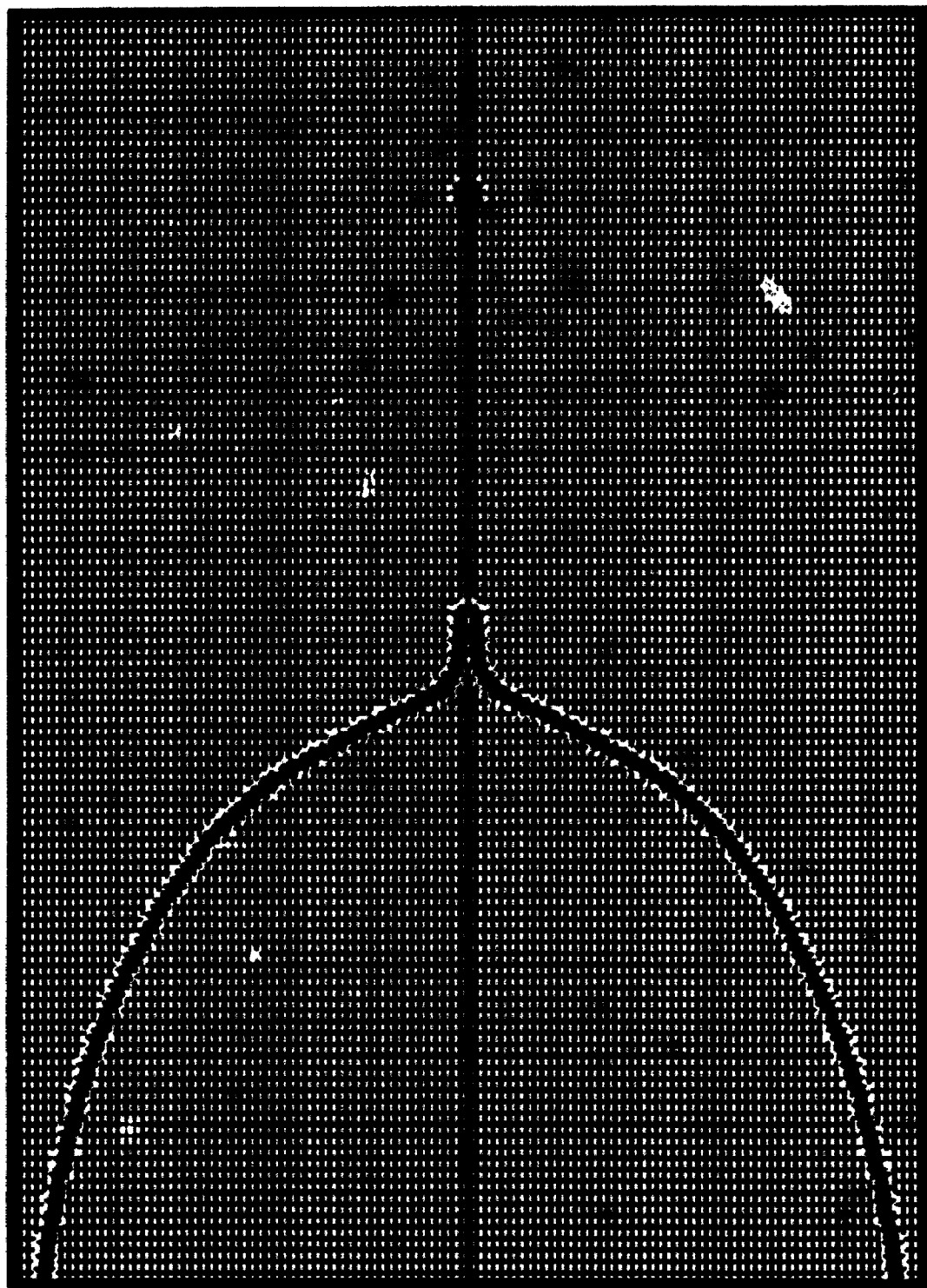


Figure 4.13: Droplet profile at $t = 36$ milliseconds.

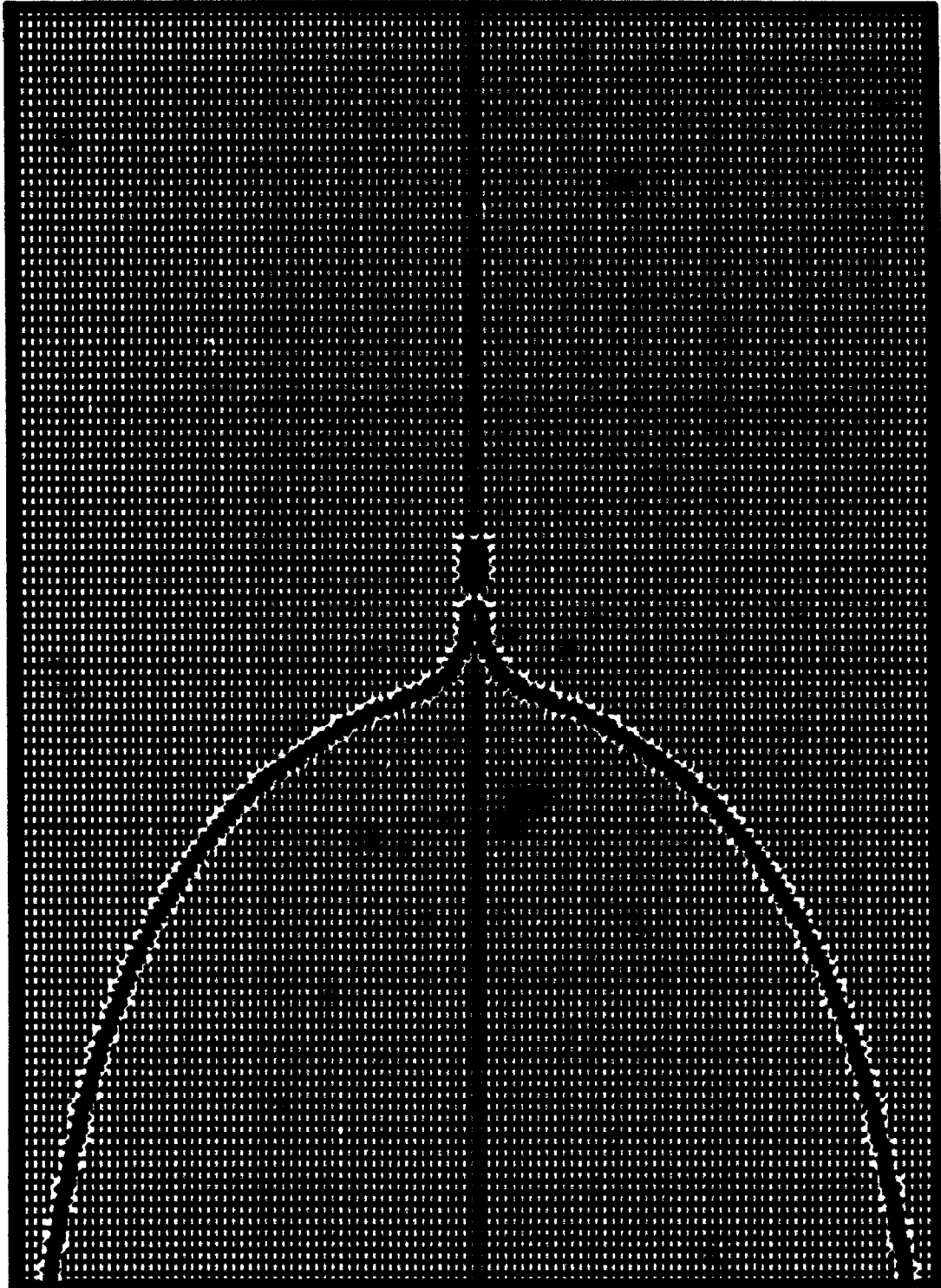


Figure 4.14: Droplet profile at $t = 28.5$ milliseconds. Second breakup occurs.

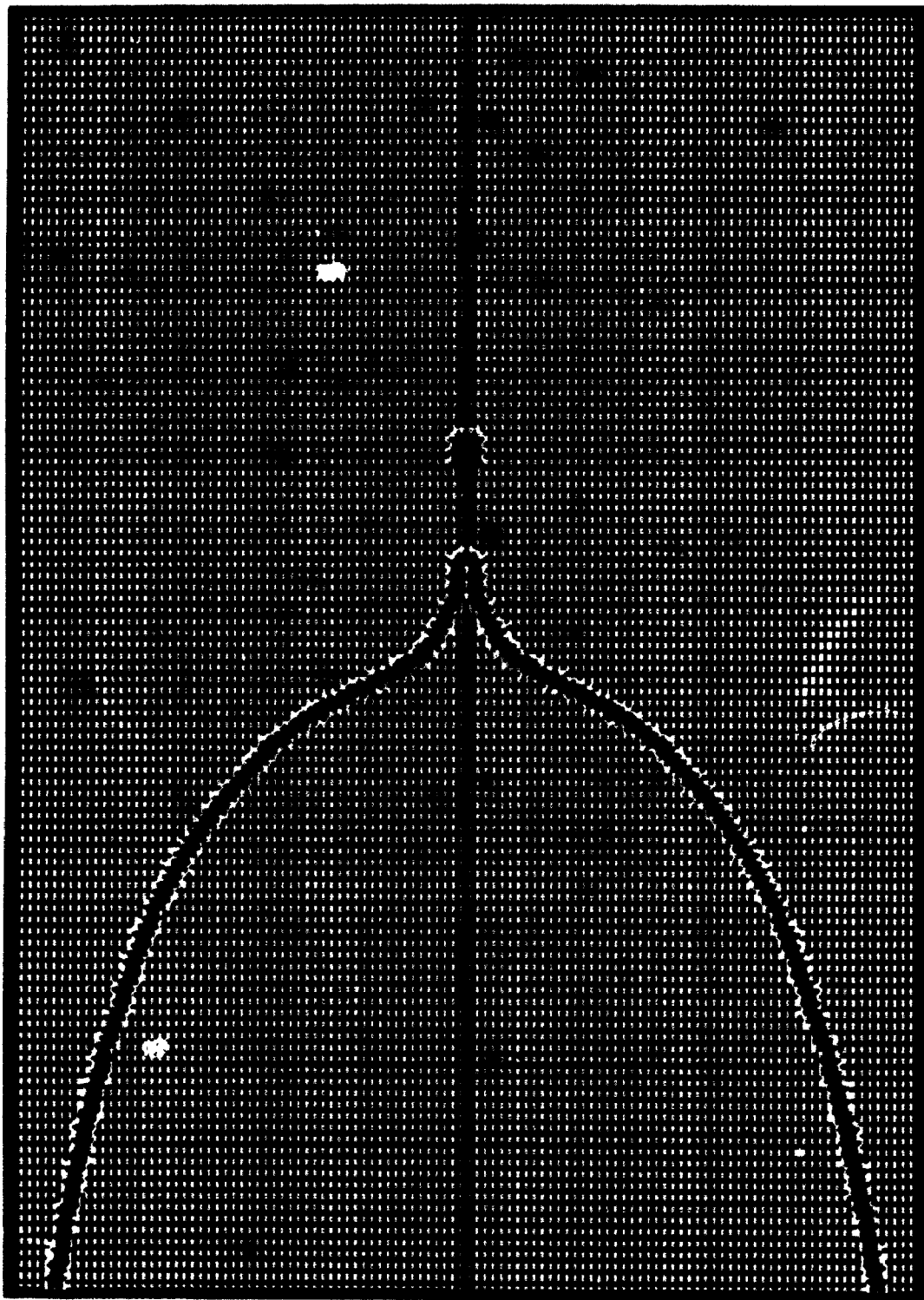


Figure 4.15: Droplet profile at $t = 51$ milliseconds.

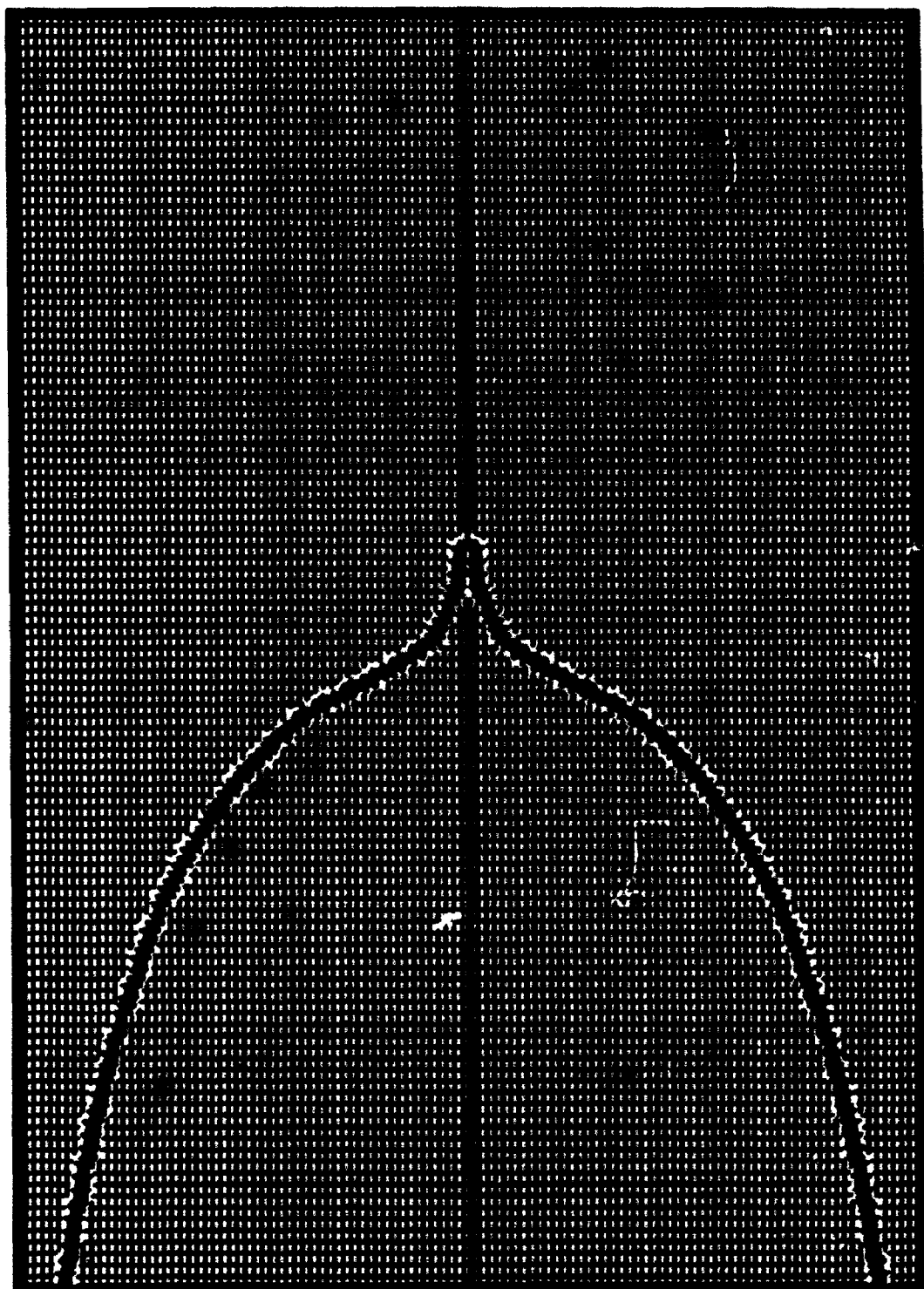


Figure 4.16: Droplet profile at $t = 52$ milliseconds.

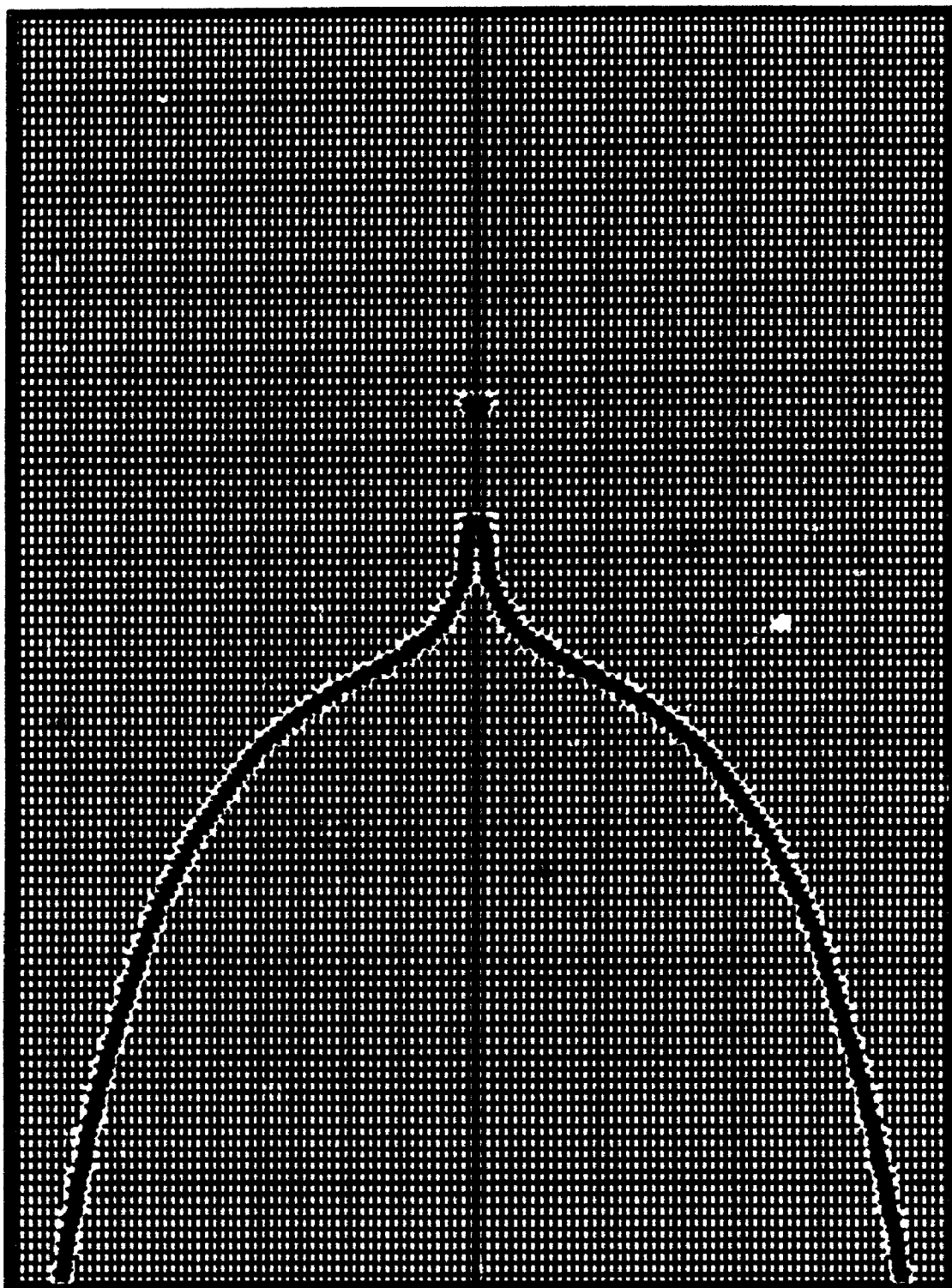


Figure 4.17: Droplet profile at $t = 54$ milliseconds. Third breakup has occurred.

Chapter 5

Conclusion

In this thesis we examined three fluid dynamic problems. First, we dealt with the hydrodynamic instability at the interface between two fluids. The stability of the flow was characterized by four parameters; the ratio of the viscosities, the ratio of the densities, the surface tension and gravity. The dispersion relation relating these parameters was solved both asymptotically and numerically. The two solutions were in excellent agreement. For the case of equal densities, the discrepancies between the numerical and the asymptotic solutions reported by Hooper and Boyd were resolved [33]. For the general case of unequal densities, long and short wavelength analyses were carried out. This result removes Hooper and Boyd's restriction on the allowable values of surface tension.

Second, we examined the electrohydrodynamic instability of the shear flow problem. Various limiting cases were investigated and the conditions for the incipience of static instability were determined. The results revealed that, in the presence of equilibrium motion, the principal of exchange of stabilities is not valid. The electric field did not have any effect on stability in the long wavelength limit. However, in the short wavelength limit the electric field had a lesser effect on the stability of the flow than the surface tension. For configurations involving finite relaxation times, the stability of the flow was characterized by the Hartmann number and by the ratio of the conductivities. In general, the Hartmann number had a destabilizing effect.

Finally, we investigated the dynamic deformation of liquid droplets by electric fields in zero gravity conditions. The core of the fluid flow problem was solved by employing a modified NASA-VOF2D algorithm developed by Torrey *et. al.*[79]. Numerical computations carried out using our model were compared with measurements obtained from microgravity experiments. The model successfully predicted the deformation of the droplet up to and including breakup. Due to the small size of the emitted droplets, the numerically computed breakups were not detected by the microgravity experiment. However, the presence of these breakups was supported by the charge measurements that were carried out during the experiment. Several modifications to the numerical model and to the experiment were recommended including a consideration of the three dimensional problem.

Appendix A

Airy Functions

The Airy differential equation is given by

$$\frac{d^2 w}{dz^2} - zw = 0. \quad (\text{A.1})$$

Two linearly independent solutions which are real when z is real are $Ai(z)$ and $Bi(z)$ which satisfy the initial conditions [1]

$$\begin{aligned} Ai(0) &= \frac{3^{-\frac{2}{3}}}{\Gamma\left(\frac{2}{3}\right)} \\ Ai'(0) &= -\frac{3^{-\frac{1}{3}}}{\Gamma\left(\frac{1}{3}\right)} \\ Bi(0) &= \frac{3^{-\frac{1}{6}}}{\Gamma\left(\frac{2}{3}\right)} \\ Bi'(0) &= \frac{3^{\frac{1}{6}}}{\Gamma\left(\frac{1}{3}\right)}. \end{aligned} \quad (\text{A.2})$$

We note that $Ai(\tilde{\omega}z)$ and $Ai(\omega z)$ also represent a pair of linearly independent solutions where $\omega = \epsilon^{\frac{2\pi i}{3}}$ [57].

The asymptotic series for $Ai(z)$ is given by

$$Ai(Z) = \pi^{-1/2} Z^{-1/4} e^{-2/3 Z^{3/2}} \left(\sum_{k=1}^{\infty} (-1)^k d_k \left(\frac{2}{3} Z^{3/2}\right)^{-k} \right) \quad (\text{A.3})$$

$$Ai'(Z) = \pi^{-1/2} Z^{1/4} e^{-2/3 Z^{3/2}} \left(\sum_{k=1}^{\infty} (-1)^k c_k \left(\frac{2}{3} Z^{3/2}\right)^{-k} \right) \quad (\text{A.4})$$

where

$$d_0 = 1 \quad d_k = \frac{\Gamma(3k + \frac{1}{2})}{54^k k! \Gamma(k + \frac{1}{2})} \quad \text{and} \quad e_1 = 1 \quad e_k = -\frac{6k + 1}{6k - 1} d_k.$$

which is valid when $|\text{Arg}z| < \pi$. [1]

The Wronskian of the functions $Ai(z)$ and $Ai(\omega z)$ is equal to

$$W(Ai(z), Ai(\omega z)) = \frac{1}{2\pi} e^{\frac{-\pi i}{6}}$$

Appendix B

The Coefficients c_{4s} and c_{5s}

$$c_{4s} = \frac{c_{41}}{S} \quad (\text{B.1})$$

$$c_{5s} = \frac{c_{51}}{S} \quad (\text{B.2})$$

where

$$\begin{aligned} c_{41} = & im^6 S^5 \left[4920 m^3 r + 4920 m^3 r^3 + 5 r^4 + 32 m^5 r + 162 m^4 r^2 + 337 r^4 m^2 \right. \\ & + 162 m^2 r^2 + 428 m^4 r + 6730 m^3 r^2 + 59 m r^4 + 1628 r^4 m^3 + 428 m^2 r^3 \\ & + 337 m^4 + 1628 m^3 + 59 m^5 + 5 m^6 + 32 m r^3 \left. \right] / \left[8192 (1+m)^9 r^4 \right] \\ & + m^4 S^3 \left[-14 m^6 - 47 m^5 r - 123 m^5 - 920 m^4 r - 691 m^4 - 435 m^4 r^2 \right. \\ & + 256 m^3 r^2 - 256 m^3 r - 368 m^3 + 368 m^3 r^3 + 435 r m^2 + 691 m^2 r^3 \\ & + 920 m^2 r^2 + 123 m r^3 + 47 m r^2 + 14 r^3 \left. \right] / \left[512 r^3 (1+m)^7 \right] \\ & + im^2 S \left[(9 r^4 m^6 + 8 m^6 + 22 m^5 r + 27 r^4 m^5 + 94 m^5 - 52 m^4 r \right. \\ & + 64 m^4 + 27 r^4 m^4 - 14 m^3 + 9 r^4 m^3 - 164 m^3 r - 5 m^3 r^2 - 52 r m^2 \\ & + 91 m^2 r^2 + 22 r m + 121 m r^2 + 17 r^2 \left. \right] / \left[64 r^2 (1+m)^5 \right] \\ c_{51} = & -m^7 S^6 i \left[7118 m^3 r^3 + 9529 m^5 r + 105872 m^4 r^2 + 1351 r^4 m^2 + 61572 m^4 r \right. \\ & + 2038 m^3 r^2 + 95 m r^4 + 9529 r^4 m^3 + 442 m^2 r^3 + 61572 r^4 m^4 + 2038 m^5 r^3 \\ & + 7118 m^5 r^2 + 95 m^7 r + 1351 m^6 r + 442 m^6 r^2 + 105872 r^3 m^4 + 1213 m^2 r^5 \\ & + 4943 m^3 r^5 + 16744 m^4 r^5 + 189 m r^5 + 4943 m^5 + 16744 m^4 + 1213 m^6 \\ & + 14 m^8 + 189 m^7 + 14 r^5 \left. \right] / \left[65536 r^5 (1+m)^{11} \right] \end{aligned}$$

$$\begin{aligned}
& + m^5 S^4 \left[-99 m^8 - 376 m^7 r - 1015 m^7 - 4920 m^6 - 4170 m^6 r - 1072 m^6 r^2 \right. \\
& - 33666 m^5 r - 17761 m^5 - 10098 m^5 r^3 - 28206 m^5 r^2 + 8973 r^4 m^4 + 11806 r^3 m^4 \\
& - 8973 m^4 - 11806 m^4 r + 17761 r^4 m^3 + 33666 m^3 r^3 + 10098 m^3 r + 28206 m^3 r^2 \\
& \left. + 4170 m^2 r^3 + 1072 m^2 r^2 + 4920 r^4 m^2 + 376 m r^3 + 1015 m r^4 + 99 r^4 \right] \\
& / \left[8192 r^4 (1+m)^9 \right] i m^3 S^2 \left[(3688 m^3 r^3 - 251 m^5 r - 2816 m^4 r^2 - 2879 m^4 r \right. \\
& - 62 m^3 r^2 + 2040 m^2 r^3 + 63 r^4 m^4 - 1029 m^5 r^2 + 68 m^7 r + 1281 m^6 r + 218 m^6 r^2 \\
& + 156 r^3 m^4 + 63 m^4 r^5 - 1029 m^3 r + 1535 m^5 + 93 m^4 + 1959 m^6 + 48 m^8 \\
& + 397 m^7 + 218 r m^2 + 81 r^4 m^6 + 153 r^4 m^5 - 36 r^4 m^8 + 189 r^5 m^5 + 189 m^6 r^5 \\
& \left. - 45 m^7 r^4 + 12 r^3 + 1470 m^2 r^2 + 352 m r^3 + 131 m r^2 + 63 m^7 r^5 \right] \\
& / \left[512 r^3 (1+m)^7 \right]. \tag{B.3}
\end{aligned}$$

Appendix C

Photographs From The Experiment

All the experiments were carried out by the Applied Electrostatic Research Center at The University of Western Ontario in conjunction with the Canadian Space Agency.

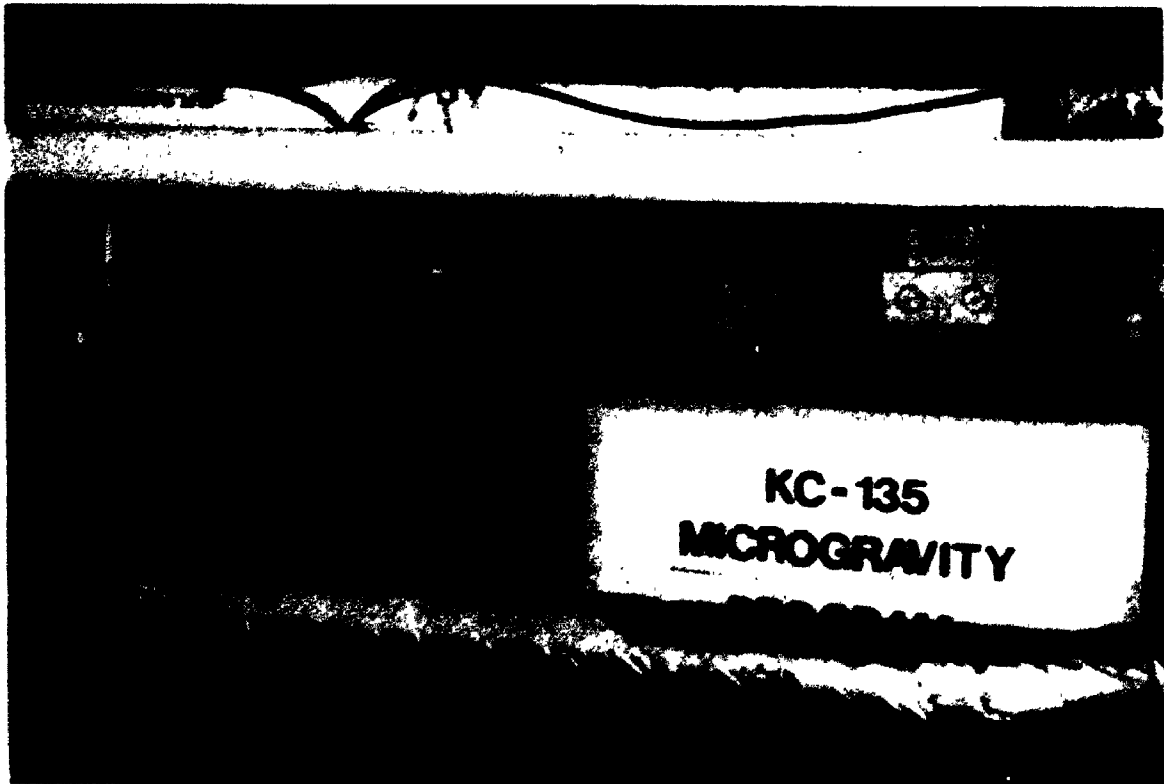


Figure C.1: The over all view of the microgravity experimental apparatus.

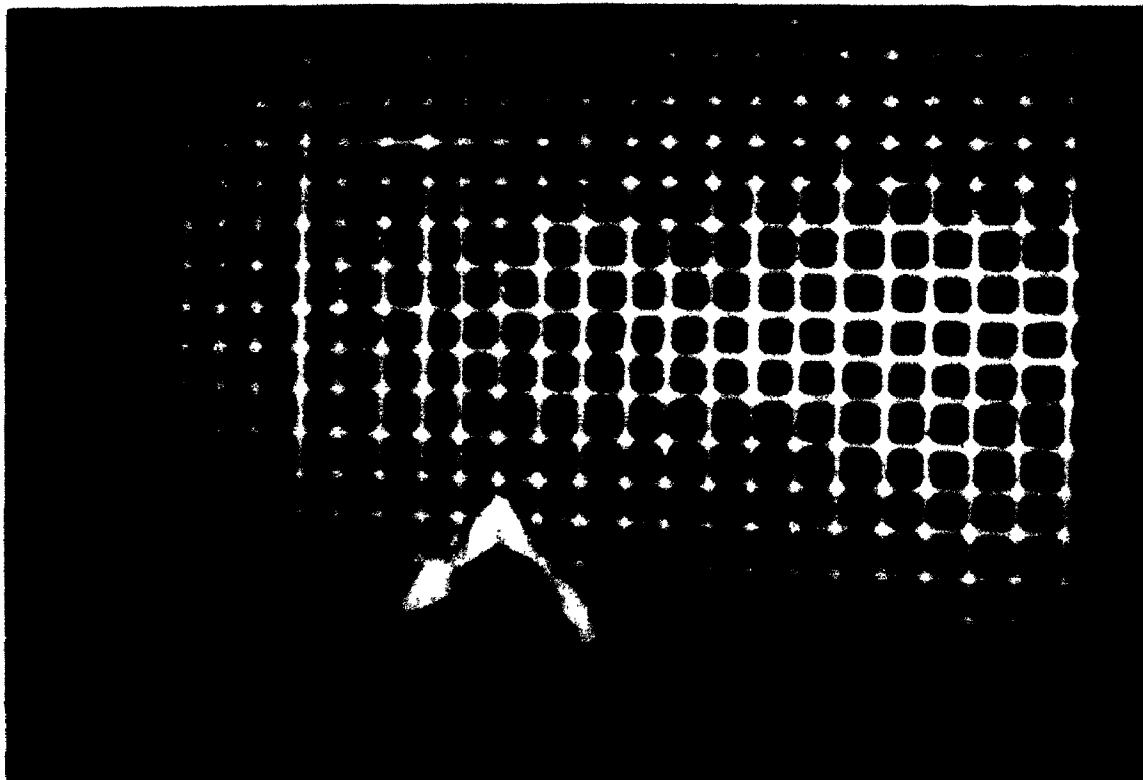


Figure C.2: The experimental droplet profile for water on a brass electrode before breakup

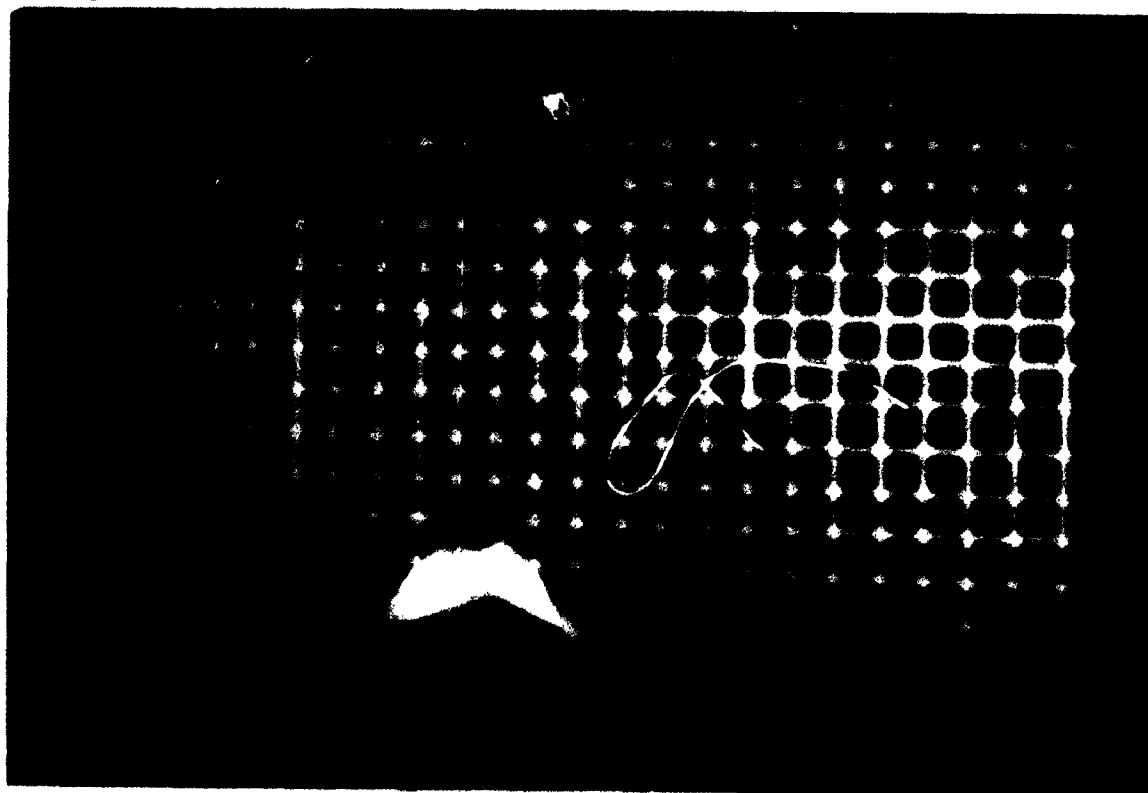


Figure C.3: The experimental droplet profile for water on a brass electrode just before breakup

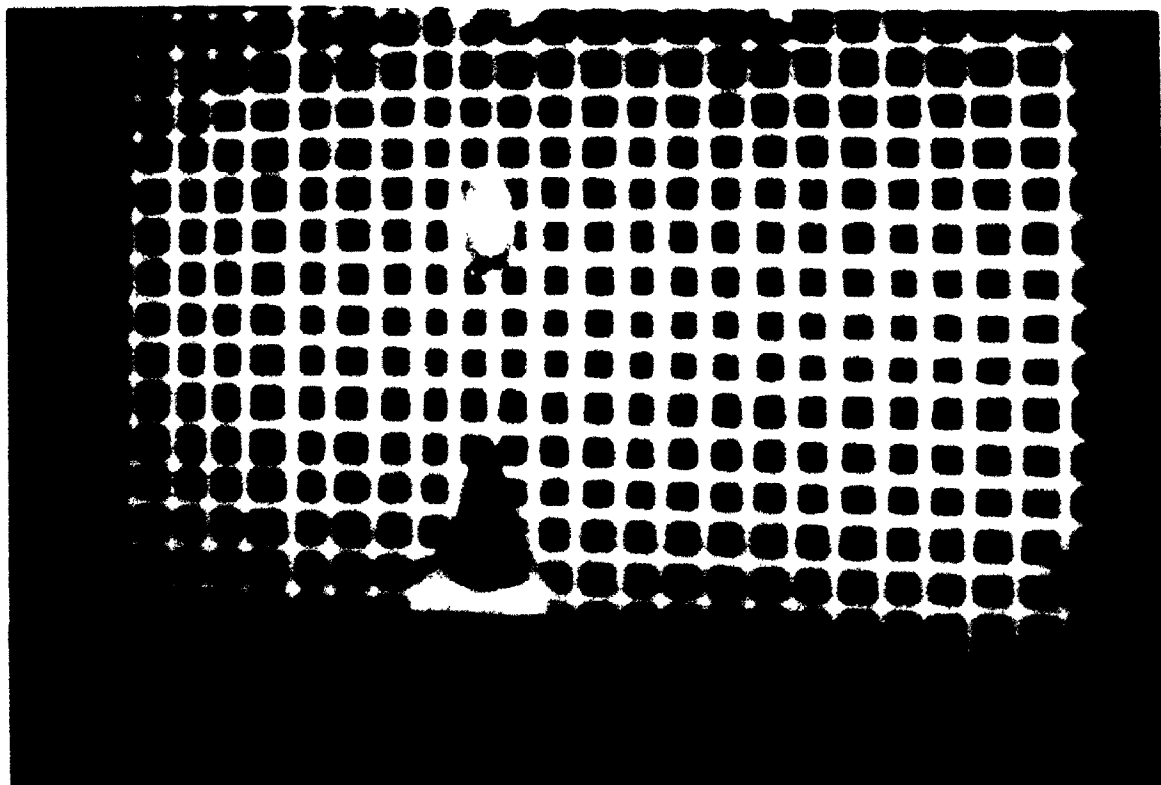


Figure C.4: The experimental droplet profile for water on a brass electrode after breakup

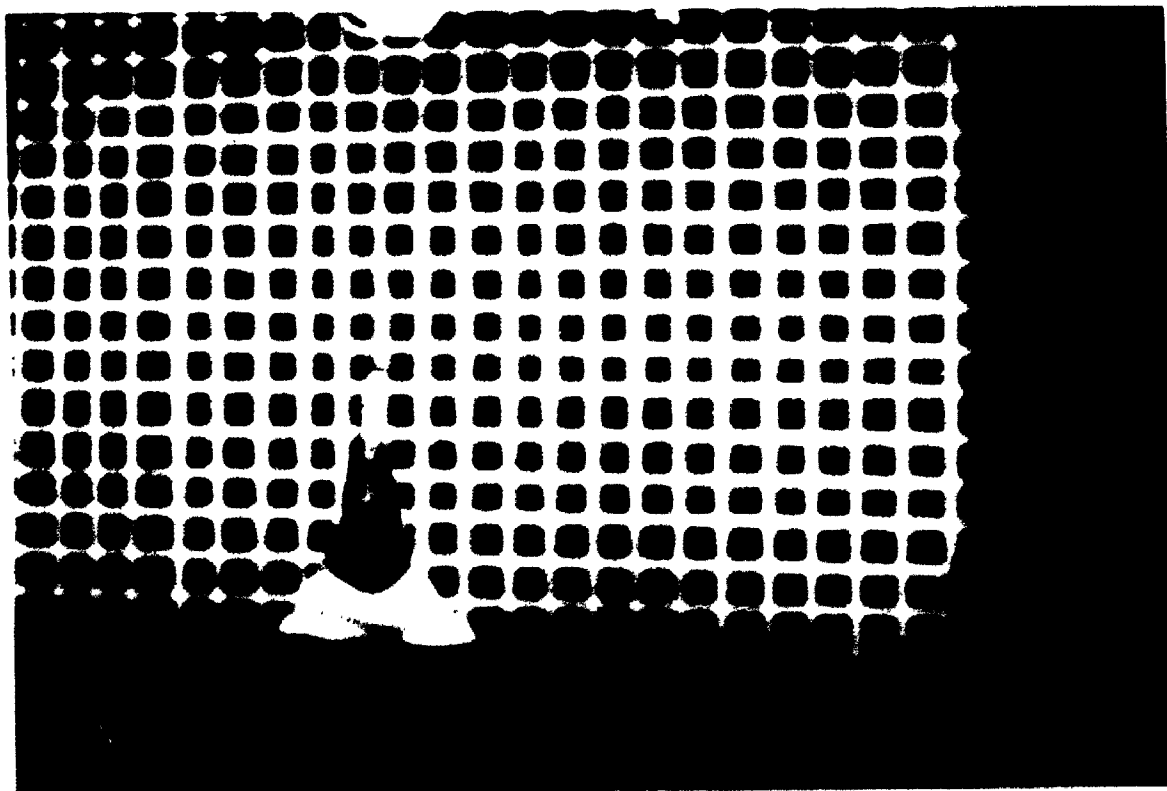


Figure C.5: The nonaxisymmetric droplet profile for water on a brass electrode after breakup

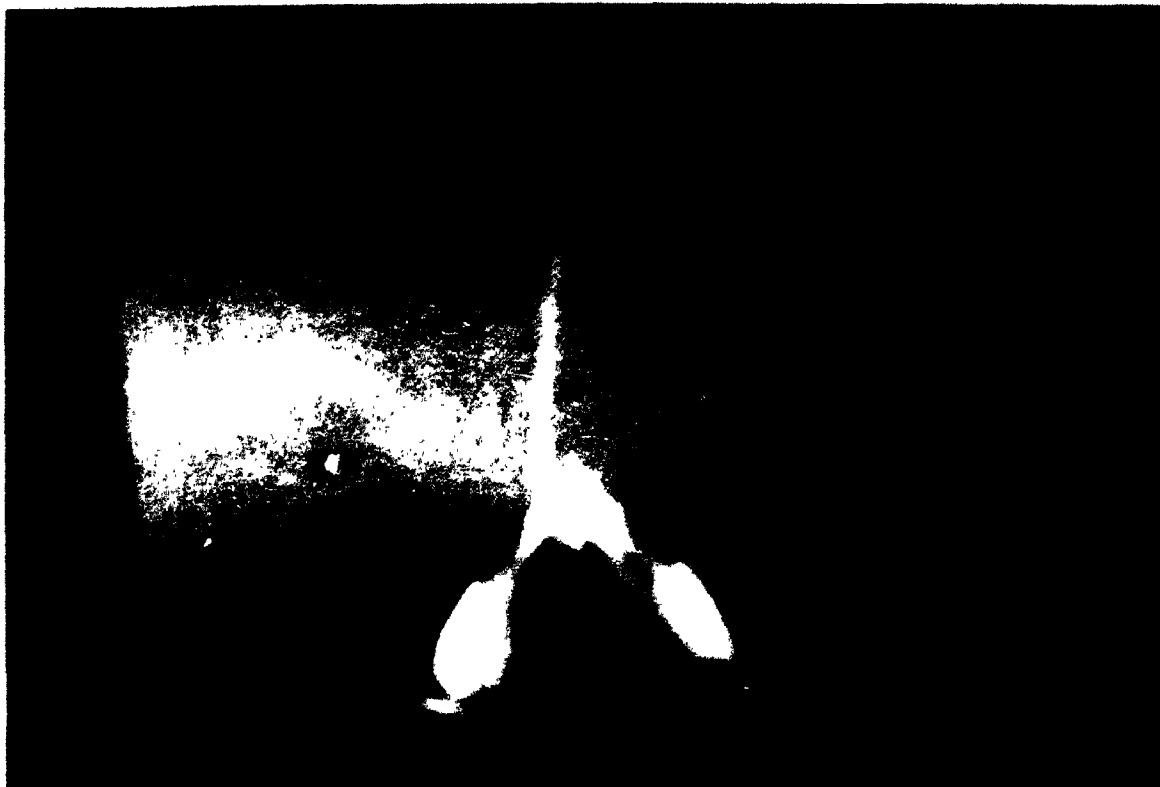


Figure C.6: The experimental droplet profile for water on an aluminium electrode before breakup

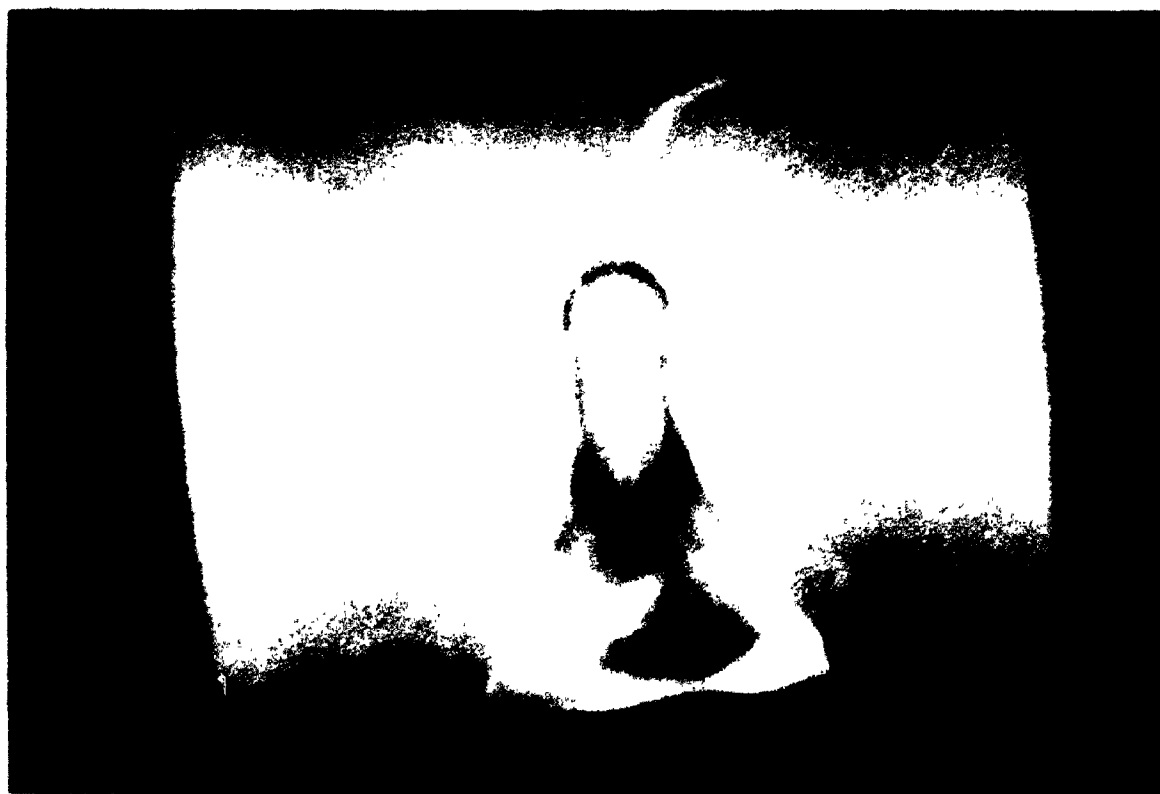


Figure C.7: The experimental droplet profile for water on an aluminium electrode just before breakup

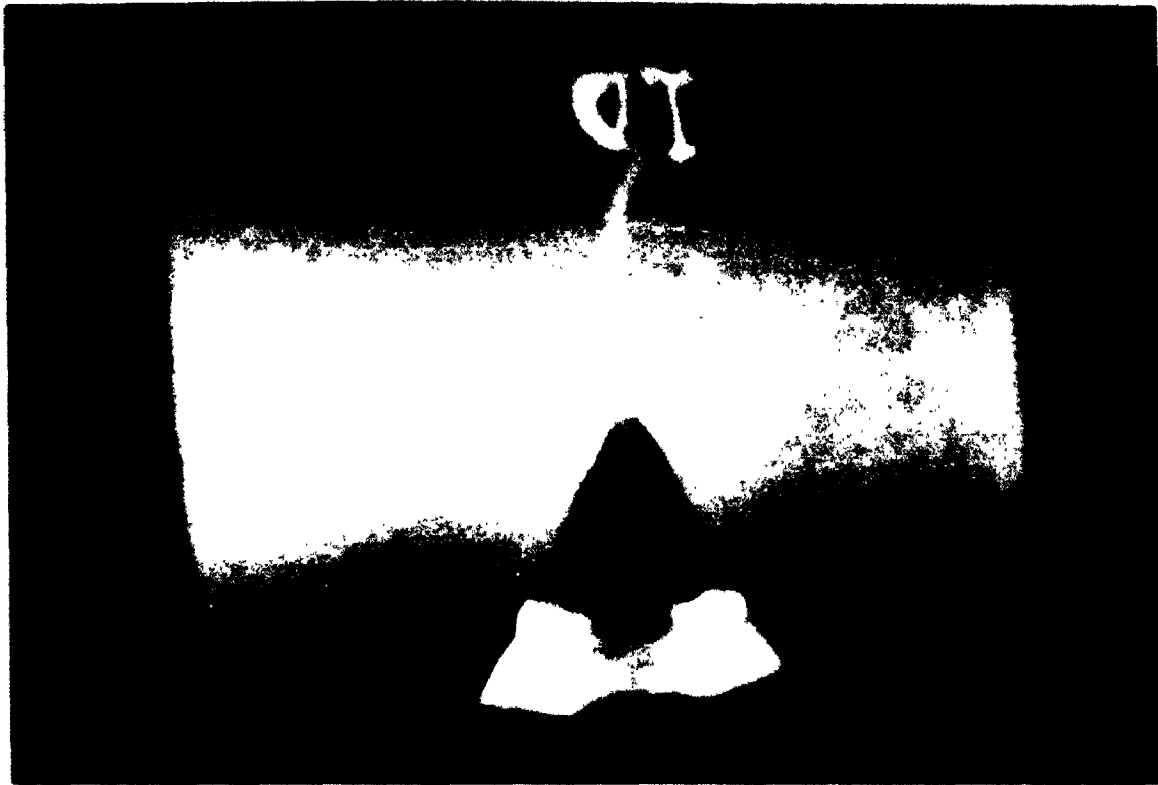


Figure C.8: The experimental droplet profile for water on an aluminium electrode after breakup



Figure C.9: The nonaxisymmetric droplet profile for water on an aluminium electrode after breakup

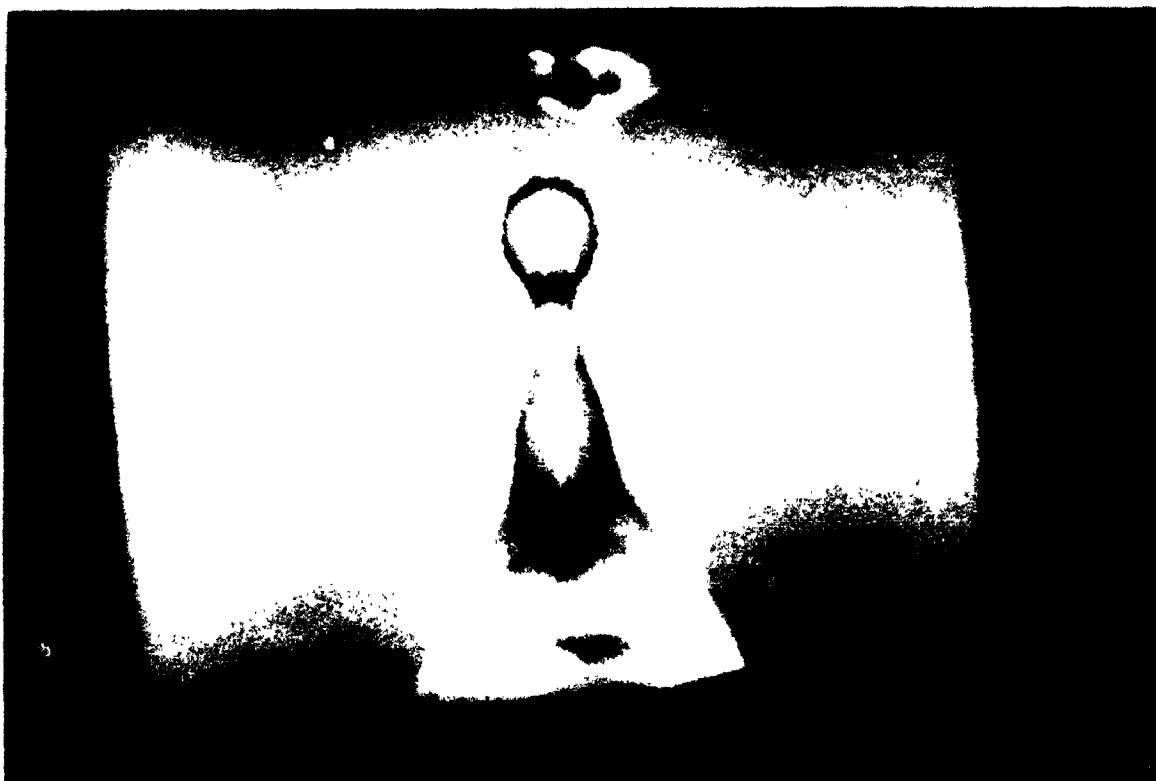


Figure C.10: The nonaxisymmetric droplet profile for water on an aluminium electrode before a second breakup

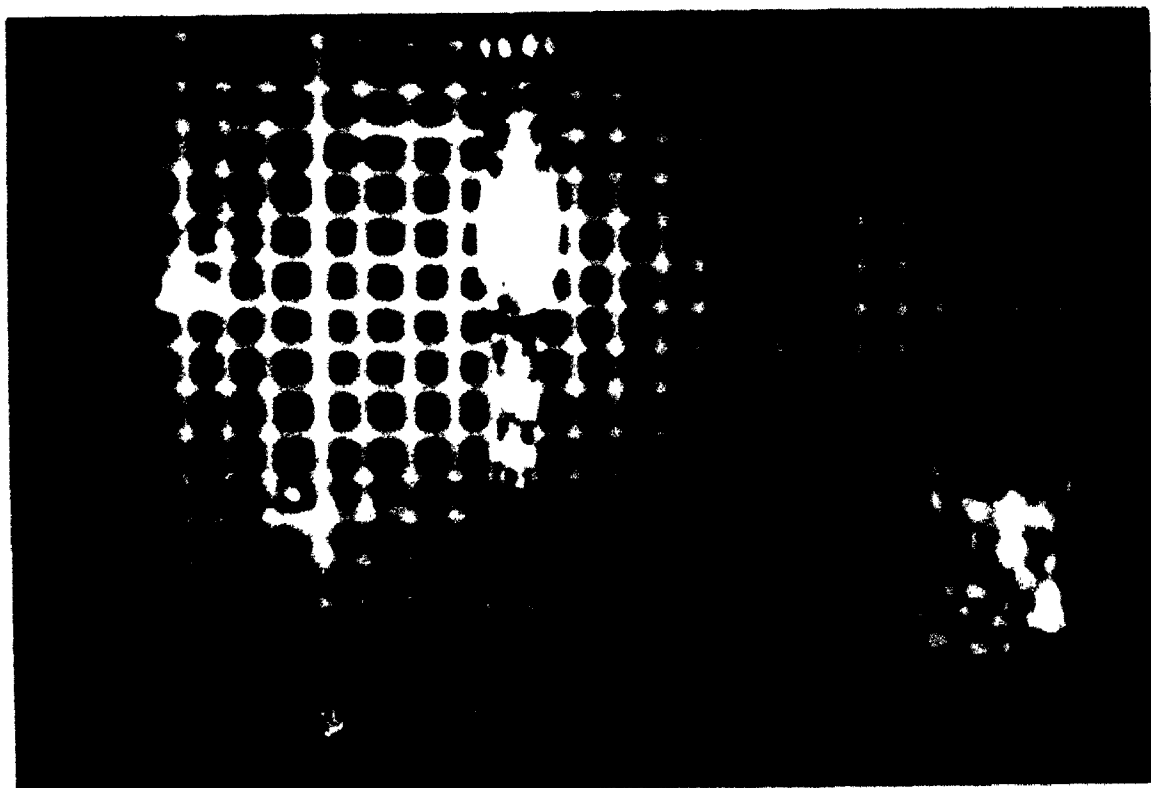


Figure C.11: The droplet profile for a highly viscous material on a brass electrode

Bibliography

- [1] Abramowitz, M. & Stegun, I. A. 1965 *Handbook of Mathematical Functions*. Dover.
- [2] Acton, F. S. 1970 *Numerical Methods That Usually Work*. Harper & Row.
- [3] Adamson, A. W. 1982 *Physical Chemistry of Surfaces*. Wiley.
- [4] Amos, D. E. 1986 Algorithm 644: a portable package for Bessel functions of complex argument and nonnegative order. *ACM Trans. Math. Software*. **12**, 265.
- [5] Batchelor, G. K. 1967 *An Introduction to Fluid Mechanics*. Cambridge University Press.
- [6] Basaran, O. A. & Scriven, L. E. 1988 The Taylor pump - viscous free surface flow driven by electric shear-stress. *Chem. Eng. Co.* **67**, 259.
- [7] Binns, K. J. & Lawrenson, P. J. 1963 *Analysis and Computation of Electric and Magnetic Field Problems*. MacMillan.
- [8] Blackmon, Jr. J. B. 1965 Collection of liquid propellants in zero gravity with electric fields. *Spacecraft Rockets*. **2**, 391.
- [9] Cercanowicz, A. E. 1981 Rayleigh limit for nonstationary charged drops. *IEEE-IAS Conf. Record*.
- [10] Chandrasekhar, S. 1961 *Hydrodynamic and Hydromagnetic Stability*. Oxford Press.

- [73] Swatic, D. S. & Hendricks C. D. 1968 Production of ions by electrohydrodynamic spraying. *AIAA J.* **16**, 1596.
- [74] Taylor, G. I. 1950 The instability of liquid surfaces when accelerated in a direction perpendicular to their plane. I *Proc. Roy. Soc. A.* **201**, 192.
- [75] Taylor, G. I. 1964 Disintegration of water drops in an electric field. *Proc. Roy. Soc.* **280**, 383.
- [76] Taylor, G. I. 1966 Studies in electrohydrodynamics. *Proc. Roy. Soc. A* **291**, 159.
- [77] Taylor, G. I. & McEwan, A.D. 1965 The stability of horizontal fluid interface in a vertical electric field. *J. Fluid Mech.* **22**, 1.
- [78] Theodossiou, G., Nelson, J.K. & Odell, G. M. 1986 A computer simulation of transient electrohydrodynamic motion in stressed dielectric liquids. *J. Phys. D.* **19**, 1643.
- [79] Torrey, M. D., Lawrence, D., Cloutman, R., Jolseness, C. M. & Hirt, C.W. 1985 NASA-VOF2D: a computer program for incompressible flows with free surfaces. *Los Alamos National Laboratory, LA-10612-MS.*
- [80] Watson, P. K. & Charbough, A. H. 1941 Conduction and breakdown in liquid dielectrics. *Progress in Dielectrics.* Vol 4, 201.
- [81] Welch J. E., Harlow, F. H., Shannon, J. P. & Daly, B. J. 1965 The MAC method; a computing technique for solving viscous incompressible transient fluid-flow problems involving free surfaces. *Los Alamos Scientific Laboratory, LA-3425.*
- [82] White, H. J. 1963 *Industrial Electrostatic Precipitation.* Addison-Wesley.
- [83] Yih, C. S. 1967 Instability due to viscous stratification. *J. Fluid Mech.* **27**, 337.
- [84] Varga, R. S. 1962 *Matrix Iterative Analysis.* Prentice-Hall.

- [22] Gunn, R. 1957 The electrification of precipitation and thunderstorms. *Proc. I.R.E.* **45**, 1331.
- [23] Harlow, F. & Welch, J. E. 1965 Numerical calculation of time dependent viscous incompressible flow of liquids with free surfaces. *Phys. Fluids*, **8**, 2182.
- [24] Harisson, W. J. 1908 The influence of viscosity on the oscillations of superposed fluids. *Proc. London Math. Soc.* **6**, 396.
- [25] Haas, W. & Adams, J. 1968 Electrophotographic imaging with cholesteric liquid crystals. *Appl. Optics*, **7**, 1203.
- [26] Hastings, D. A. 1975 Computational method for electrical potential and other field problems. *Am. J. Phys.* **43**, 518.
- [27] Hendricks, C. D. 1962 Charged droplet experiments. *J. Colloid Sci.* **17**, 249.
- [28] Hendricks, C. D. & Schneider, J. M. 1963 Stability of a conducting droplet under the influence of surface tension and electrostatic forces. *Am. J. Phys.* **31**, 450.
- [29] Hung, R. J., Tsao, Y. D. & Leslie, F. W. 1988 *Drops and Bubbles*. AIP.
- [30] Hirt, C. W. & Nichols, B. D. 1980 A computational method for free surface hydrodynamics. *Los Alamos Scientific Laboratory, LA-8355*.
- [31] Hirt, C. W. & Nichols, B. D. 1981 Volume of fluid (VOF) method for the dynamics of free boundaries. *J. Comp. Phys.* **39**, 201.
- [32] Hogan, J. J. & Heendricks, C. D. 1965 Investigation of charge to mass ratio of electrically sprayed liquid particles. *AIAA J.* **3**, 296.
- [33] Hooper, A. P. & Boyd, W. G. C. 1983 Shear-flow instability at the interface between two viscous fluids. *J. Fluid Mech.* **128**, 507.

- [34] Inculet, I. I. & Kromann, R. 1989 Breakup of large water droplets by electric fields. *IEEE Trans. Ind. Appl. Ia-25*, 945.
- [35] Inculet, I. I., Floryan, J. M. & Haywood R. 1990 Dynamics of water droplets break-up in electric fields. *IEEE Ind. Appl. Soc. Conf. Rec. Seattle*, 1915.
- [36] Inculet, I. I., Adamiak, K., Rasmussen, H., Abdella, K. & Base, T.E. 1991 Dynamics of sessile droplets distortion and disruption by electric field in micro gravity conditions. *Proc. Space Bound.* 101.
- [37] Kamotani, Y., Prasad, A. & Ostrach, S. 1981 Thermal convections in an enclosure due to vibrations aboard a spacecraft. *AIAA J.* **19**, 511.
- [38] Jeffreys, H. 1926 The stability of a layer of fluid heated below. *Phil. Mag.* **2**, 833.
- [39] Kelvin, Lord 1871 Hydrokinetic solutions and observations. *Phil. Mag.* **42**, 362.
- [40] Kim, K. & Turnbull, R. J. 1976 Generation of charged drops of insulating liquid by electrostatic spraying. *J. Appl. Phys.* **47**, 1964.
- [41] Lamb, H. 1932 *Hydrodynamics*. Cambridge University Press.
- [42] Lewis, D. J. 1950 The instability of liquid surfaces when accelerated in a direction perpendicular to their plane. II *Proc. Roy. Soc. A.* **117**, 81.
- [43] Lin, C. C. 1945 On the stability of two-dimensional parallel flows. Parts I, II, III. *Quart. Appl. Math.* **3**, 117, 218, 277.
- [44] Lopez, J., Milleer, C. A. & Ruckenstein, E. 1976 *J. Colloid Interface Sci.* **56**, 460.
- [45] Marcus, P. S. & Press, W. H. 1977 On the Green's functions of small disturbances of plane Couette flow. *J. Fluid Mech.* **79**, 525.
- [46] Melcher, J. R. 1963 *Field Coupled Surface Waves*. MIT Press.

- [47] Melcher, J. R. 1966 Travelling-wave induced electroconvection. *Phys. Fluids*. **9**, 1548.
- [48] Melcher, J. R. & Ferebaugh, M. S. 1967 Traveling-wave bulk electroconvection induced across a temperature gradient. *Phys. Fluids*. **10**, 1178.
- [49] Melcher, J. R. & Smith, C. V. 1967 Electrohydrodynamic charge relaxation and interfacial perpendicular-field instability. *Phys. Fluids*. **12**, 778.
- [50] Melcher, J. R. & Mathew, H. 1967 Gradient stabilization of electrohydrodynamically oriented fluids. *J. Space Craft and Rockets*. **4**, 864.
- [51] Melcher, J. R. & Taylor, G. I. 1969 Electrohydrodynamics. *Ann. Rev. Fluid Mech.* **55**, 48.
- [52] Miles, J. W. 1960 The hydrodynamic stability of a thin film of liquid in uniform shearing motion. *J. Fluid Mech.* **8**, 593.
- [53] Mohamed, A. A., Elshehawy, E. F. & Dib, Y. O. E. 1986 Electrohydrodynamic stability of a fluid layer. *J. Chem. Phys.* **85**, 445.
- [54] Muller, D. E. 1956 A method for solving algebraic equations using an automatic computer. *Mathematical tables and aids to computation*. **10**, 208.
- [55] Nicholas, B. D., Hirt, C. W. & Hotchkiss, R. S. 1980 SOLA-VOF: A Solution Algorithm For Transient Fluid Flow With Multiple Free Boundaries. *Los Alamos Scientific Report*, **LA-8355**.
- [56] Noh, W. F., Adleer, B., Fernbach, S. & Rotenberg, M. 1964 CEL: a time-dependant two-space dimensional, coupled Eulerian-Lagrange code. *Methods Comp. Phys.* **3**, 117.
- [57] Olver, F. W. J. 1974 *Asymptotics and Special Functions*. Academic.

- [58] Olver, F. W. J., Piessens, R., deDoncker-Kapenga, E., Uberhuber, C. W. & Kahaner, D. K. 1983 *QUADPACK*. Springer-Verlag.
- [59] Orr, W. M'F. 1907 The stability or instability of the steady motions of a perfect liquid and of viscous liquid. *Proc. Roy. Irish. Acad.* **27**, 9 & 69.
- [60] Pohl, H. A. 1960 *Sci. Am.* **203**, 107.
- [61] Poincare, H. 1885 sur l'equilibre d'une masse fluide animee d'un mouvement de rotation. *Acta Math.* **7**, 259.
- [62] Proudman, J. 1953 *Dynamical Oceanography*. John Wily & Sons.
- [63] Rayleigh, Lord 1879 On the instability of jets. *Proc. London Math. Soc.* **10**, 4.
- [64] Rayleigh, Lord 1916 On convection currents in a horizontal layer of fluids, when the higher temperature is on the under side. *Phil. Mag.* **32**, 529.
- [65] Rayleigh, Lord 1882 On the equilibrium of liquid conducting masses charged with electricity. *Phil. Mag.* **14**, 184.
- [66] Rosensweig, R. E. 1966 Magnetic fluids. *Intl. Sci. Tech.* **10**, 1178.
- [67] Ruckenstein, E. & Dunn, C. S. 1977 *J. Colloid Interface Sci.* **59**, 135.
- [68] Shaw, F. S. 1953 *An Introduction to Relaxation Methods*. Dover.
- [69] Smith, K. M. & Stephen, H. D. 1982 The instability of shear liquid layers. *J. Fluid Mech.* **121**, 187.
- [70] Southwell, R. V. 1946 *Relaxation Methods in Theoretical Physics*. Oxford University Press.
- [71] Stratton, J. A. 1941 *Electromagnetic Theory*. McGraw Hill.
- [72] Stroud, A. H. & Secrest, D. 1966 *Gaussian Quadrature Formulas*. Prentice-Hall.

- [73] Swatic, D. S. & Hendricks C. D. 1968 Production of ions by electrohydrodynamic spraying. *AIAA J.* **16**, 1596.
- [74] Taylor, G. I. 1950 The instability of liquid surfaces when accelerated in a direction perpendicular to their plane. I *Proc. Roy. Soc. A.* **201**, 192.
- [75] Taylor, G. I. 1964 Disintegration of water drops in an electric field. *Proc. Roy. Soc.* **280**, 383.
- [76] Taylor, G. I. 1966 Studies in electrohydrodynamics. *Proc. Roy. Soc. A* **291**, 159.
- [77] Taylor, G. I. & McEwan, A.D. 1965 The stability of horizontal fluid interface in a vertical electric field. *J. Fluid Mech.* **22**, 1.
- [78] Theodossiou, G., Nelson, J.K. & Odell, G. M. 1986 A computer simulation of transient electrohydrodynamic motion in stressed dielectric liquids. *J. Phys. D.* **19**, 1643.
- [79] Torrey, M. D., Lawrence, D., Cloutman, R., Jolseness, C. M. & Hirt, C.W. 1985 NASA-VOF2D: a computer program for incompressible flows with free surfaces. *Los Alamos National Laboratory, LA-10612-MS.*
- [80] Watson, P. K. & Charbough, A. H. 1941 Conduction and breakdown in liquid dielectrics. *Progress in Dielectrics. Vol 4*, 201.
- [81] Welch J. E., Harlow, F. H., Shannon, J. P. & Daly, B. J. 1965 The MAC method; a computing technique for solving viscous incompressible transient fluid-flow problems involving free surfaces. *Los Alamos Scientific Laboratory, LA-3425.*
- [82] White, H. J. 1963 *Industrial Electrostatic Precipitation.* Addison-Wesley.
- [83] Yih, C. S. 1967 Instability due to viscous stratification. *J. Fluid Mech.* **27**, 337.
- [84] Varga, R. S. 1962 *Matrix Iterative Analysis.* Prentice-Hall.

- [85] Zeleny J. 1914 The electrical discharge from liquid points and hydrostatic method of measuring the electric intensity at their interfaces. *Phys. Rev.* [2] **3**, 1914.
- [86] Zeleny, J. 1915 On the condition of instability of electrified drops, with application to the electrical discharge from liquid points. *Proc. Cambridge Phil. Soc.* **18**, 17.